The Power Systems Decarbonization Transition Planning and Operating: A Comprehensive Carbon Management Framework

YI YANG

Ph.D. (Engineering)

THE UNIVERSITY OF SYDNEY

Supervisor: Dr. Jeremy (Jing) Qiu
Associate Supervisor: A.Prof. Dong Yuan

A Thesis submitted in fulfilment of
requirements for the degree of
Doctor of Philosophy

This research reported in this thesis was supported by the award of a
Vanzone Green Hydrogen Postgraduate Research Scholarship
to the PhD Candidate

School of Electrical and Computer Engineering
Faculty of Engineering
The University of Sydney
Australia

30 May 2024

To my family and friends, especially to my parents & grandparents

Declaration

This is to certify that to the best of my knowledge, the content of this thesis is my own work. It contains no material previously published or written by another person except duly referenced within the text. The contents of this thesis reflect the work I have carried out since the commencement of my higher degree by Ph.D. research candidature and do not involve a substantial part of work submitted for any other academic degree or diploma from any university or other institution of higher education. I consent to this copy of my thesis, when deposited in the University Library, being made available for loan and photocopying subject to the provisions of the Copyright Act 1968.

I hereby certify that the intellectual content of this thesis is the product of my own work and that all the assistance received in preparing this thesis and sources have been acknowledged. Furthermore, the works involved in this thesis include chapters/scholarly works that have been published or are under review, of which I am the joint author.

Chapter 2 of this thesis is partly published as [C. Zhang, Y. Yang*, J. Qiu, J. Ruan, G. Liang, and L. Yang, "Comprehensive Approaches to a Low-Carbon Transition of the Power Grid," 8th IEEE Conference on Energy Internet and Energy System Integration (IEEE EI2 2024), Shenyang, China, pp. 1-6, Dec. 2024]. I designed the study, reviewed the models, and wrote the drafts.

Chapter 3 of this thesis is currently under review and submitted as [Y Yang, C Zhang, Y Wang, J Ruan, and J Qiu, "A Two-Stage Generation Expansion Planning Considering Coal-to-Gas Conversion in Coal-Fired Power Plants," Energy, under review]. I designed the study, analyzed the data, and wrote the drafts.

Chapter 4 of this thesis is currently under review and submitted as [C Zhang, Y Yang*, J Qiu, J Lin, and J Zhang, "Fuzzy Inference-based Power System Planning Considering Collaborative Decarbonization on the Supply-Demand Side," IEEE Transactions on Industry Applications, under review]. I designed the model, analyzed the data, and wrote the drafts.

Chapter 5 of this thesis is published as [Y. Yang, J. Qiu, and C. Zhang, "Distribution Network Planning Towards a Low-Carbon Transition: A Spatial-Temporal Carbon Response Method," IEEE Transactions on Sustainable Energy, vol. 15, no. 1, pp. 429 - 442, Jan. 2024]. I designed the study, analyzed the data, and wrote the drafts.

Chapter 6 of this thesis is published as [Y. Yang, J. Qiu, C. Zhang, J. Zhao, and G. Wang, "Flexible Integrated Network Planning Considering Echelon Utilization of Second Life of Used Electric Vehicle Batteries," IEEE Transactions on Transportation Electrification, vol. 8, no. 1, pp. 263–276, Mar. 2022]. I designed the study, analyzed the data, and wrote the drafts.

Author:

In addition to the statements above, in cases where I am not the corresponding author of a published item, permission to include the published material has been granted by the corresponding author.

Yi Yang

June 2024

Approved by Principal Supervisor:

As supervisor for the candidature upon which this thesis is based, I can confirm that the authorship attribution statements above are correct.

Dr. Jing Qiu

June 2024

Acknowledgements

The doctoral study period holds profound significance for me, and therefore, I hope to be granted permission to deviate from formalities in this chapter to express my gratitude.

A hymn to courage:

It's beyond imagination that I have indeed successfully completed the requirements of my doctoral thesis and paper, about to obtain my coveted Ph.D. degree. Reflecting on this journey, the overwhelming excitement leaves me at a loss for words, unsure of how to put pen to paper. For me, the journey to obtaining a doctoral degree demanded not just knowledge but also courage. The pursuit of knowledge was fraught with various challenges and trials, testing me physically and mentally. Therefore, before expressing my sincerest gratitude to others, I must first express gratitude to myself. I am grateful to myself for persevering through this journey of life, despite experiencing anxiety, stress, depression, and various physiological reactions that accompanied them. Looking back, I wonder if I could have achieved what I have today if given the chance to start over. I am thankful to the version of myself who was so courageous and relentlessly pursued my dream.

Among those who have provided me with invaluable assistance, I must first express my gratitude to my supervisor, Dr. Jeremy Qiu. I am thankful to him for granting me this opportunity to pursue my Ph.D. at the Centre for Future Energy Networks, University of Sydney. I appreciate his patience, trust, and encouragement throughout my academic journey. He has been more than just an advisor but also a friend during my doctoral life. Not only has he provided ample academic guidance, but he has also extended support in life and finances whenever possible. Additionally, I would like to thank my co-supervisor, A.Prof. Dong Yuan sincerely.

Furthermore, special thanks are extended to Prof. Junhua Zhao. I am grateful for his assistance and guidance during the pandemic. His dedication, pragmatism, and

innovative approach to academia deeply inspired and influenced me. I owe a great deal of my achievements today to his help and support.

Without the support of friends, I could not have achieved accomplishments today. Firstly, I want to express my gratitude to a special friend: my girlfriend, Dr. Chenxi Zhang. She embodies numerous beautiful qualities, such as loveliness, beauty, and intelligence. We met in Australia and became lovers during the previous stage of my academic journey. I will never forget that it was with her help that I obtained the opportunity to pursue a doctoral degree. I also cherish the years we have spent together, hand in hand. I am grateful for her companionship, support, encouragement, and care. Over these years, we have experienced many things together, and I appreciate our ability to be there for each other during countless challenging times.

Furthermore, I need to express gratitude to the numerous colleagues and collaborators in the laboratory, thanking them for their outstanding contributions to some experimental results and mathematical modeling aspects of this thesis. Graduating with a doctoral degree does not signify an end but rather marks the beginning of a research career. I also sincerely appreciate the many friends who shared information and provided advice during the job-seeking period. Special thanks to Dr. Yunqi Wang, Dr. Xianzhuo Sun, Dr. Yuechuan Tao, Dr. Jiaqi Ruan, and Ph.D. Candidate Jiafeng Lin for their contributions to the listed publication.

Life without friends would be dull and colorless. Over the past few years, the support and encouragement of friends around me have been one of the reasons I have been able to persevere. I am grateful to my friends from China, Shuo Tong, Zhekai Wu, and Rujia Zhan. Growing up together since childhood, even though we are miles apart, our frequent interactions on the internet have added much joy to my life. I also want to thank my lovely neighbors, Dr. Jinjin Gu, Ph.D. Candidate Xinlei Wang, Dr. Xin Lu, and Ph.D. Candidate Xinyan Yu. Our daily gatherings and outings have been a continuous source of happiness for me.

Besides friends who have accompanied me in real life, anime and games have also provided great spiritual support and solace during my doctoral studies. I am grateful to "Frieren: Beyond Journey's End" for teaching me anew what courage means. I appreciate the companionship of the virtual character “Takane Manaka” from the "Love Plus" series of games. And I am thankful to "Hyouka: Classic Literature Club series," both the novel and anime, for bringing me a calming period.

Finally, special thanks are dedicated to my family. My parents and *the best parents*, **Mr. Lixin Yang** and **Ms. Xiuxiang Wu**, as well as their parents, my grandparents, **Mr. Wenbin Yang** and **Ms. Lianhua Yan**, **Mr. Yuanqing Wu** and **Ms. Xiulian Lin**.

Without their hard work and dedication, I would not be who I am today. I am grateful for the spiritual and material support they have provided, allowing me the freedom and confidence to pursue my dreams. Though, at times, my parents may struggle to express their love, I am happy to see that this is gradually improving. Most importantly, I wholeheartedly believe that we deeply appreciate each other's existence and love each other immensely.

As I put pen to paper to write this letter of gratitude, it signifies the conclusion of my Ph.D. journey. Regardless of whether the outcome meets expectations, my life will usher in a new chapter. I hope everyone reading this can find the happiness and joy they seek. Once again, I sincerely thank all those who have helped me along the way.

List of Publications

The following publications have been completed as the Ph.D. research results, where I was listed as the first and corresponding author.

(P: Published; UR: Under Review; *: corresponding author)

[P1] **Y. Yang**, J. Qiu, and C. Zhang, “Distribution Network Planning Towards a Low-Carbon Transition: A Spatial-Temporal Carbon Response Method,” *IEEE Transactions on Sustainable Energy*, vol. 15, no. 1, pp. 429 - 442, Jan. 2024.

[P2] **Y. Yang,** J. Qiu, C. Zhang, J. Zhao, and G. Wang, “Flexible Integrated Network Planning Considering Echelon Utilization of Second Life of Used Electric Vehicle Batteries,” *IEEE Transactions on Transportation Electrification*, vol. 8, no. 1, pp. 263–276, Mar. 2022.

[P3] **Y. Yang**, J. Qiu, J. Ma, and C. Zhang, "Integrated grid, coal-fired power generation retirement and GESS planning towards a low-carbon economy", *International Journal of Electrical Power & Energy Systems*, vol. 124, p. 106409, Jan. 2021.

[P4] **Y. Yang**, C. Zhang, and J. Qiu, “Low-Carbon System Transition Considering Collaborative Emission Reduction on Supply-Demand Side,” in 2023 *IEEE International Conference on Energy Technologies for Future Grids* (ETFG), Wollongong, Australia, pp. 1–6. Dec. 2023, doi: 10.1109/ETFG55873.2023.10408546.

[P5] C. Zhang[1], **Y. Yang**[1], Y. Wang, J. Qiu, and J. Zhao, “Auction-based peer-to-peer energy trading considering echelon utilization of retired electric vehicle second-life batteries,” *Applied Energy*, vol. 358, p. 122592, Mar. 2024. (equal contributions)

[P6] C. Zhang, J. Qiu, and **Y. Yang***, “A Two-Stage Time-shiftable Flexible Demand-based Negawatt Trading Framework in Low-voltage Distribution Networks,” *Applied Energy*. vol. -, p. -, Dec. 2024.

[P7] C. Zhang, **Y. Yang***, J. Qiu, J. Ruan, G. Liang, and L. Yang, “Comprehensive

Approaches to a Low-Carbon Transition of the Power Grid," in 2024 *IEEE Conference on Energy Internet and Energy System Integration* (IEEE EI^2 2024), Shenyang, China, pp. 1–6. Dec. 2024.

[P8] B. Zhang, C. Zhang, **Y. Yang***, and J. Qiu, "A Scenario-Driven Bi-Level Programming Model for Optimal Distributed Generation Planning: Integrating Fuzzy C-Means (FCM) Clustering and Enhanced Whale Optimization (EWOA)," in 2024 *4th International Conference on Smart City and Green Energy* (ICSCGE), Sydney, Australia, pp. 1–6. Dec. 2024. (Conference Best Paper)

[P9] W. Liao, **Y. Yang***, Q. Wang, R. Wang, X. Fu, Y. Xie, and J. Zhao, "Interpretable Hybrid Experiment Learning-Based Simulation Analysis of Power System Planning under the Spot Market Environment," Energies, vol. 16, no. 12, p. 4819, Jun. 2023.

[UR1] **Y Yang**, C Zhang, Y Wang, J Ruan, and J Qiu, "A Two-Stage Generation Expansion Planning Considering Coal-to-Gas Conversion in Coal-Fired Power Plants," *Energy*. Under Review.

[UR2] C. Zhang, **Y. Yang***, J. Qiu, J. Lin, and J. Zhang, "Fuzzy Inference-based Power System Planning Considering Collaborative Decarbonization on the Supply-Demand Side," *IEEE Transactions on Industry Applications*. Under Review.

The following papers have also been completed in the course of the PhD studies, where I was listed as the co-author.

(P: Published; UR: Under Review)

[P1] C. Zhang, J. Qiu, and **Y. Yang**, "A Peer-to-Peer Joint Kilowatt and Negawatt Trading Framework Incorporating Battery Cycling Degradation," *IEEE Transactions on Power Systems*, pp. 1–12, 2024, doi: 10.1109/TPWRS.2024.3360606.

[P2] C. Zhang, J. Qiu and **Y. Yang**, "A Two-Stage Adaptive Supply-Demand Management Framework for Microgrids: Aging-Aware Asset Planning and Peer-to-Peer Negawatt Trading," *IEEE Transactions on Power Systems*, pp. 1-12, 2024, early access, doi: 10.1109/TPWRS.2024.3510700.

[P3] J. Lin, J. Qiu, **Y. Yang**, and W. Lin, "Planning of Electric Vehicle Charging

Stations Considering Fuzzy Selection of Second Life Batteries,” *IEEE Transactions on Power Systems*, vol. 39, no. 3, pp. 5062–5076, May 2024.

[P4] C. Zhang, J. Qiu, **Y. Yang**, and J. Zhao, “Residential customers-oriented customized electricity retail pricing design,” International Journal of Electrical Power & Energy Systems, vol. 146, p. 108766, Mar. 2023

[P5] C. Zhang, J. Qiu, **Y. Yang**, and J. Zhao, “Trading-oriented battery energy storage planning for distribution market,” International Journal of Electrical Power & Energy Systems, vol. 129, p. 106848, Jul. 2021.

[P6] X. Lu, J. Qiu, **Y. Yang**, C. Zhang, J. Lin and S. An, "Large Language Model-based Bidding Behavior Agent and Market Sentiment Agent-Assisted Electricity Price Prediction," *IEEE Transactions on Energy Markets, Policy and Regulation*, pp. 1-12, 2024, early access, doi: 10.1109/TEMPR.2024.3518624.

I warrant that I have obtained, where necessary, permission from the copyright owners to use any third-party copyright material reproduced in the thesis or to use any of my own published work (e.g., journal chapters) in which the copyright is held by another party (e.g., publisher, co-authors).

Abstract

The ongoing exacerbation of global climate change, fueled by the continuous growth in human societal emissions, remains a pressing concern. Excessive emissions continue to escalate temperatures, challenging the temperature control goals outlined in the Paris Agreement. As one of the largest sources of emissions, the decarbonization transition of power systems has garnered attention from academia, industry, and government sectors. The system transition process is complicated due to the involvement of various entities such as power generation, transmission networks, active customers, etc. Traditional emission mitigation methods targeting individual entities may struggle to achieve the expected outcomes at the systemic level. Coordinating operations and planning among various stakeholders is essential to achieve the desired results. With the gradual phasing out or retrofitting of traditional high-emission power generators, the system will certainly incorporate a significant influx of renewable energy to meet the increasing electricity demands. Moreover, coupling between power and emission markets can incentivize proactive participation from both the supply and demand sides, while flexible market mechanisms facilitate emission control, thus reducing overall emissions.

To promote overall system emissions reduction, solely considering direct and indirect emissions generated from energy combustion in the production process, i.e., Scope 1 and Scope 2 emissions, is insufficient. The system also encompasses a large amount of other indirect emissions occurring throughout the system value chain, that is, Scope 3 emissions. These emissions are relatively more challenging to quantify and control as they are generated by third-party actions, such as reusing or scraping second-life electric vehicle batteries. While the specific emissions reductions from these actions are difficult to measure precisely, they effectively enhance overall system resource utilization efficiency, reducing total societal emissions. Furthermore, the coupling of transportation networks with electricity networks becomes increasingly inseparable with the expansion of electric vehicles, further decreasing the fossil fuel reliance on systems. In summary, the above novel emission curb paradigm considers more complex

physical, economic, and emission constraints, presenting new opportunities and challenges for the planning and operation of power systems.

This thesis focuses on the decarbonization transition of power systems, especially the modeling and optimization of planning and operational strategies to achieve a net-zero emission society. In this thesis, a comprehensive carbon management framework is proposed, which covers various emission reduction strategies ranging from the supply side to the demand side and partial Scope 3 emissions, to analyze the pathways for carbon-oriented power system emission reduction. In the main body of the thesis, from Chapter 3 to Chapter 6, analyses are conducted on topics such as the low-carbon transformation of Coal-Fired Power Plants (CFPPs) on the generation side, supply-demand side coordinated emission reduction, spatial-temporal carbon response of demand-side flexibility load, and echelon utilization of second-life electric vehicle batteries, respectively. Among these, coordinated planning involves the mutual influence among networks such as the power grid and transportation network. Operational problems consider the dynamic response of various system demand-side entities, including data centers, large industrial loads, and mobile energy storage, to node carbon intensity. Additionally, economic and planning measures such as carbon taxes, carbon allowance trading, and flexible carbon targets allow for measuring the costs associated with system emissions.

In this thesis, the effectiveness and reliability of the proposed models and methods are demonstrated through simulations in several benchmark test systems of different scales and voltage levels. The experimental results fully certify that the proposed approach can effectively reduce system emissions, and the coordination of emission reduction methods at various levels can facilitate a smooth system transition.

Contents

Glossary

AEMO	Australian Energy Market Operator
BESSs	Battery Energy Storage Systems
BOM	Bureau of Meteorology
CCS	Carbon Capture and Storage
CCUS	Carbon Capture, Utilization, and Storage
CDF	Cumulative Distribution Function
CEF	Carbon Emission Flow
CFPPs	Coal-Fired Power Plants
CPs	Charging Posts
CSIRO	Commonwealth Scientific and Industrial Research Organization
CtG	Coal-to-Gas
DDCs	Distributed Data Centers
DL	Deep Learning
DOD	Depth of discharge
ESSs	Energy Storage Systems
EVs	Electric Vehicles
FCSs	Fast Charging Stations
FIS	Fuzzy Inference System
GANs	Generative Adversarial Networks
GDLs	Geographically Dispatchable Loads
GEP	Generation Expansion Planning
GESSs	Gas Energy Storage Systems
GFPPs	Gas-Fired Power Plants

HRSG	Heat Recovery Steam Generator
IDCs	Internet Data Centers
LILs	Large Industrial Loads
LSTM	Long short-term memory
LSTM-A	LSTM and attention
MES	Multi-Energy System
MESSs	Mobile Energy Storage Systems
MFs	Membership Functions
P2G	Power-to-Gas
PLET	Peukert Lifetime Energy Throughput
PV	Photovoltaic
QoS	Quality of Service
SLBs	Second-Life Batteries
SOH	State of health
UETAM	User equilibrium-based traffic assignment model

List of Figures

List of Tables

Chapter 1 Introduction

1.1 Background and motivation

The escalating carbon dioxide emissions aggravate climate challenges and pose significant barriers to sustainable development, and net-zero emission targets are attracting unprecedented attention from scholars and politicians. Countries worldwide are committing to achieving carbon neutrality to curb carbon emissions. According to a December 2020 World Bank report [1], 127 countries, 823 cities, and 101 regions have pledged to decarbonize by mid-century. Wherein, the Australian government has released a long-term emissions reduction plan that is expected to deliver a 35% reduction by 2030 and net zero emissions by 2050 [2]. Germany is committed to achieving a fully decarbonized energy sector by 2035 [3][4]. Moreover, the United States and China have also announced intentions to achieve carbon neutrality before 2050 and 2060, respectively.

Among these key emission sectors, the power industry is the major emitter, accounting for about one-third of the overall emissions [5]. Its emissions are mainly from the combustion of fossil fuels in the process of power generation, especially coal-fired power generation [6]. In 2020, coal-fired power generation in the United States accounted for 20% of total power generation, and emissions accounted for 54% [7]. More than 60% of Australia's electricity came from coal-fired power plants (CFPPs) in 2021, and its emissions accounted for about an astonishing 90% [8].

Over the past few years, the method of system decarbonization on the supply side of the power grid, that is, the generation and transmission side, has been studied. The existing research on emission reduction is mainly focused on the retirement of aged coal-fired generators [9], the co-planning of gas networks [10], the expansion of transmission lines [11], and the installation of renewable stations and energy storage systems (ESS) [12]. Some literature points out that installing renewable energy combined with applying ESS is ideal for accomplishing net zero emissions in the power system. Due to problems such as intermittency and high investment costs, completing 100% renewable energy output for the current power system is still challenging [13-15]. Regarding power plant transformation, it can substantially curb the carbon footprint from the electricity production process and allow for a smoother system transition. From the workability perspective, the existing technical solutions for generator transformation include generator retirement, generation efficiency modification, carbon capture and storage (CCS), bioenergy co-combustion, and coal-to-gas (CtG) conversion. Among them, considering factors such as cost and emission reduction efficiency, generator decommissioning, CCS, and CtG conversion are the solutions that have more possibilities for large-scale implementation [16].

To achieve the goal of net-zero emissions across the power industry, exclusively considering supply-side emissions abatement is not comprehensive. Reference [17] has pointed out that based on the carbon flow tracking, it can be yielded that the electricity load is the virtually underlying driver of the emission, which means rather than "producers", the "consumers" need to be responsible for CO_2 emitted during the electricity production. Although there are few high-emission generators in the distribution system, numerous feeders and substations in the system connect to the upstream transmission network. Reducing the carbon intensity of the distribution system can also effectively facilitate the emission mitigation of the main grid [18-19]. In the distribution network, a large number of distributed energy resources, data centers, electric vehicles (EVs), and other highly flexible devices give more possibilities for system emission reduction planning [20-22]. Compared to the supply side, the emission reduction of the demand side is also worthwhile to investigate.

On the demand side, as one of the typical dispatchable flexible loads, EVs are gradually replacing internal combustion vehicles and becoming increasingly prevalent due to their low-emission advantages and good driving experience [23]. With the prevalence of EVs, how to effectively recycle and reuse a large number of retired on-board batteries has become an urgent problem. Efficient utilization of recyclable resources can significantly reduce system scope three emissions. Studies show that 11 million tons of retired batteries are expected to be produced globally by 2030 [24]. The remaining capacity of retired EV batteries still retains almost 80% of their original capacity, which means they have high secondary utilization values [25-27]. Although the Battery Energy Storage System (BESS) cost has declined in recent years, it still maintains a relatively high price. According to the latest report of the Australian Energy Market Operator (AEMO) in 2020, the wholesale cost of BESS composed of fresh batteries is approximately $300 [28]. Correspondingly, the price of the EV battery pack is cheaper. BloombergNEF's report shows that brand-new Lithium-ion battery pack prices have fallen to $137 in 2020 [29]. Compared with fresh batteries, secondary utilization of second-life batteries (SLBs) currently has evident cost advantages. SLBs usually refer to retired EV batteries that have been tested, sorted, and reassembled [30]. Under ideal circumstances, compared with fresh batteries, the shortcomings of SLBs include shorter service life, less rated capacity, and lower charge and discharge efficiency. In actual situations, SLBs may have more hidden troubles, so they are usually used in some application scenarios with lower power quality requirements, such as microgrids and auxiliary service markets [31]. The reasonable utilization of SLBs can significantly reduce the investment cost of the system, and the echelon utilization of SLBs can improve the overall energy efficiency of society and further reduce emissions.

In conclusion, the novel emission reduction paradigm presents new opportunities and challenges for the planning and operation of systems. Building upon the knowledge gained, this thesis aims to develop and apply innovative emission reduction methods, promoting emissions mitigation in system planning and operation processes from multiple dimensions and perspectives. Additionally, it investigates various indicator characteristics such as economic feasibility, sustainability, and reliability. In the following sections, 1.2 summarizes the contributions of this thesis, and section 1.3 presents its outline.

1.2 Contribution

This thesis builds the framework and innovations and aims to develop power system emission reduction methods to fill the research gaps mentioned above. The novel contributions of this Ph.D. thesis are:

A generation expansion planning (GEP) framework incorporating CtG conversion is proposed. The system could select the appropriate generator transformation strategy for the current system conditions by comparing generator retirement, CCS retrofit, and CtG conversion.

Developing a CtG conversion planning model for CFPPs, which could help the system reduce emissions at a lower cost. Meanwhile, plant utilization rates could be improved as the plant's fuel is switched from high-emitting coal to low-emitting natural gas.

A linear carbon target model to facilitate the system decarbonization transition is proposed. The exterior point method is deployed to relax the carbon target relevant constraint, embed the carbon target into the objective function as a penalty item, and adjust the implemental intensity of the carbon target by bringing in different penalty coefficients.

A novel Fuzzy Inference System (FIS) based method is introduced for selecting candidate locations to enhance optimization accuracy and improve the practical feasibility of the results. FIS primarily narrows the selection of candidate locations for Carbon Capture, Utilization, and Storage (CCUS) retrofit and power-to-gas (P2G) installation and computes the upper bound of dispatchable internet data centers (IDCs) and Large Industrial Loads (LILs).

A spatial-temporal carbon response method is proposed based on dispatchable loads incorporating data centers, large in dustrial factories, and mobile energy storage systems (MESSs). Compared to traditional temporal-scale carbon scheduling, this method can enhance the resource utilization rates of existing systems, including renewable energy and low-emission power generation. It can also restrain the output of coal-fired generators through demand-side load shifting, resulting in more significant reductions in system emissions.

Considering the carbon intensity change after the CCUS retrofit and during the MESS movement, the modified carbon emission flow (CEF) models based on CCUS and MESS are proposed, respectively, to improve the applicability of the traditional model. By cooperating with the modified CEF model and spatial-temporal carbon response method, the system carbon intensity can be adjusted at the temporal and spatial scales, further reducing emissions.

Developing an echelon utilization planning strategy for SLBs in the long-term process that can reduce the energy system costs effectively. Simultaneously, to ensure the power reliability of the system during the entire planning process, this thesis considers multiple life cycles to retire and replace the BESSs periodically.

A novel planning model that can help the system to select fresh and reuse BESS is proposed. Compared with the existing research, the system has more diverse and flexible choices for BESS. Moreover, it can more clearly show the impact of different types of BESS on the system and ensure that this investment strategy is optimal under the current system conditions.

The overall flexibility of the system planning results of different cases is considered by comparing the system adaptation cost. Analyze the impact of stochastic features caused by uncertainty prediction error on the planning robustness.

1.3 Outline of the Thesis

The decarbonization transition of the power system represents a complex systemic challenge that necessitates cooperation among various stakeholders to ensure a rapid, smooth, and cost-effective transformation process. Within the proposed framework, the decarbonization of the power system can be categorized into four key levels: supply, transmission network, demand side, and market design, which comprehensively includes the emission from scope 1 to scope 3. Among these, the transformation of power plants on the supply side, as the primary source of system emissions, plays a pivotal role in determining the overall success of the transition. The retirement of coal-fired power plants, coupled with the optimization of gas-electricity integration, can significantly enhance the utilization of alternative fuels such as natural gas and hydrogen. As an essential mechanism to drive the transformation, policy and market strategies, including carbon allowances, green certificate trading, and carbon taxes, can accelerate the phase-out of high-emission coal-fired generators. These strategies also incentivize greater engagement in demand-side carbon response initiatives. Facilitated by these market and policy incentives, demand-side carbon response becomes a critical component in achieving a net-zero power system. By flexibly dispatching loads such as electric vehicles, data centers, and mobile energy storage systems, the system can not only achieve further emission reductions but also enhance resource utilization efficiency. The coordination scenarios diagram involving various entities within the framework are shown as follows:

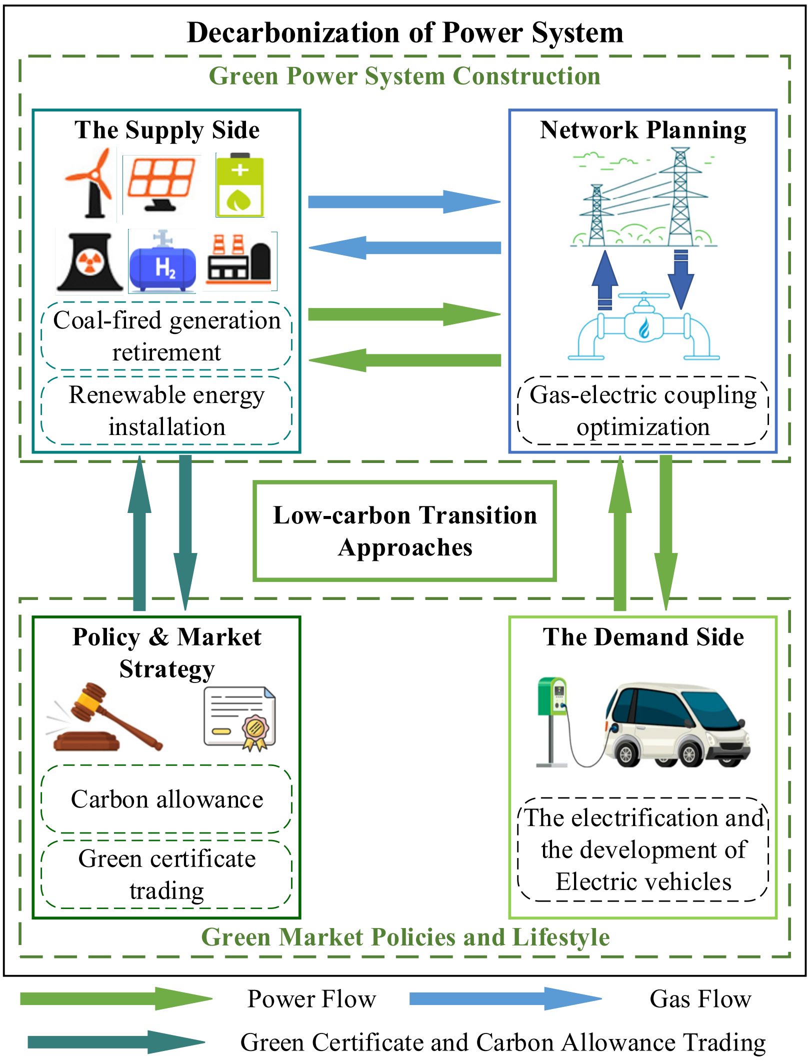

Figure 1-1 The overview of the proposed framework

The outlines of each following chapter are shown below:

Chapter 2 provides a systematic overview of the power system low-carbon transition. It outlines traditional pathways for decarbonizing CFPPs, including CCS retrofitting and generator retirement. Market and policy instruments such as carbon taxes and carbon allowance trading are introduced. Foundational models for system decarbonizing are listed. This chapter also reviews the topics related to system carbon management, such as traffic flow and battery energy storage systems.

Chapter 3 explores a novel low-carbon gasification conversion planning approach to facilitate a cost-effective transition of CFPPs. Moreover, a comprehensive two-stage GEP framework, including CtG conversion, generator retirement, and CCS retrofit, is introduced. In the first stage, a linear emission reduction target is also integrated as a penalty term in the objective function to maximize emission reduction while avoiding excessive emission reduction costs. Upon completing the first stage, the second stage evaluates the flexibility of these planning schemes by comparing adaptation costs, thereby ensuring a smoother transition.

Chapter 4 introduces a novel FIS-based two-stage integrated framework for system decarbonization that addresses emission mitigation from both perspectives. On the supply side, the framework considers the retrofitting of CFPPs with CCUS technologies, facilitating a substantial reduction in emissions. Additionally, the captured gas can be converted into natural gas using P2G equipment, further improving the utilization of CCUS. On the demand side, a modified carbon emission flow model based on CCUS is proposed to capture the impact of the demand side on carbon reduction. The typical dispatchable demand, including IDCs and LILs, can effectively reduce system emissions by responding to carbon intensity fluctuations without affecting production progress. Furthermore, considering some off-site factors that may exist in the actual construction and production process that affect planning and operation results, the FIS is implemented to model those factors that affect both emission reduction methods on the supply and demand side.

Chapter 5 proposes a distribution system planning method with a specific emission reduction target, in which the emission target is embedded in the objective function via the exterior point method rather than considered as a constraint. Simultaneously, a spatial-temporal carbon response model is proposed, which is based on geographically dispatchable loads (GDLs) incorporating distributed data centers (DDCs) and MESSs. This model can be extended to further mitigate system emissions without changing the current system framework.

Chapter 6 proposes a novel multi-stage system planning model including BESSs. BESS designed in this chapter involves not only the use of fresh batteries but also the echelon utilization of SLBs and considers the multiple lifespan cycles based on its State of Health (SOH). Moreover, the proposed planning strategy integrates the electricity and transportation networks in the first stage and evaluates the flexibility of the planning system by comparing the adaptation costs of each system in the second stage.

Finally, **Chapter 7** summarizes the main conclusions and discusses the direction of future works.

The structure and relationship between the main contents of this thesis are displayed in

Figure 1-2. As outlined above, the proposed system transition framework addresses emissions across Scope 1, Scope 2, and Scope 3. Specifically, the generation transformation planning discussed in Chapter 3 falls under the control strategies for Scope 1 emissions. Chapters 4 and 5 primarily focus on mitigation strategies for Scope 2 emissions. Furthermore, the echelon utilization of second-life batteries is categorized as a measure to reduce Scope 3 emissions.

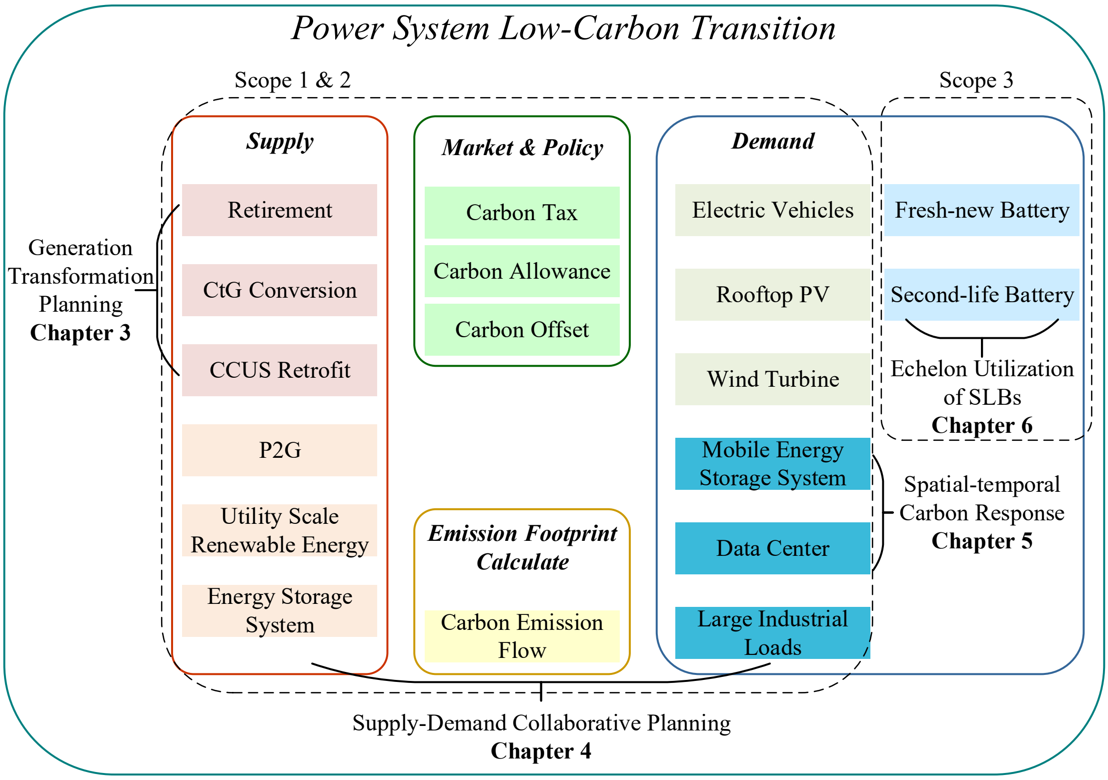

Figure 1-2 Mind map for the thesis outline

Chapter 2 Literature Review

As a major source of carbon emissions, the power system plays an indispensable role in carbon neutrality by decarbonization. To achieve the ambitious climate goals set by countries, the future low-carbon power system should be an integrated multi-energy system with renewable energy, including solar photovoltaic and wind power as the core, and supported by energy storage, natural gas power generation, and demand response [4]. Simultaneously, with the popularity of electric vehicles and the increasing coupling in electricity-gas networks, the low-carbon energy system will also support clean electrification for transportation, industry, and many other sectors so as to achieve comprehensive decarbonization of human society. However, the existing power grid has strict operating requirements. The increasing proportion of renewable energy generation and the retirement of coal-fired generators keep challenging the system stability and reliability. On the other hand, the classical control paradigm is being fundamentally reshaped by the future integrated multi-energy system, where multi-department and cross-industry collaborative operations will become the norm, thereby improving and ensuring the flexibility and reliability of the system. This chapter will categorize emission reduction methods according to the classifications, as Figure 2-1 shows, such as network level and the emission categories from scope 1 to scope 3. A systematic and comprehensive review of relevant existing literature and typical models will be conducted.

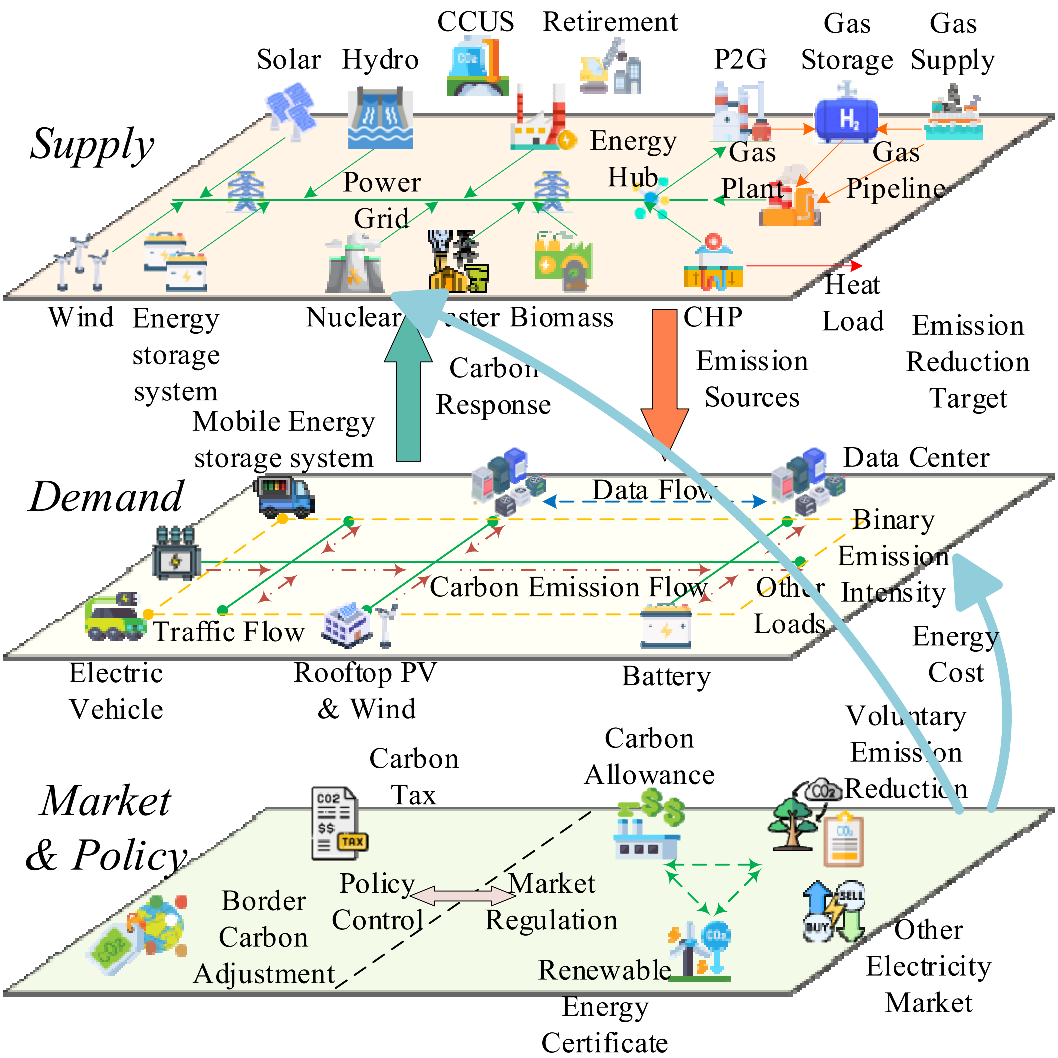

Figure 2-1 The low-carbon transition approaches of the power system

In detail, subchapter 2.1 primarily reviews relevant literature on low-carbon transformation strategies for the power generation and transmission sectors. This includes an overview of power generation transformation strategies (2.1.1), traditional CFPPs retirement methods (2.1.2), RES planning (2.1.3), and power-gas coupling planning (2.1.4). These approaches can all be considered strategies that utilize low-emission or zero-emission alternative fuels for power generation, aligning with Scope 1 emission reduction efforts. Subsection 2.2 focuses on reviewing various demand-side emission reduction strategies. These strategies, whether involving demand-side carbon response or power-transportation joint optimization, indirectly affect emissions and are classified as Scope 2 emission reduction methods. Additionally, Subsection 2.3 discusses existing emission reduction policies across different countries and reviews various low-carbon market trading models. Finally, Section 2.4 examines methods for battery echelon utilization as part of Scope 3 emission control strategies.

2.1 Generation and Transmission Expansion Planning

2.1.1 Generation Transformation Schemes

Since a substantial portion of emissions (referred to as Scope 1 emissions) originates from the generation process of CFPPs, existing research has extensively explored the planning challenges associated with CFPP retirement. Reference [32] proposes a CFPP retirement planning model that considers the generator's service age and takes the renewable energy prediction deviation into the planning process through the risk index. In [9], a concept about the optimal per unit cost of emission reduction is proposed, and the system planning includes retiring generators and installing gas energy storage systems. However, reference [9] also points out that the simultaneous retirement of numerous generators may lead to supply shortages due to load uncertainty and potentially challenging system stability and reliability. Other references remind problems such as insufficient system spinning reserves caused by CFPP decommissioning as well [33-34]. Careful planning and coordination regarding the timing and location of generator retirements are imperative. Conversely, CCUS represents another viable technical avenue toward achieving net-zero emissions, capable of mitigating system emissions while safeguarding system reliability.

As a technical approach that could probably execute net-zero emissions, CCS retrofit of CFPP has attracted attention from academia and industry. As of 2022, CCUS projects for industrial applications worldwide currently encompass 30 operational projects, with 11 under construction and 153 in various stages of development [35]. According to data from the Commonwealth Scientific and Industrial Research Organization (CSIRO) [36], Australia currently hosts 18 CCUS projects in different stages of advancement, comprising two test facilities. The planned projects are anticipated to sequester 20 million tons of CO_2 annually by 2035. In the literature, many researchers have studied CCUS retrofit and operation methods during the planning process. Reference [37] considers CCS during the planning and calculates the costs and revenue of CCS simultaneously. A planning model for the CCS retrofitting of traditional power plants is proposed in [38], and the model's effectiveness is verified through deterministic, stochastic, and robust optimization. However, research also denotes that there are still barriers to CCS retrofitting, including cost, technology, and social acceptability.

Reference [39] indicates that the CCS retrofit suitable generator should meet the following conditions, namely, the rated capacity is greater than 300MW, and the service age is less than 35 years. Reference [40] mentions that large-scale onshore CCS projects may not be expected to be developed in Germany in the short term due to poor social acceptability.

Compared with the above two solutions, CtG conversion of CFPP has the advantages of low investment cost and high environmental benefit. According to the actual case of TransAlta Corporation in Canada, the total cost of converting a 463MW CFPP to a gas-fired power plant (GFPP) fueled by natural gas is about 77M$, and emissions are reduced to about half of the original ones [41]. Such obvious advantages make it necessary to consider CtG conversion in the GEP framework to accelerate the process of system emission abatement. However, most of the existing papers involving CtG mainly focus on analyzing its economic and environmental benefits from the macro level [16] [40] [42].

2.1.2 Traditional model of CFPPs retirement

Aging coal-fired generators will affect the overall efficiency of the system due to increased maintenance cost, reduced generation, and emissions efficiency [43]. Meanwhile, coal-fired generators are still the main source of electric power supply in most countries, resulting in high carbon intensity. Hence, the gradual retirement of these generators is an essential pathway to achieve carbon neutrality in the power system. However, retiring a large number of generators at the same time could cause supply shortages due to load uncertainty [11]. The centralized decommissioning of coal-fired units in a region may adversely affect the reliability of the regional power grid. Therefore, the retirement time and location of the generators need to be carefully considered and coordinated. The specific mathematical equations for describing the retirement of generators can be expressed as follows:

$$Min\ C^{retire} = \begin{cases} \underbrace{(\kappa_i - \varepsilon_i) \cdot (\delta_{i,t}^{re} - \delta_{i,t-1}^{re})}_{demolition\ cost} \\ + \underbrace{C^{mt} \cdot \left(1 + \rho_t^{re}\right)^{t-1} \cdot \left(1 - \delta_{i,t}^{re}\right)}_{maintenance\ cost} \end{cases} \tag{2.1}$$

$$s.t.\ \delta_{i,t-1}^{re} \le \delta_{i,t}^{re} \tag{2.2}$$

$$0 \le P_{i,t}^{G} \le P_{rate}^{G} \cdot \left(1-\delta_{i,t}^{re}\right) \tag{2.3}$$

where κ_i denotes the equipment demolition cost at location i, and ε_i represents the salvage income obtained by selling the valuable components of equipment; $\delta_{i,t}^{re}$ and $\delta_{i,t-1}^{re}$ are binary decision variables that indicate whether the generator is retired at time t and $t-1$; C^{mt} is the maintenance cost of remaining equipment; ρ_t^{re} is the increasing rate of maintenance cost; $P_{i,t}^{G}$ and P_{rate}^{G} denote the generator's output at time t and rate output of unit.

The optimization of generator retirement usually has the following difficulties. First, how to avoid repeated retiring of the same generators; second, how to ensure that the retired generators are not reactivated; third, how to find a trade-off in minimizing costs and emissions by retiring generators. To solve the problem one and two, the method of combining the formula $(\delta_{i,t}^{re} - \delta_{i,t-1}^{re})$ and $\delta_{i,t-1}^{re} \le \delta_{i,t}^{re}$ is adopted in [32]. For question three, due to the high emission rate of coal-fired age-generators, retiring those generators could reduce system emissions but increase system investment and retirement costs. It is necessary to find appropriate methods to minimize both factors during the system decarbonization transition. In [32], system emissions and costs are simultaneously embedded into a multi-objective problem to solve the mentioned problem. In [9], by introducing a carbon tax, the carbon emissions are converted into carbon costs, so that the problem is transformed into single-objective optimization.

2.1.3 RES&ESS Planning and the typical models

To prevent supply shortages due to the retirement of aging generators, other types of new generators need to be installed. Among many candidates, wind energy and solar power dominate increasing generation proportions on a year-to-year basis due to their advantages of relatively mature technology and low cost. In the power system, due to a series of operating conditions such as transmission line capacity and regional climate conditions, the location and capacity of renewable energy are important factors that can determine whether the system can operate economically. In addition, due to the intermittency of renewable energy, the system usually needs to be equipped with a certain capacity of the energy storage system. Reference [44] proposes a hybrid shared energy storage framework integrating private storage and independent energy storage operators to address the challenge of sizing storage capacity amidst uncertain renewable energy outputs. According to [45], a coordinative planning framework is presented for decarbonizing urban multi-energy systems by integrating public transport electrification, renewable energy sources, and energy networks. The framework comprises three levels: investment decision models for RESs, ENs, and PTE at the upper level, a carbon emission-security assessment at the middle level, and a hybrid energy pricing mechanism at the lower level. In [21], an integrated methodology is presented for planning distribution systems toward low-carbon sustainability, incorporating renewable distributed generation and demand response enabled by real-time pricing. Reference [46] proposes a unified decision-making structure for partitioning power networks into interconnected areas to mitigate the risk of system collapse during natural disasters and cyber-attacks. It also addresses optimal operational planning to allocate renewable generation and energy storage systems within the partitions. In [47], a battery-based energy storage transportation method is proposed as a solution for managing transmission congestions in power systems with high Renewable Energy penetration. Reference [48] introduces a stochastic multi-period multi-objective transmission planning model to address uncertainty challenges from renewable energy generation and other sources.

The typical equations of PV, wind and ESS can be expressed as follows:

$$Min\ C^{rew} = C^W n_i^W + C^S \alpha_i^S + C^{ESS} E_{rate}^{ESS} \tag{2.4}$$

$$s.t.\ P^W\left(v_{i,t}^W\right) = \begin{cases} 0 & v_{i,t}^W < v_{in}^W, v_{i,t}^W > v_{out}^W \\ n_i^W \cdot P_{i,rate}^W \cdot \dfrac{v_{i,t}^W - v_{in}^W}{v_{rate}^W - v_{in}^W} & v_{in}^W < v_{i,t}^W < v_{rate}^W \\ n_i^W \cdot P_{i,rate}^W & v_{rate}^W < v_{i,t}^W < v_{out}^W \end{cases} \tag{2.5}$$

$$0 \le n_i^W \le n_i^{W,MAX} \tag{2.6}$$

$$P^S\left(H_{i,t}\right) = H_{i,t} \cdot \alpha_i^S \cdot \mu_i^S \tag{2.7}$$

$$0 \le \alpha_i^S \le \alpha_i^{S,MAX} \tag{2.8}$$

$$E_{i,t+1}^{ESS} = E_{i,t}^{ESS} + \left[P_{i,t}^{ESS,c} u^c - \left(P_{i,t}^{ESS,d} / u^d\right)\right]\Delta t \tag{2.9}$$

$$E_{rate}^{ESS} \cdot \underline{SoC} \le E_{i,t}^{ESS} \le E_{rate}^{ESS} \cdot \overline{SoC} \tag{2.10}$$

where C^{rew}, C^W, C^S, C^{ESS} are the capital cost of all devices, wind turbines, photovoltaic (PV) panels, and batteries; $v_{i,t}^W$ denotes the wind speed, and P^W is the output power of wind turbine; v_{in}^{W}, v_{rate}^{W}, v_{out}^{W} present the cut-in, rated, and cut-out wind speed, respectively; $P_{i,rate}^{W}$ is the rated power; n_i^W and $n_i^{W,MAX}$, α_i^S and $\alpha_i^{S,MAX}$ are the number and maximum quantities of wind turbines, and the area and maximum area of the solar power equipment; P^S represents the solar output power; $H_{i,t}$ and μ_i^S are the solar radiation and the conversion efficiency of PV panels; E_{rate}^{ESS}, $E_{i,t}^{ESS}$, $P_{i,t}^{ESS,c}$ and $P_{i,t}^{ESS,d}$ represent the rate stored energy, stored energy, charging power and discharging power of energy storage system; u^c and u^d are the charge and discharge efficiency; Δt is the time interval; $\underline{SoC}$ and $\overline{SoC}$ denote the minimum and maximum state-of-charge. Eq. (5)-(8) represent the output power constraints of wind energy and solar power, respectively. Eq. (9)-(10) is the mathematical models of energy storage system. Considering that regions have different natural conditions such as solar exposure, temperatures, and wind speed, the site selection of renewable energy will tremendously affect the output of devices. Therefore, installation in a reasonable location by using decision variables n_i^W and α_i^S can maximize the utilization efficiency of the equipment. Meantime, due to the different loads in various locations, reasonable capacity planning will not cause a waste of investment costs.

In the planning process, the uncertainty in renewable energy outputs makes decision-making even more challenging. Uncertainties in wind and solar mainly come from wind speed and solar irradiation intensity. In some literature dealing with renewable energy, the methods of dealing with uncertainty prediction usually include probability distribution and machine learning [32] [49]. Moreover, due to the participation of the energy storage system, excess electricity can be sold at a suitable time. Aiming at the problem of the power trading benefits loss caused by the large difference between the electricity price of time-of-use and feed-in-tariff, [50] proposed a bilateral auction mechanism called the average pricing market mechanism.

2.1.4 Power-Gas coupling Planning and the typical models

In terms of transmission expansion planning, compared with the traditional single-energy network, the multi-energy system (MES) has obvious emission reduction potential in covering the complete energy supply chain from the energy source to the end-user [51]. MES integrates multiple networks including electricity, heat, gas, cooling, and transport, and can effectively combine emission reduction approaches for the generation and consumer side. Considering coal-fired generators are gradually retired in the process of system decarbonization, the application of alternative energy sources is a cost-effective approach that can effectively supplement energy supply gaps and play a key role in maintaining system reliability. Natural gas has become one of the most attractive alternative fuels for traditional power generation due to its low emissions and relatively mature technology [52]. Reference [53] proposes a coordinated planning strategy for integrating electricity networks with hydrogen refueling and production stations for fuel cell electric vehicles. The system includes hydrogen refueling stations, production stations, storage, and delivery networks, utilizing both gas pipeline and truck logistics delivery. In [54], a two-stage credit-based sharing model is introduced for energy sharing between a coordinator managing an energy storage system and prosumers. Both capacity and energy sharing are integrated, considering electricity and hydrogen. Reference [55] proposes an integrated energy-sharing model encompassing hydrogen and electricity, where aggregators, including P2G and plug-in hybrid electric and hydrogen vehicles aggregators, serve as coupling points between the electricity and gas networks. The schematic diagram of the gas-electric coupling network is shown in Figure 2-2.

The classic gas flow equations and utility function as shown below:

$$Max\ f(P_i^{gas}) = a_i + b_i P_i^{gas} + c_i \left(P_i^{gas}\right)^2 \tag{2.11}$$

$$s.t.\ S_{ij}^{gas} = \operatorname{sgn}\left(\rho_i, \rho_j\right) \cdot \phi_{ij} \cdot \sqrt{\left|\rho_i^2 - \rho_j^2\right|} \tag{2.12}$$

$$\operatorname{sgn}\left(\rho_i, \rho_j\right) = \begin{cases} 1 & \rho_i \geq \rho_j \\ -1 & \rho_i \leq \rho_j \end{cases} \tag{2.13}$$

$$P_i^{gas,s} + \sum S_{ij}^{gas} = \sum S_{ji}^{gas} + P_i^{gas} \tag{2.14}$$

where P_i^{gas} is gas demand at bus i; a_i, b_i and c_i are price coefficients; S_{ij}^{gas} denotes the gas flow rate between $i-j$; sgn is gas flow direction index; ρ_i, ρ_j are nodal gas pressures; ϕ_{ij} presents the flow constant; $P_i^{gas,s}$ is gas supply at bus i.

In the integrated energy system, synthetic natural gas can be used in industries such as chemical and transportation, stimulating the decarbonization potential of other industries. However, the introduction of the gas network turns the optimization problem into mixed-integer nonlinear programming, which greatly increases the difficulty of solving. To improve computational efficiency, reference [52] introduced two linearization methods to deal with the nonlinear properties in the two systems, namely piecewise linear approximation, and first-order Taylor series approximation. Moreover, the gas-electric coupling system can increase the benefits of carbon emission reduction, which was confirmed in [56]. With the continuous maturity of technology and appropriate policy support, the integrated energy network with P2G technology can become a key approach to energy transition and climate change mitigation.

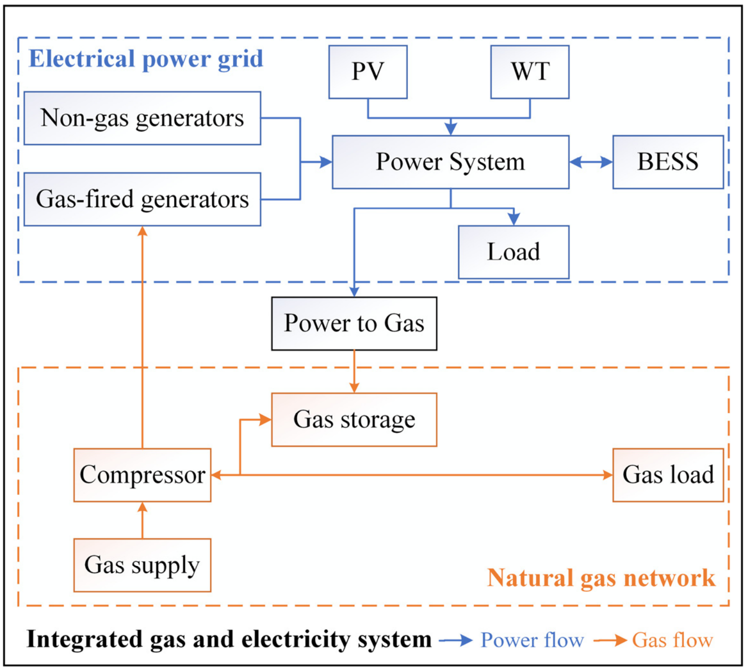

Figure 2-2 The paradigm of gas-electric integrated energy system.

2.2 Carbon-Oriented Flexible System Operation for Demand Side

2.2.1 Demand Side Carbon Response Schemes

As emission reduction on the power generation and transmission side has been in-depth studied, more studies in the literature have pointed out that the demand side also needs to respond to emission reduction actively in recent years. This method of reducing overall emissions through demand-side response represents a typical strategy for controlling Scope 2 emissions. Reference [17] proposes a CEF model, thus specifying the corresponding emissions on the consumer side. Reference [57] mentions a method to calculate the buses marginal carbon intensity, that is, the change in the overall system emission caused by the change of unit demand on that bus. References [19], [58-50] proposed methods to enable the demand side to actively participate in emission reduction based on real-time nodal carbon intensity. Among them, a carbon-aware distribution locational marginal pricing is proposed in [19], and demands can be real-time dispatched according to carbon-oriented price signals. In [58], an electricity-transportation collaborative planning model is proposed, where the second stage minimizes the associated emissions of electric vehicle charging stations according to the nodal carbon intensity. Reference [59] allocates carbon allowances to the demand side and promotes the overall system emission reduction through the carbon allowance trading between the demands. In [60], an emission scheduling method is proposed, which dispatches the power of mobile battery systems and distributed data centers based on emission intensity in real time.

With the calculation based on dynamic node carbon intensity, demand-side resources are no longer passively accepting corresponding emission responsibilities; instead, they can actively promote emissions reduction by flexibly adjusting usage patterns. To enhance the utilization of whole system resources and accelerate the achievement of industry-wide emissions reduction targets, there are the following major challenges that need to be addressed: (1) How to ensure that the planning methods can target the emission reduction; How to obtain a trade-off solution between emission reduction targets and system economic benefits? (2) How to proactively deploy the existing system resources to maximize the effectiveness of equipment for cutting emissions?

For the first challenge, conventionally, the regular methods of controlling emissions in the system planning process are carbon taxes and carbon allowances. Ref [61] proposes a planning strategy considering the echelon utilization of second-life batteries, and the carbon tax has been exploited to control system emissions. The authors in [62] establish a blockchain application in electricity and carbon allowance trading in microgrids and model the trading and benefit distribution by means of the cooperative game.

In addition to the aforementioned cost-based system emissions control scheme, formulating the emission targets as constraints in the optimization models is also a typical approach for emission control planning research. Ref [63] formulates a two-level system expansion planning considering emission constraints and allocates the total emission cap to different systems through the CEF model. Ref [64] presents a capacity expansion planning model embedded with unit commitment and maintenance constraints and incorporates emission targets into the constraints to satisfy the emission limits.

For the second challenge, most existing studies focus on the demand-side carbon response at the temporal scale. For example, renewable energy sources and ESS can be planned in a cooperative way to optimize distribution system operation and decline system emissions [61]. However, the ESS may be underutilized since it is installed at a fixed location and can only locally dispatch with the temporal scale [65]. As an alternative, MESSs can not only be dispatched at the temporal scale but also at the spatial scale, which can markedly improve system benefits and flexibility.

In the distribution system, besides MESS, other types of GDLs are DDCs, electric vehicles, etc. To date, only a few studies have mentioned the GDLs' function of spatial-temporal carbon response. Ref [19] proposes a peer-to-peer joint power and carbon trading model that combines CEF. The peer-to-peer trading causes the load to have a spatial transfer-like effect. Ref [58] achieves carbon intensity transfer in a two-stage planning model by optimizing the minimum carbon emissions of electric and fuel cell vehicle charging stations.

Furthermore, the current emission reduction technologies may have unsatisfactory economic benefits or emission reduction effects due to off-site factors during actual planning and operation. Before optimization, utilizing fuzzy inference systems (FIS) to model these expectable off-site factors is crucial. FIS is a computational framework well-suited for modeling uncertain and imprecise details that cannot be adequately expressed in traditional mathematical models. FIS enables the simultaneous handling of multiple off-site variables as inputs and generates interpretability outputs, facilitating a broader decision-making process. In [66], FIS-based control is used to regulate power flow in hybrid systems comprising electric vehicles and wind turbines. Reference [67] utilizes fuzzy inference-based control to manage the state-of-charge of superconducting magnetic energy storage in wind power systems. In [68], FIS is applied to pre-evaluate candidate construction sites for the secondary battery site selection problem, thereby enhancing accuracy in optimization during planning and reducing solution time.

2.2.2 Transportation-Electrification Coupling Optimization

On the demand side, industry, transportation, and construction account for the vast majority of energy consumption. In terms of transportation, the transport sector produces about a quarter of the EU's total greenhouse gas emissions [69]. Therefore, electric vehicles replacing traditional fuel vehicles is one of the approaches to accelerate the realization of the low-carbon transition. The popularity of electric vehicles has also made possible the co-optimization of traffic flow and the power system. Reference [70] proposes an adaptive fast charging station strategy to address the challenges brought by the increasing charging demand of electric vehicles to future smart grids. In [71], a novel carbon-oriented expansion planning model is proposed for integrated electricity and natural gas systems with electric vehicle fast-charging stations to create a low-carbon charging infrastructure. Furthermore, a coordination planning method is introduced in [72] for integrated energy systems incorporating charging stations for electric buses with battery swapping technology, aiming to reduce carbon emissions. According to [73], a market-based mechanism is proposed for EV charger planning, aiming to achieve a competitive strategy in future smart cities. Using Sydney as a case study, it introduces a predict-then-optimized framework employing a multi-relation graph convolutional network for EV charging demand prediction and a Cournot competition game model for resource allocation. Reference [74] introduces a comprehensive model for urban electrified transportation network expansion planning, simultaneously optimizing investment strategies for transportation networks and power distribution networks. Reference [75] presents a multidisciplinary approach to jointly plan plug-in electric vehicle charging stations and distributed photovoltaic power plants on a coupled transportation and power network. In [76], an analytical method is presented to study the optimal topology and maximum capacity of existing distribution networks for accommodating electric vehicle charging demands. The calculation of traffic flow has different expressions in many papers, the user equilibrium-based traffic assignment model is one of the common methods [77].

$$Min\ J^t = \sum_{r \in \Omega^R} \int_0^{x_r} t_r(\omega) d\omega \tag{2.15}$$

$$s.t. \sum_{a \in \Omega_{se}^a} f_a^{se} = q^{se} \tag{2.16}$$

$$f_a^{se} \geq 0 \tag{2.17}$$

$$x_r = \sum_{a \in \Omega_{se}^a} \left(f_a^{se} \cdot \delta_{a,r}^{se} \right) \tag{2.18}$$

where $t_r(\omega)$ is the road impedance function; Ω^R denotes the set of road section; x_r is the traffic flow on rth road section; f_a^{se} and q^{se} are the traffic flow of ath path of OD section and traffic demand from s to e; Ω_{se}^a represents the set of the link of the OD section from s to e; $\delta_{a,r}^{se}$ is rth road is on ath path of OD section from s to e.

After the result of the traffic flow is calculated, it can be coupled with the power system through the following method:

$$Min\ E^{FCS} = \sum_{i\in\Omega^{bus}} \sum_{t\in T} P_{i,t}^{FCS} \cdot e_{i,t}^{FCS} \tag{2.19}$$

$$P_{i,t}^{FCS} = C \cdot \beta \cdot \frac{f_{i,t}^{trip}}{\sum_{t\in T} f_{i,t}^{trip}} \cdot \frac{f_{i,t}}{\sum_{i\in\Omega^{bus}} f_{i,t}} R_{i,t}^{FCS} \tag{2.20}$$

$$f_i = \sum_{r\in\Omega^R} (x_r \cdot u_{i,r}) \tag{2.21}$$

Where E^{FCS} is the total emission of fast charging stations (FCSs); $P_{i,t}^{FCS}$, $e_{i,t}^{FCS}$ are the charging power and nodal carbon intensity of FCS; C, β, $f_{i,t}^{trip}$ denote the total charging demand, the choosing ratio, and the travel ratio of FCS, respectively; $f_{i,t}$ indicates the traffic flow captured by FCS; $u_{i,r}$ is whether the FCS is connected to the road. The effect of traffic flow participation in emission reduction has been verified in [58].

The difficulty in the comprehensive optimization of the power system and the transportation system is that the charging and discharging of electric vehicles will further increase the uncertainty of the power load. The behavior of electric vehicle charging is extremely flexible, and traditional methods of dealing with uncertainty based on probability distributions may no longer be applicable. In [61], an approach based on Generative Adversarial Networks (GANs) was adopted to construct a set of scenarios according to historical data. Moreover, the planning of the two systems is often not synchronized. In [77], the multi-objective collaborative planning method (MCPM) is adopted to simultaneously solve these two planning problems. At present, references have shown that the simultaneous planning of two networks can effectively improve efficiency and reduce costs.

2.3 Carbon Market and policy

Excepting the emission reduction methods on the power generation side and demand side, on the market side, the low-carbon mechanism is needed to promote the spontaneous optimal allocation of resources by enterprises. The core concept of the carbon pricing mechanism is that each entity needs to pay a corresponding fee for emitting a certain amount of carbon dioxide. Its purpose is to improve the efficiency of resource utilization, increase investment in clean energy, and encourage the development and sales of low-carbon products and services. According to the latest report of the World Bank in 2021, as of May 2021, a total of 64 carbon pricing mechanisms have been implemented in the world, covering 21.4% of total global greenhouse gas emissions [1]. These mechanisms combine administrative methods and market forces and will serve as the internal driving force to continuously promote the process of low-carbon transition of the power system. The classic formulas for carbon tax and carbon allowance trading are as follows:

$$Min\ C^{tax} = \left(\sum_{t} \sum_{i} P_{i,t}^{G} \cdot e_{i,t}^{G} \cdot \Delta t \right) \cdot p^{tax} \tag{2.22}$$

$$Min\ C^{cap} = \sum_{i} \left(\sum_{t} P_{i,t}^{G} \cdot e_{i,t}^{G} \cdot \Delta t - Cap_i \right) \cdot p_i^{cap} \tag{2.23}$$

where $e_{i,t}^{G}$ is the carbon intensity of generators; Cap_i denotes the emission cap; p^{tax} and p_i^{cap} are carbon tax and carbon allowance trading price.

Carbon tax, as a price-oriented emission reduction policy tool, has been widely implemented in many countries around the world. Among countries that have already imposed carbon taxes, tax rates vary widely, ranging from less than \$1/ton CO_2 emission (tCO_2e) to as high as \$137/tCO_2e [1]. The advantage of the carbon tax is that it is easy to implement, does not need to design complex market products and trading rules, and has low management and operating costs. However, carbon tax suffers from less flexibility in price changes, and uncertainty about the effect of emission reduction due to the size of the enterprise.

Carbon allowance trading, as a market exchangeable product, has the natural attributes of finance, which can expand the scope of market participation and attract more participation from banks, funds, and enterprises. Compared with the carbon tax, carbon allowance trading can more effectively improve the efficiency of resource allocation, and the market price changes are relatively flexible. The disadvantage of carbon allowance trading mainly comes from the high regulatory cost and possible moral hazard.

The impact of carbon taxes and carbon allowance on emission reductions has been well studied. According to the data in [78], due to the high carbon tax rate, Sweden's total carbon dioxide emissions fell by 13% during the period 1990-2008. In terms of carbon allowance, [79] modeled 35 industrial sectors in China. As the overall scale of carbon allowance trading increased from 1.48 billion tons to 1.83 billion tons, its contribution to emission reduction also increased from 58.68% to 62.09%. Furthermore, in some literature, market-relevant topics also include the electricity and carbon coupling markets, carbon-oriented electricity balancing markets, and market clearing mechanisms for a high proportion of renewable energy. Reference [80] proposes a decentralized transactive solution for local energy markets leveraging direct peer-to-peer trading, aiming to increase prosumer participation and ensure a reliable energy supply. According to [81] a spot market framework is introduced for managing the coordination problem between renewable energy sources and flexible resources in a scenario where renewable energy penetration approaches 100%. In [82], the Nash Equilibrium Point is investigated in a joint Peer-to-Peer electricity market and carbon emission auction market among prosumer microgrids in the distribution network. Reference [83] proposes a blockchain-enabled distributed market framework for bi-level carbon and energy trading between coal mine integrated energy systems and a virtual power plant with network constraints. Moreover, a novel carbon-oriented balancing market model is introduced in [84] to align with environmental targets in both day-ahead and real-time balancing markets. The dual-stage market aims to minimize economic and environmental costs, resulting in increased balancing service costs but a larger drop in carbon costs, ultimately reducing total costs and incentivizing decarbonized energy resources in scheduling and balancing actions. Reference [85] analyzes and quantifies the multi-elasticity of multi-energy demands in integrated electricity and gas markets, aiming for market efficiency improvement and demand cost reduction.

2.4 Echelon Utilization of BESS

In addition to the above-mentioned emission reduction strategies addressing Scope 1 and Scope 2 emissions, Scope 3 emissions in the power system must also be considered to achieve a comprehensive and effective net-zero carbon transformation. Among these, battery recycling is expected to be a key factor influencing future Scope 3 emissions in the system. Among various ESSs, BESS possess advantages such as short response times and high charge-discharge efficiency. However, constrained by their lifespan, the rated capacity and efficiency of BESS will decline after a certain number of operating cycles. The echelon cascading utilization of BESS can maximize the efficiency of system resource utilization and, to some extent, reduce Scope 3 emissions, thereby facilitating the smooth attainment of emission reduction goals. In the literature, the planning and operation models of BESS have been well studied. The application scenarios of BESS usually include peak load shaving [86], mitigation of renewable energy fluctuations [87], energy management [88], and frequency regulation [89], etc. In [90], a two-stage stochastic optimization planning model was proposed, which involved solar PV, BESS, and microturbine. Reference [91] discussed the optimal allocation of BESS in the distribution system to adjust the bus voltage and reduce energy costs. In [92], the optimal size planning of the BESS in the fast-charging station considering the resilience of EV load was proposed. The result shows that the resilience does not have a great impact on the BESS size during the initial installation, but it cannot be ignored in the later size adjustment. In these papers, the operation and location of BESS were optimized. However, the impact of changes in battery lifespan on system operations and costs had not been discussed in detail.

The battery lifespan mainly depends on the operation and control strategy during daily usage. Depth of discharge (DOD) and frequency are generally considered to be the main factors affecting the degradation of BESS [93]. In the existing research, the battery life cycle model has been applied to scenarios such as energy dispatch [94], and frequency regulation [95]. Reference [96] analyzed the economic feasibility of applying retired EV batteries to power grid auxiliary services. In [97], the market potential of SLBs based on grid energy storage applications was explored. For the relationship between battery's life and its operation, several papers [98]-[101] discussed the cycle lives of the battery at different DOD, in [98] studied the optimal bidding strategy for battery storage in the electricity market and discussed the cycle life model of the battery. The battery's capacity reduction from its cycle was calculated in [99]. Reference [100] applied a battery life model to better manage BESS in the microgrid. In [102], consider employing a virtual energy hub to combine PV generation with BESS, and apply it to an electric transportation system that includes a battery-powered bus charging station and an EV parking lot.

During the system planning process, the evaluation of BESS economy is also a considerable issue. In the market environment, the common approach for BESS to gain profits is to buy or store energy during off-peak hours and sell energy during peak times. According to [103], arbitrage of BESS mainly depends on its energy storage and generation capacity rather than violating the market prices. In [104], the economics of different energy storage technologies were studied, and the results showed that BESS has a high probability of obtaining positive NPV values. This means that BESS is economically feasible. At the same time, the study also pointed out that the impact of charge and discharge efficiency on the economy of BESS may even be greater than its cost.

For the echelon utilization of BESS, Reference [30] proposed an operational framework that combined centralized charging stations, PV, and SLBs, which made full use of the remaining value of SLBs. In [105], the whole-life cycle planning of BESS was discussed, which served the power grid frequency regulation auxiliary service market and energy arbitrage market in the first and second lifespan of BESS, respectively.

2.5 Chapter Summary

This chapter presents a detailed literature review, encompassing generation and transmission expansion planning, carbon-oriented flexible system operation, carbon markets and policies, as well as echelon utilization of BESS. The various planning and operation methods discussed in the literature contribute to a deeper understanding of low-carbon transition strategies and modeling methods for power systems. Moreover, through the comparison of literature in this chapter, the shortcomings of existing research are clearly identified, laying the groundwork for research proposals in subsequent chapters.

Chapter 3 Generation Transformation Planning Considering Coal-to-Gas Conversion

This chapter proposes a novel two-stage GEP framework that simultaneously includes three technical solutions: generator retirement, CCS retrofit, and CtG conversion. Wherein the impact of different generator transformation schemes on the planning results is considered in the first stage, and the flexibility of each planning result is analyzed in the second stage. The proposed model is rigorously tested on the IEEE benchmark system, providing insightful analysis of the impact of different CFPP transformation schemes on system cost and emissions.

3.1 Proposed Two-Stage Generation Transformation Planning Framework

To completely decarbonize the power system, it is necessary to invest in large amounts of renewable energy and ESS and retrofit existing power plants. A reasonable power plant transformation scheme can quickly drop system emissions in a short period, making system decarbonization smoother. As shown in Figure 3-1, within the proposed framework, the transformation of power plants includes three approaches: generator retirement, CCS retrofit, and CtG conversion.

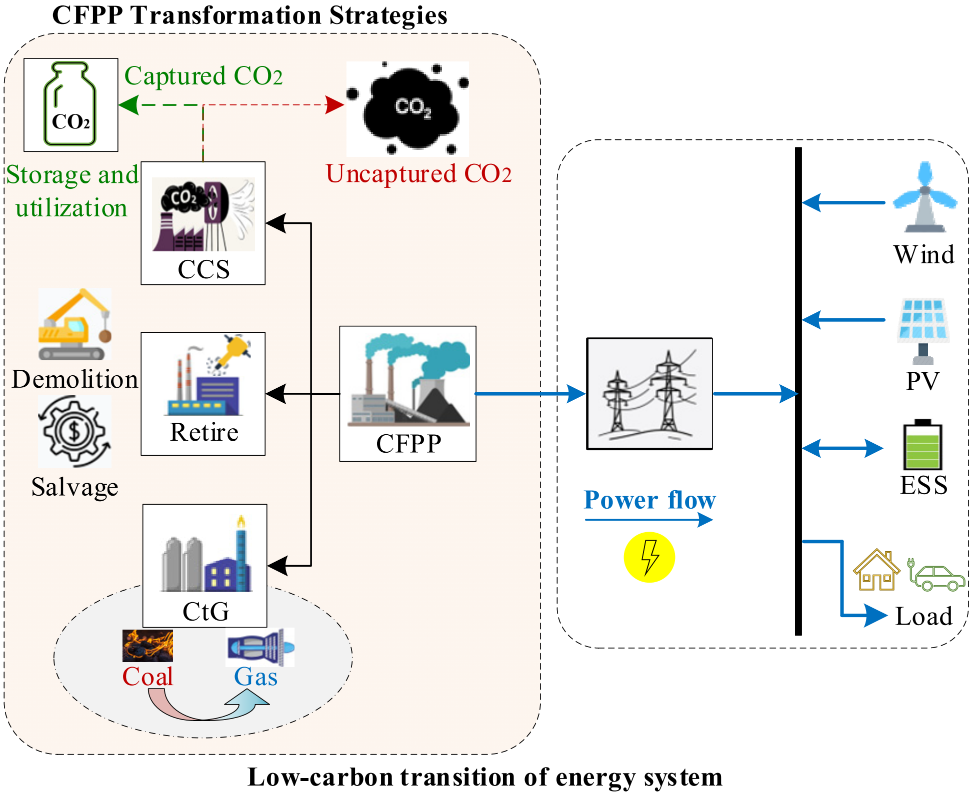

Figure 3-1 CFPP transformation approaches and system operation architecture.

Retirement is a relatively direct way to emission reduction transition for some aging CFPPs with low generation efficiency. The retiring process usually involves dismantling devices and selling reusable items. CCS retrofit can fully exploit the existing system generation capacity and capture most emissions generation [71]. The captured CO_2 is usually stored and reused, and the uncaptured CO_2 is released into the atmosphere. CtG conversion takes advantage of gas-fired power generation producing fewer emissions and transforms generators from coal-fired to gas-fired. In this chapter, the choice of generator transformation method is mainly based on its economic and environmental benefits, and the specific system framework is shown in Figure 3-2.

In the first stage, it is necessary to employ a deep learning-based uncertainty prediction model (LSTM-A, the combination of long short-term memory and attention) to predict uncertain factors involving load and renewable energy. Subsequently, system operation variables can be obtained during the planning process, including whether CFPP is retired, CCS retrofitted, or CtG converted. At this stage, an emission mitigation target is embedded into the objective function using the exterior point method to motivate the system emission reduction.

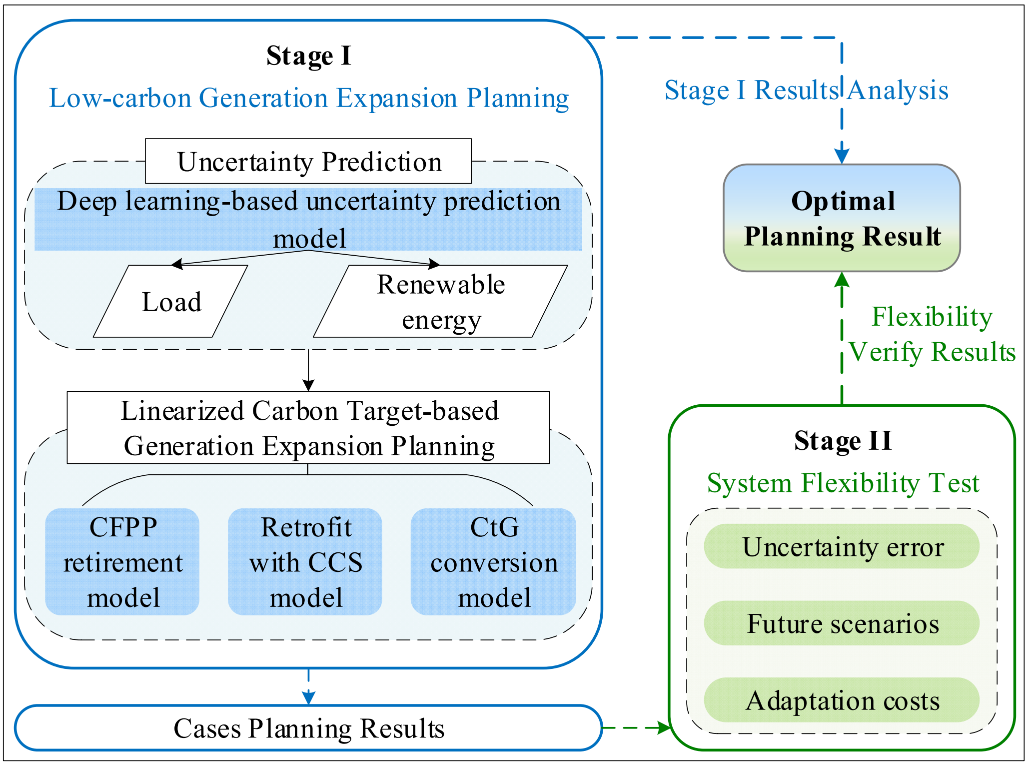

Figure 3-2 The Proposed two-stage system framework

In the second stage, the system generates multiple sets of future scenarios based on uncertainty errors. The systemic flexibility of the previous stage planning results is tested by comparing the adaptation costs. Finally, through the comprehensive comparison of the results of the first stage and the second stage, the optimal GEP result is obtained.

3.2 Mathematical Modeling

A. The CtG conversion of CFPP

The CtG conversion of CFPP is not simply replacing the generator fuel from coal to natural gas but requires the modification of existing equipment, such as coal-fired boilers. Existing modification methods can generally be divided into in-series coupled systems and parallel coupled systems modernization [106]. The CtG conversion in this chapter defaults to adopt the modification method of the parallel coupled system, considering its cost and efficiency advantages [107]. The schematic of the generator output after CtG conversion is shown below.

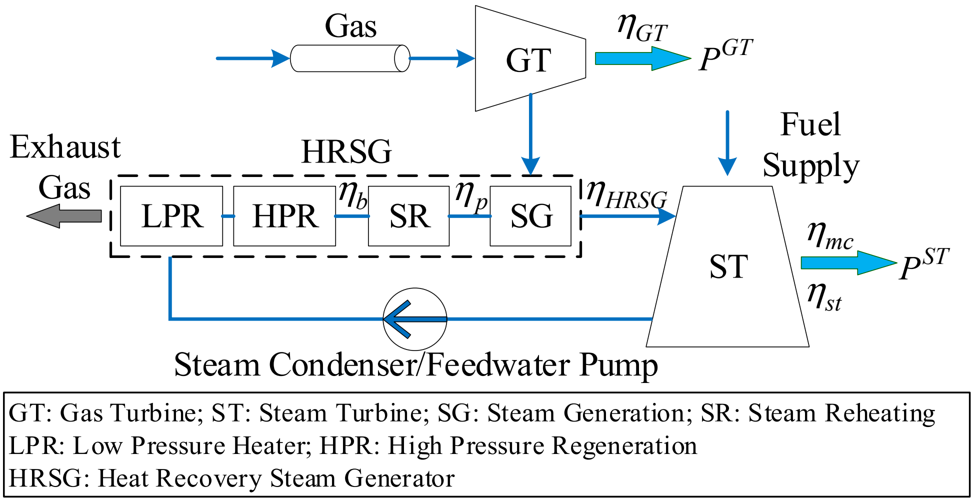

Figure 3-3 The schematic of the gas-steam combined cycle in the parallel system

In the parallel system, the heat recovery steam generator (HRSG) replaces the coal-fired boiler [107]. The overall generator output is composed of gas turbine power output $P_{i,t,y}^{GT}$ and steam turbine power output $P_{i,t,y}^{ST}$, the model of which is shown as follows:

$$P_{i,t,y}^{GT} = q_p \cdot E_{ch,t}^{coal} \cdot \eta_{GT} \tag{3.1}$$

$$P_{i,t,y}^{ST} = E_{ch,t}^{coal} \cdot \left[q_p (1-\eta_{GT}) \eta_{HRSG} + \eta_b \right] \cdot \eta_p \cdot \eta_{st} \cdot \eta_{mc} \tag{3.2}$$

where $E_{ch,t}^{coal}$ represents the chemical energy of coal combustion in boilers of repowered power plant; q_p is the share of the chemical energy of the gas of the parallel system in the chemical energy of the coal combustion in the modified power plant $q_p \in (0,1.4)$ [107]; η_{GT}, η_{HRSG}, and η_b are the gross efficiency of the gas turbine, HRSG, and boiler, respectively; η_p and η_{st} denote the energy efficiency of the collector system and steam turbine, the collector system feeds steam into the turbine; η_{mc} is the electromechanical efficiency of the turbogenerator.

Since the power balance in the whole system is attracting more attention than the efficiency transfer within the generator during the planning process, equations (3.1) and (3.2) are transformed into the following constraints:

$$P_{i,t,y}^{GT} \le \xi^{GT} \cdot \overline{P_i^{CtG}} \cdot \Theta_{i,y}^{cv} \tag{3.3}$$

$$P_{i,t,y}^{ST} \le \xi^{ST} \cdot \overline{P_i^{CtG}} \cdot \Theta_{i,y}^{cv} \tag{3.4}$$

$$P_{i,t,y}^{CtG} = P_{i,t,y}^{GT} + P_{i,t,y}^{ST} \tag{3.5}$$

$$E_{i,t,y}^{CtG} = e_{i,y}^{C} \cdot P_{i,t,y}^{C} \cdot \left(1 - \Theta_{i,y}^{cv}\right) + e_{i,y}^{G} \cdot P_{i,t,y}^{CtG} \cdot \Theta_{i,y}^{cv} \tag{3.6}$$

$$\Theta_{i,y-1}^{cv} \leq \Theta_{i,y}^{cv} \tag{3.7}$$

$$C^{cv} = \varpi_{i,y}^{cv} \cdot \left(\Theta_{i,y}^{cv} - \Theta_{i,y-1}^{cv}\right) \cdot \overline{P_{i}^{CtG}} \tag{3.8}$$

where ξ^{GT} and ξ^{ST} are the total output efficiency of gas and steam turbine; $\Theta_{i,y}^{cv}$ represents the decision variable of CtG conversion; $\overline{(\cdot)}$ is the upper bound of that value. Based on equations (3.3) and (3.4), CFPP is modified into GFPP by CtG conversion with a power output of $P_{i,t,y}^{CtG}$. Moreover, the emission becomes $P_{i,t,y}^{CtG}$ multiplied by the emission intensity of gas generator $e_{i,y}^{G}$. $P_{i,t,y}^{C}$ denotes the coal-fired generator output and $e_{i,y}^{C}$ is its carbon intensity. $\varpi_{i,y}^{cv}$ is the cost coefficient of the CtG conversion investment cost C^{cv}.

B. Linear emission reduction target model

Due to the diminishing marginal benefits in the emission reduction-related investment costs, the complete realization of the emission reduction target may lead to an exponential increase in cost. Utilizing the exterior point method to embed the emission reduction target into the objective function could promote system emission reduction while keeping the system cost within an acceptable range. The model is as follows:

$$\sum_{i \in \Omega^{G,bus}} \sum_{t \in \Omega^{T}} \sum_{y \in \Omega^{Y}} \left(E_{i,t,y}^{N} + E_{i,t,y}^{CtG}\right) \leq e^{target} \tag{3.9}$$

$$f(e) = \sum_{i \in \Omega^{G,bus}} \sum_{t \in \Omega^{T}} \sum_{y \in \Omega^{Y}} \left(E_{i,t,y}^{N} + E_{i,t,y}^{CtG}\right) - e^{target} \leq 0 \tag{3.10}$$

$$\varepsilon_e = \left[\max\left\{0, f(e)\right\}\right]^2, \; emission\ penalty = \Pi_e \varepsilon_e \tag{3.11}$$

where e^{target} is the specific emission reduction target of this planning; $\Omega^{G,bus}$, Ω^{T}, and Ω^{Y} are the set of generator location buses, time, and year, respectively. Equation (3.10) expresses the constraint in terms of a function $f(e)$. Equation (3.11) is the quadratic form of the barrier function [108], that is, when $f(e)$ is less than 0, it is 0, and when $f(e)$ is greater than 0, $\varepsilon_e = [f(e)]^2$. The system emission penalty is equal to ε_e times the penalty coefficient Π_e, and the penalty item will be manually removed when calculating the final total cost. For easier solving, the above equations can be converted in the following way.

$$0 \le \Im, f(e) \le \Im \tag{3.12}$$

$$\begin{cases} f(e) \ge \Im - \Pi\left(1-\Theta_1^f\right) \\ 0 \ge \Im - \Pi\left(1-\Theta_2^f\right) \\ \sum_{i=1,2} \Theta_i^f \le 1 \end{cases} \tag{3.13}$$

$$\varepsilon_e = \Im^2 \tag{3.14}$$

set the new auxiliary variable $\Im$, auxiliary decision variables Θ_1^f and Θ_2^f, and disjunctive factor Π. Through equations (3.12) and (3.13), $\Im$ can only be equal to $f(e)$ or 0. Therefore, the barrier function ε_e is converted to $\Im^2$.

C. The retirement and CCS retrofit model of CFPP

1) The retirement model of CFPP

The retirement cost of CFPP is typically related to its dismantling and salvage costs. The specific model is formulated as follows:

$$C^{rt} = \left(\Theta_{i,y}^{rt} - \Theta_{i,y-1}^{rt}\right) \cdot \left[\mu_i^{rt} - \varsigma_i^{rt} \big/ \left(1+\Lambda_y^{rt,c}\right)\right] \cdot \overline{P_i^C} \tag{3.15}$$

$$E_{i,t,y}^C = e_{i,y}^C \cdot P_{i,t,y}^C \tag{3.16}$$

$$0 \le P_{i,t,y}^C \le \overline{P_i^C} \cdot \left(1-\Theta_{i,y}^{rt}\right) \tag{3.17}$$

$$\Theta_{i,y-1}^{rt} \le \Theta_{i,y}^{rt} \tag{3.18}$$

where C^{rt} denotes the retirement cost of CFPP; $\Theta_{i,y}^{rt}$ and $\Theta_{i,y-1}^{rt}$ are the decision variables that decides whether CFPP of bus i is retired or not at y and $y-1$ year; μ_i^{rt} and ς_i^{rt} are the uninstallation and salvage costs of CFPP, and the specific amount is related to the nameplate capacity $\overline{P_i^C}$; considering the residual value of salvageable components decreases yearly, $\Lambda_y^{rt,c}$ is the declining rate of salvage costs. The emission $E_{i,t,y}^C$ of CFPP at time t is equal to the coal-fired generator output multiplied by its carbon emission intensity. Equation (3.17) expresses that the ith CFPP can no longer generate electricity after deciding to retire. Equation (3.18) limits the repeated retiring of CFPP.

2) The CCS retrofit of CFPP

After the retrofit of CCS, the power output and emission are calculated as follows:

$$P_{i,t,y}^{N} = P_{i,t,y}^{C} - P_{i,t,y}^{CCS} \tag{3.19}$$

$$P_{i,t,y}^{CCS} = \lambda_i^{rf} \cdot E_{i,t,y}^{CCS} \tag{3.20}$$

$$E_{i,t,y}^{N} = E_{i,t,y}^{C} - E_{i,t,y}^{CCS} \tag{3.21}$$

$$0 \le E_{i,t,y}^{CCS} \le \psi_i^{ccs} \cdot e_{i,y}^{C} \cdot P_{i,t,y}^{C} \cdot \Theta_{i,y}^{rf} \tag{3.22}$$

$$\Theta_{i,y-1}^{rf} \le \Theta_{i,y}^{rf} \tag{3.23}$$

$$C^{rf} = \varpi_{i,y}^{rf} \cdot \left(\Theta_{i,y}^{rf} - \Theta_{i,y-1}^{rf}\right) \cdot \overline{P_i^{C}} \tag{3.24}$$

where $P_{i,t,y}^{N}$ represents the net power output after CCS retrofit; $P_{i,t,y}^{CCS}$ denotes the power consumption of CCS equipment. Its value equals to the captured emission $E_{i,t,y}^{CCS}$ multiplied by the power coefficient λ_i^{rf} [109]. Therefore, the net emission $E_{i,t,y}^{N}$ equals the difference between the original and captured emission. ψ_i^{ccs} indicates the capture rate, and $\Theta_{i,y}^{rf}$ is the decision variable to implement the CCS retrofit. Equation (3.23) expresses that the CCS retrofit of ith CFPP can only be executed once. Equation (3.24) shows the calculation process of the investment cost of CCS retrofit C^{rf}, where $\varpi_{i,y}^{rf}$ is the cost coefficient.

D. Deep learning-based uncertainty prediction model

Uncertain factors, including renewable energy and load, generally exhibit intense volatility, intermittence, and randomness. To improve the prediction accuracy, these data's nonlinear features and invariant structures should be considered comprehensively. Deep learning (DL) is a superior technique for achieving the above. As a variant of the recurrent neural network, the LSTM network exploits the gate-based mechanism to process data, effectively extracting data characteristics such as temporal features, formulated as follows:

$$i_d = Sigmoid\left(W_i\left[x_d \,||\, h_{d-1}\right] + b_i\right) \tag{3.25}$$

$$o_d = Sigmoid\left(W_o\left[x_d \,||\, h_{d-1}\right] + b_o\right) \tag{3.26}$$

$$f_d = Sigmoid\left(W_f\left[x_d \parallel h_{d-1}\right]+b_f\right) \tag{3.27}$$

$$c_d = f_d \odot c_{d-1} + i_d \odot \tanh\left(W_c\left[x_d \parallel h_{d-1}\right]+b_c\right) \tag{3.28}$$

$$h_d = o_d \odot \tanh\left(c_d\right) \tag{3.29}$$

where $x_d \in \mathbb{R}^n$ is the time series input containing n features on day d, and the LSTM cell state $c_d \in \mathbb{R}^m$ will be controlled by the input gate i, the output gate o, and the forget gate f [110]; i_d, o_d, f_d, $h_d \in \mathbb{R}^m$ are the input, output, forget gate state, and current target hidden state in LSTM, respectively; W_i, W_o, $W_f \in \mathbb{R}^{m\times 2n}$ denote learnable matrix parameters; b_i, b_o, b_f represent the bias vectors in the LSTM layer; the symbol $\parallel$ and $\odot$ are the concatenation operation and the element-wise Hadamard product operation, respectively. To avoid indiscriminate compression of all information and strengthen the intrinsic correlation of the extracted features, LSTM-Attention was proposed. The attention mechanism can give higher weight to valuable features of h_d [111], as follows:

$$F_{as}\left(h_d, h_{as}\right) = ReLU\left(h_{as}^T W_{as} h_d\right) \tag{3.30}$$

$$a_{as} = Sigmoid\left(F_{as}\left(h_d, h_{as}\right)\right) \tag{3.31}$$

$$h_d' = W_a\left[h_d \parallel a_d^T H_s\right] \tag{3.32}$$

where F_{as} is the attention score function to assess the relevance of h_d with each source hidden state $h_{as} \in \mathbb{R}^m$; $W_{as} \in \mathbb{R}^{m\times m}$ represents a learnable attention score mapping matrix; $ReLU(\cdot)$ is the activation function to enhance the feature differences and concentrate weight distribution; $a_{as} \in \mathbb{R}$ denotes the attention weight, and $a_d = [a_{d-D+1}, \cdots, a_d] \in \mathbb{R}^D$ is the attention weight vector which includes attention weight for all source hidden state vectors; $H_s \in \mathbb{R}^{D\times m}$ is the source hidden state vectors; $W_a \in \mathbb{R}^{m\times 2m}$ indicates the learnable attention matrix, and h_d' is the output of the attention layer.

The above equation can process the time series of load and renewable energy under the LSTM-A learning architecture. Furthermore, weather information such as temperature is essential to load and renewable energy forecasting. By giving a meteorological input $y_d \in \mathbb{R}^k$ with k features, the fully connected layer is employed to extract latent information.

$$y_d{}' = \vartheta(\mathrm{W}y_d + b_v) \tag{3.33}$$

$$F_L(Z, \widehat{Z}) = \min \left\| Z - \widehat{Z} \right\|_l \tag{3.34}$$

where $y_d{}' \in \mathbb{R}^l$ is the features mapped; $W \in \mathbb{R}^{l\times k}$ is the learnable parameters; b_v is the bias vector; $\vartheta(\cdot)$ is the activation function used. After that, a fusion layer is employed to concatenate $h_d{}'$ and $y_d{}'$ for combining the features from time series and meteorological data. Several stacked fully connected layers can be further used for feature extraction and prediction. The equation (3.34) is used to train the DL model, wherein Z, $\hat{Z}$ represent the true and predicted values for all training samples. The norm-l can be 1 or 2 for the mean-absolute-error (MAE) or mean-square-error (MSE) training criterion. Finally, the prediction model is formulated as follows:

$$\widehat{Z}_{d+1} = \aleph\left(X_d, \widehat{Y}_{d+1}\right) \tag{3.35}$$

where $\hat{Z}_{d+1}$ denotes the predicted value; X_d is the available time series data; $\hat{Y}_{d+1} \in \mathbb{R}^L$ is the meteorological data which contains L relevant meteorological conditions; $\aleph(\cdot)$ represents the well-trained DL model. The trained model will be used for a one-year prediction, and the scenario probability distribution based on the one-year prediction result will be calculated for subsequent planning.

3.3 Two-Stage Generation Expansion Planning Model

A. Stage I: Linear carbon target-based generator transformation planning

The optimization of the first stage is to select the optimal CFPP transformation planning scheme. Embedding the aforementioned equations (3.1) - (3.24), the objective function of stage I consists of five parts: investment cost C^{Inv}, operation cost C^O, maintenance cost C^M, emission cost C^E, and linear carbon target penalty $\Im$.

$$Min\ C = \left\{ \frac{C^{Inv}}{(1+\Lambda)^{Y-1}} + \sum_{y=1}^{Y} \frac{C^O + C^M + C^E}{(1+\Lambda)^{y-1}} + \Pi_e \Im^2 \right\} \tag{3.36}$$

where C is the system total cost; Λ and Y denote the discount rate and total planning period; Π_e is the penalty coefficient. It should be noted that the emission penalty item $\Pi_e \Im^2$ needs to be removed when calculating the actual total cost after the planning is completed.

The investment costs are divided into the following parts: CFPP retiring costs, CCS retrofit costs, CtG conversion costs, and investment costs for renewable energy, ESS, and transmission lines.

$$
\begin{aligned}
&C^{Inv} = C^{rt} + C^{rf} + C^{cv} + C^{re} + C^{ESS} + C^{TL} \\
&= \left\{ \begin{aligned}
&\sum_{i \in \Omega^{G,bus}} \left[\begin{aligned}
&\left(\Theta_{i,y}^{rt} - \Theta_{i,y-1}^{rt}\right)\left[\mu_i^{rt} - \varsigma_i^{rt} / \left(1 + \Lambda_y^{rt,c}\right)\right]\overline{P_i^C} \\
&+\varpi_{i,y}^{rf}\left(\Theta_{i,y}^{rf} - \Theta_{i,y-1}^{rf}\right)\overline{P_i^C} \\
&+\varpi_{i,y}^{cv}\left(\Theta_{i,y}^{cv} - \Theta_{i,y-1}^{cv}\right)\overline{P_i^{CtG}}
\end{aligned} \right] \\
&+\sum_{r \in \Omega^R} \sum_{i \in \Omega^{re,bus}} \left(\varpi_{r,i,y}^{re} \cdot \Theta_{r,i,y}^{re} \cdot \overline{P_{r,i}^{re}}\right) \\
&+\sum_{i \in \Omega^{ESS,bus}} \left(\varpi_{i,y}^{ESS} \cdot \Theta_{i,y}^{ESS} \cdot \overline{E_i^{ESS}}\right) \\
&+\sum_{n \in \Omega^{TL}} \sum_{i,j \in \Omega^{bus}} \varpi_{n,ij,y}^{TL} \cdot \Theta_{n,ij,y}^{TL} \cdot L_{n,ij}^{TL}
\end{aligned} \right\}
\end{aligned} \tag{3.37}
$$

Where $\Theta_{r,i,y}^{re}$, $\Theta_{i,y}^{ESS}$, $\Theta_{n,ij,y}^{TL}$ are the decision variables of renewable energy, ESS, and transmission lines, and $\varpi_{r,i,y}^{re}$, $\varpi_{i,y}^{ESS}$, $\varpi_{n,ij,y}^{TL}$ are the cost coefficient of those facilities; r and Ω^R represent the types and sets of renewable energy sources including solar and wind; $i \in \Omega^{(\cdot,bus)}$ indicates the set of buses where various types of devices locate; $L_{n,ij}^{TL}$ is the length of the line $i-j$; n and Ω^{TL} are the number and quantity set of lines.

The operating cost of the system is mainly composed of the operating cost of CFPP $C^{o,C}$, the CCS operating cost $C^{o,CCS}$, and the operating cost of GFPP $C^{o,CtG}$.

$$
\begin{aligned}
&C^O = C^{o,C} + C^{o,CCS} + C^{o,CtG} \\
&= \sum_{s \in \Omega^S} \left\{ \begin{aligned}
&\delta_s \times \\
&\sum_{i \in \Omega^{G,bus}} \sum_{t \in \Omega^T} \left[\begin{aligned}
&a_i\left(P_{i,t,y}^C\right)^2 + b_i P_{i,t,y}^C + c_i \\
&+\left(\varpi_i^{c\&s} \cdot E_{i,t,y}^{CCS}\right) \\
&+\alpha_i\left(P_{i,t,y}^{CtG}\right)^2 + \beta_i P_{i,t,y}^{CtG} + \gamma_i
\end{aligned} \right]
\end{aligned} \right\}
\end{aligned} \tag{3.38}
$$

where a_i, b_i, c_i are the cost coefficient of CFPP; $\varpi_i^{c\&s}$ is the cost coefficient of CCS including capture, transportation, and storage; α_i, β_i, γ_i represent the generation cost coefficient of GFPP; δ_s is the probability that sth scenario appears in the scenario set Ω^S.

Maintenance costs are similar to investment costs, depending on whether the equipment is installed or retired.

$$
\begin{aligned}
C^{M} &= C^{mt,Gen} + C^{mt,re} + C^{mt,ESS} \\
&= \left\{
\begin{array}{l}
\sum\limits_{i\in\Omega^{G,bus}} \left[
\begin{array}{l}
\varpi_{i,y}^{mt,C}\left(1-\Theta_{i,y}^{rt}\right)\left(1+\Lambda_{y}^{mt,C}\right)\overline{P_{i}^{C}} \\
+\varpi_{i,y}^{mt,CCS}\Theta_{i,y}^{rf}\left(1+\Lambda_{y}^{mt,CCS}\right)\overline{P_{i}^{CCS}} \\
+\varpi_{i,y}^{mt,CtG}\Theta_{i,y}^{cv}\left(1+\Lambda_{y}^{mt,CtG}\right)\overline{P_{i}^{CtG}}
\end{array}
\right] \\
+\sum\limits_{r\in\Omega^{R}}\sum\limits_{i\in\Omega^{re,bus}}\left(\varpi_{r,i,y}^{mt,re}\cdot\Theta_{r,i,y}^{re}\cdot\overline{P_{r,i}^{re}}\right) \\
+\sum\limits_{i\in\Omega^{ESS,bus}}\left(\varpi_{i,y}^{mt,ESS}\cdot\Theta_{i,y}^{ESS}\cdot\overline{P_{i}^{ESS}}\right)
\end{array}
\right\}
\end{aligned}
\tag{3.39}
$$

where $C^{mt,Gen}$, $C^{mt,re}$, $C^{mt,ESS}$ are the maintenance costs of the power plant, renewable energy, and ESS, respectively; $\varpi_{i,y}^{mt,C}$, $\varpi_{i,y}^{mt,CCS}$, $\varpi_{i,y}^{mt,CtG}$, $\varpi_{r,i,y}^{mt,re}$, and $\varpi_{i,y}^{mt,ESS}$ indicate the maintenance cost coefficients of the corresponding equipment; $\Lambda_{y}^{mt,C}$, $\Lambda_{y}^{mt,CCS}$, $\Lambda_{y}^{mt,CtG}$ denote the annual growth rate of maintenance costs.

When calculating the emission cost, if CFPP chooses to fulfill the CCS retrofit, the total emission should be minus the captured part. After CtG conversion, the emission of CFPP will be converted into the emission of GFPP.

$$
C^{E} = \sum_{s\in\Omega^{S}} \left\{
\begin{array}{l}
\delta_{s}\times \\
\sum\limits_{t\in T}\sum\limits_{i\in\Omega^{G,bus}}\left[
\begin{array}{l}
e_{i,y}^{C}\cdot P_{i,t,y}^{C} - P_{i,t,y}^{CCS}/\lambda_{i}^{rf} \\
+e_{i,y}^{G}\cdot P_{i,t,y}^{CtG}
\end{array}
\right]\cdot\varpi_{i,t,y}^{car}
\end{array}
\right\}
\tag{3.40}
$$

where $\varpi_{i,t,y}^{car}$ represents the carbon price.

To ensure the security system operation while obtaining the optimal transformation planning, the system constraints are as follows:

$$
\left\{
\begin{array}{l}
S_{ij,t,y} + P_{i,t,y}^{C} - P_{i,t,y}^{CCS} + P_{i,t,y}^{CtG} \\
+\sum\limits_{r\in\Omega^{R}} P_{r,i,t,y}^{re} + P_{i,t,y}^{ESS,dis} - P_{i,t,y}^{ESS,ch}
\end{array}
\right\} = \Gamma_{i,t,y}^{P}\left(1+\Lambda_{y}^{p}\right)
\tag{3.41}
$$

$$
S_{ij,t,y}^{ex} - B_{ij}\left(\theta_{i,t,y}-\theta_{j,t,y}\right) = 0
\tag{3.42}
$$

$$
S_{n,ij,t,y}^{ca} - B_{n,ij}^{ca}\left(\theta_{n,i,t,y}^{ca}-\theta_{n,j,t,y}^{ca}\right) \le \left(1-\Theta_{n,ij,y}^{TL}\right)\Pi_{TL}
\tag{3.43}
$$

$$\left|S_{ij,t,y}\right| \le \overline{S^{ex}_{ij,t,y}} + \sum_{n\in\Omega^{TL}} \overline{S^{ca}_{n,ij,t,y}} \cdot \Theta^{TL}_{n,ij,y} \tag{3.44}$$

$$E^{ESS}_{i,t+1,y} = \begin{Bmatrix} E^{ESS}_{i,t,y} + \left(P^{ESS,ch}_{i,t,y} \cdot \varphi^{ch}_i\right) \cdot \Delta t \\ -\left(P^{ESS,dis}_{i,t,y} \big/ \varphi^{dis}_i\right) \cdot \Delta t \end{Bmatrix} \tag{3.45}$$

$$0 \le E^{ESS}_{i,t,y} \le \overline{E^{ESS}_{i,t,y}} \cdot \Theta^{ESS}_{i,y} \tag{3.46}$$

$$\begin{cases} 0 \le P^{ESS,ch}_{i,t,y} \le \overline{P^{ESS,ch}_{i,t,y}} \cdot \Theta^{ch}_{i,t,y} \\ 0 \le P^{ESS,dis}_{i,t,y} \le \overline{P^{ESS,dis}_{i,t,y}} \cdot \Theta^{dis}_{i,t,y} \\ \Theta^{ch}_{i,t,y} + \Theta^{dis}_{i,t,y} \le 1 \end{cases} \tag{3.47}$$

$$P^{re}_{r,i,t,y} = g^{re}_{r,i,t,y} \cdot \Theta^{re}_{r,i,y} \tag{3.48}$$

$$0 \le P^{CCS}_{i,t,y} \le \lambda^{rf}_i \cdot \psi^{ccs}_i \cdot e^C_i \cdot \overline{P^C_i} \cdot \Theta^{rf}_{i,y} \tag{3.49}$$

$$0 \le P^C_{i,y} \le \overline{\left(P^C_i\right)} \cdot \left(1 - \Theta^{cv}_{i,y}\right) \tag{3.50}$$

$$0 \le P^{CtG}_{i,t,y} \le \left(\xi^{GT} + \xi^{ST}\right) \cdot \overline{P^{CtG}_i} \cdot \Theta^{cv}_{i,y} \tag{3.51}$$

$$\Theta^{rt}_{i,y} + \Theta^{cv}_{i,y} + \Theta^{rf}_{i,y} \le 1 \tag{3.52}$$

$$\begin{cases} 0 \le \Theta^{re}_{r,i,y} \le \overline{\Theta^{re}_{r,i,y}} \\ 0 \le \Theta^{ESS}_{i,y} \le \overline{\Theta^{ESS}_{i,y}} \\ 0 \le \Theta^{TL}_{n,ij,y} \le \overline{\Theta^{TL}_{n,ij,y}} \end{cases} \tag{3.53}$$

where $S_{ij,t,y}$ is the power flow on line $i-j$; $P^{re}_{r,i,t,y}$ indicates the renewable energy power output; $P^{ESS,dis}_{i,t,y}$ and $P^{ESS,ch}_{i,t,y}$ are discharge and charge power of ESS; $\Gamma^{P}_{i,t,y}$ is the load on bus i; Λ^{p}_{y} is the load annual growth rate; $S^{ex}_{ij,t,y}$, $S^{ca}_{n,ij,t,y}$, B_{ij}, $B^{ca}_{n,ij}$, $\theta_{i,t,y}$, $\theta^{ca}_{n,i,t,y}$ represent the power flow, line susceptance, and voltage phase angle of existing and candidate lines, respectively; Π_{TL} is an enormous auxiliary parameter. Equation (3.44) means the overall power flow limitation of line $i-j$. $E^{ESS}_{i,t,y}$, $P^{ESS,ch}_{i,t,y}$, $P^{ESS,dis}_{i,t,y}$ are the stored energy, charge power, and discharge power of ESS; φ^{ch}_i and φ^{dis}_i denote the charge and discharge efficiency; Δt is the time interval between time t and $t+1$. $\Theta^{ch}_{i,t,y}$ and $\Theta^{dis}_{i,t,y}$ are decision variables limiting that ESS cannot be charged and discharged simultaneously. In (3.48), $g_{r,i,t,y}^{re}$ represents the output function of different types of renewable energy. Equations (3.49) to (3.52) are additional constraints on CFPP transformation. Where equation (3.49) gives an upper bound on the power consumption of CCS. Equation (3.50) indicates that when CFPP chooses CtG conversion, the former power output must be 0. Equation (3.51) defines the upper limit of GFPP output. Equation (3.52) limits CFPP can only choose one transformation method. Finally, Equation (3.53) is about the upper limit of the quantities of renewable energy, ESS, and transmission lines. Other constraints about CFPP transformation and linear carbon targets are mentioned above, which is:

(3.3)-(3.7), (3.10)-(3.14), (3.17)-(3.23)

B. Stage II: The flexibility test of planned network

During planning implementation, the deviation of uncertain prediction may force the adjustment of planning schemes, resulting in an exorbitant cost for the system [61]. Therefore, it is necessary to test the system's flexibility by comparing the adaptation cost before determining the planning scheme. The system flexibility evaluation algorithm is as follows:

Algorithm 1 System Flexibility Evaluation

for $w = 1{:}W$

Initialization: Parameters ($\Theta_{i,y}^{rt}$, $\Theta_{i,y}^{rf}$, $\Theta_{i,y}^{cv}$, $\Theta_{r,i,y}^{re}$, $\Theta_{i,y}^{ESS}$, $\Theta_{n,ij,y}^{TL}$);

Variables under wth Uncertain prediction deviation scenario ($\Theta_{n,ij,y}^{TL,w}$, $\Gamma_{i,t,y}^{lc,w}$)

if *in* wth scenario, are the system security constraints satisfied?

$Adaptation\ Cost\ (w) = 0$

$w = w + 1$

else

$Adaptation\ Cost\ (w) = C_2$

$w = w + 1$

end

Firstly, the first stage planning results will be regarded as parameters during the planning process of stage II. Then, generate W random scenarios with uncertain prediction errors. When the first stage planning result can satisfy the operational security constraints in the wth scenario, the adaptation cost is 0. If the security constraints cannot be satisfied, the system needs to be re-expanded, and calculates the adaptation cost. The re-expanded model is calculated as follows:

$$Min\ C_2 = \left\{ \begin{array}{l} \dfrac{\sum\limits_{n\in\Omega^{TL}} \sum\limits_{i,j\in\Omega^{bus}} \varpi_{n,ij,y}^{TL} \cdot \Theta_{n,ij,y}^{TL} \cdot L_{n,ij}^{TL}}{(1+\Lambda)^{Y-1}} \\ + \sum\limits_{i\in\Omega^{bus}} \sum\limits_{t\in\Omega^{T}} \sum\limits_{y\in\Omega^{Y}} \dfrac{\Pi_{ct} \cdot \Gamma_{i,t,y}^{lc}}{(1+\Lambda)^{y-1}} \end{array} \right\} \quad (3.54)$$

where C_2 is the system re-expanded cost which involves two parts, the transmission line re-expanded cost and load curtailment cost; $\Gamma_{i,t,y}^{lc}$ denotes the power of load curtailment under w th scenario; Π_{ct} indicates the penalty coefficient of load curtailment. The constraints of system operation are:

$$\left\{ \begin{array}{l} S_{ij,t,y} + P_{i,t,y}^{C} - P_{i,t,y}^{CCS} + P_{i,t,y}^{CtG} \\ + \sum\limits_{r\in\Omega^{R}} P_{r,i,t,y}^{re} + P_{i,t,y}^{ESS,dis} - P_{i,t,y}^{ESS,ch} \end{array} \right\} = \Gamma_{i,t,y}^{P} - \Gamma_{i,t,y}^{lc} \quad (3.55)$$

(3.3)-(3.7), (3.17)-(3.23), (3.42)-(3.51)

In this chapter, all equations are satisfied $\forall i,j \in \Omega^{bus}, \forall n \in \Omega^{TL}, \forall r \in \Omega^{R}, \forall t \in \Omega^{T}, \forall y \in \Omega^{Y}, \forall s \in \Omega^{S}, \forall w \in \Omega^{W}$.

3.4 Chapter Case Study

A. Test System and Parameters Settings

In the proposed optimization problem, the generation expansion planning considering CtG conversion in stage I is mix-integer quadratic programming. The system flexibility verification in stage II is mix-integer linear programming. The two-stage optimization simulations are conducted using MATLAB® on a laptop with a 3.3 GHz AMD Ryzen 9 5900HX CPU and 16GB RAM. The planning models are programmed on the Gurobi solver within the YALMIP toolbox. The formulation and training process of DL models are performed on the NVIDIA GeForce RTX 3070Ti GPU by Python. The proposed two-stage model is simulated on the modified IEEE 24-bus transmission network, and the total planning time is about ten years. The basic parameters of the network are quoted from [9]. To verify the effectiveness of the proposed CFPP transformation strategy, the following cases are designed:

Case1: CFPPs can only be retired during the GEP process

Case2: CFPPs can be retired, and CCS retrofitted during the GEP process

Case3: CFPPs can be retired, CCS retrofitted, and CtG converted during the GEP process

Case4.1: based on case3, GEP considers only emission cost without linear carbon target

Case4.2: based on case3, GEP considers only emission constraints without linear carbon target

Among cases 1-3, Case 3 will be utilized as a base case to compare CFPP's choice when it has multiple transformation strategies. Case 1 and Case 2 are comparative cases to verify the effectiveness of the proposed models and method from cost and emissions. Compared with CtG conversion, both retirement and CCS retrofit may lead to a substantial increase in investment costs, and emission reduction efficiency also needs to be verified. Moreover, Case 4.1 and Case 4.2 are established to validate the proposed linear emission reduction target. Among them, Case 4.1 removes the part about the emission target in the objective function. Case 4.2 additionally considers equation (3.19)-(3.24) in the constraint part. After the simulation of the first stage, stage II will evaluate the system flexibility of Cases 1 to 3. The main parameters of the simulation are shown in Table 3-1.

TABLE 3-1 MAIN PARAMETERS OF SYSTEM

Parameter	Value	Parameter	Value
μ_i^{rt}	0.16 (M$/MW)	ψ_i^{ccs}	0.8
ς_i^{rt}	16000 ($/MW)	e_i^C	0.895 (tCO_2/MWh)
$\varpi_{i,y}^{rf}$	3 (M$/MW)	e_i^G	0.427 (tCO_2/MWh)
$\varpi_{i,y}^{cv}$	0.346 (M$/MW)	ξ^{GT}, ξ^{ST}	0.588
e_y^{target}	25000000 (ton)	$\varpi_i^{c\&s}$	19.4 ($/MWh)

Regarding the CtG conversion cost $\varpi_{i,y}^{cv}$, this chapter mainly refers to the cost in the realistic case [41] and the reference [107] and takes the average value. Considering the influence of the cost setting of CtG conversion on the planning scheme, this chapter tests its price sensitivity in the follow-up experiments. Furthermore, the relevant costs and parameters of CCS retrofit mainly refer to [112-113], and the retirement-related costs refer to [32]. The maintenance cost is set as 2% of the investment cost in this experiment. During the training process of the DL model, the load data comes from the actual electric load of the California Independent System Operator (CAISO) [114], and the meteorological data comes from the Australian Bureau of Meteorology [115].

B. Numerical Analysis of simulation results

In the simulation test system, 8 CFPPs are located on different buses, which are bus 1, 7, 10, 14, 18, 22, 23, and 24. In various cases, CFPP can choose retirement, CCS retrofit, and CtG conversion as its transformation strategies. To ensure that the system maintains sufficient generation capacity after CFPP retires, eight candidate buses are set up to install ESS and renewable energy including solar and wind farms. The system topology diagram and planning results of each case are shown in Figure 3-4.

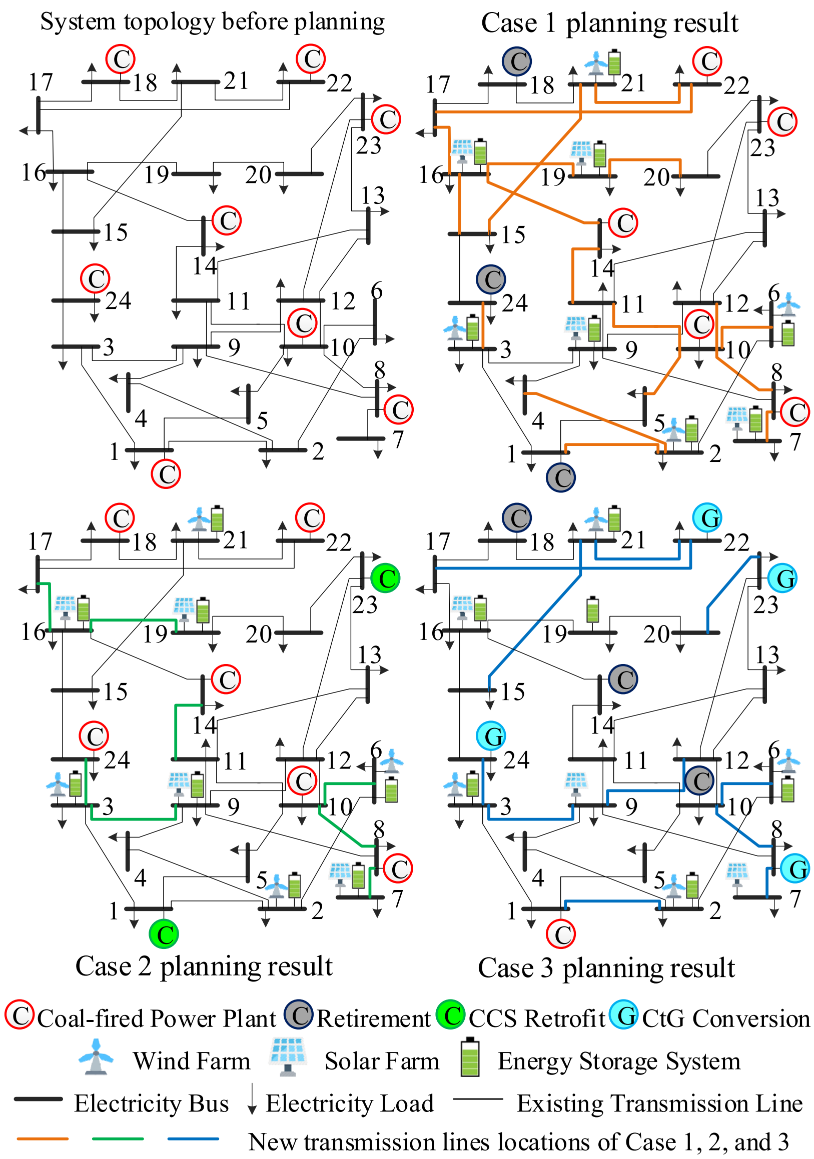

Figure 3-4 System topology and planning results for each case

It can be seen from the figure that the CFPPs in Cases 1, 2 and 3 have chosen different transformation technologies. This demonstrates that the proposed model can effectively choose between multiple techniques. To achieve the emission reduction target to the greatest extent, three CFPPs in Case 1 choose to retire. All CFPPs in Case 2 remain operational, but two opted for CCS retrofit. In Case 3, 4 CFPPs are modified to GFPPs by CtG conversion. Three of them decided to retire, and only one CFPP remained unchanged. Moreover, it can be seen that all three cases choose to install renewable energy and ESS as a supplement power supply to the system, and the specific installed capacity is shown in Table 3-2.

TABLE 3-2 STAGE 1 RESULTS OF DIFFERENT CASES

Item	Case 1	Case 2	Case 3
The penalty coefficient Π_e($)	4600	4600	4600
Solar (MW)	2040	2040	1428
Wind (MW)	1800	1800	1797
ESS (MWh)	2611	3516	845
Transmission Lines (unit)	31	13	19

According to the results in Table 3-2, under the same penalty coefficient, the installed capacity of solar, wind, and ESS in Case 3 is smaller than that of Case 1 and Case 2. The number of new-constructed transmission lines in Case 3 is slightly higher than that of Case 2 and much lower than that of Case 1. Regarding the installed capacity of renewable energy and ESS, Case 2 and Case 1 are basically the same, and Case 2 is slightly higher than Case 1. The reason for this result is CFPPs have high emission coefficients. The system tries to avoid emission target penalties and balance the demand and supply. However, in Case 3, since the emission coefficient of GFPP is vastly lower than that of CFPP, the need for renewable energy equipment is smaller than that of Cases 1 and 2. The system power output corresponding to the current planning results is shown in Figure 3-5.

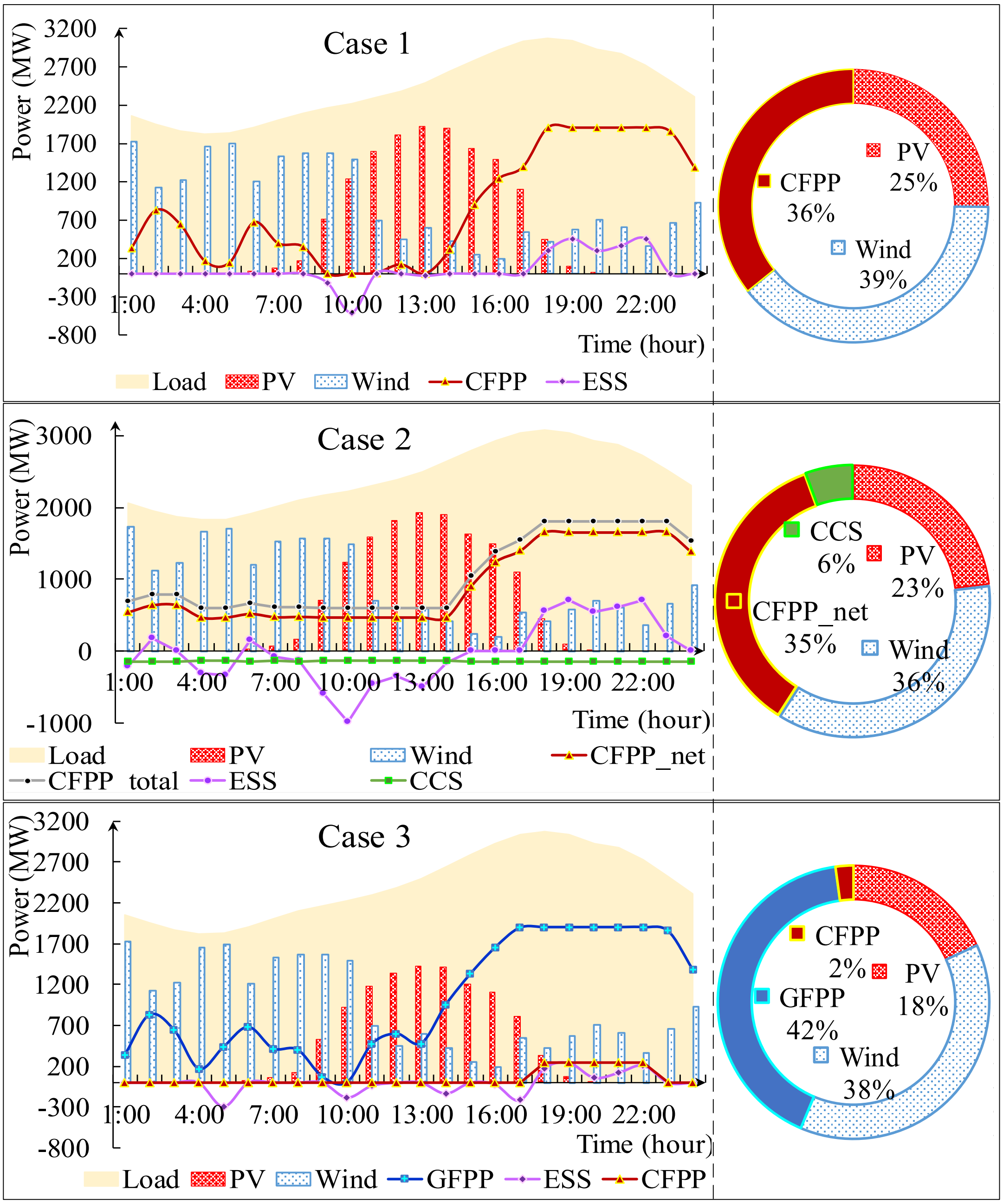

Figure 3-5 The system operation situations of each case

In the results of Figure 3-5, the power output situation of Case 1 and Case 2 can be summarized as follows: during the day, renewable energy is the primary power output source, while at night, the power demand is mainly from the supply of CFPPs and ESSs. Moreover, according to the proportion of total power generation throughout the day on the right-hand side, CFPP output basically accounts for 35% or more of the total power supply. In case 3, the output of ESS decreased, but the output of GFPP increased significantly.

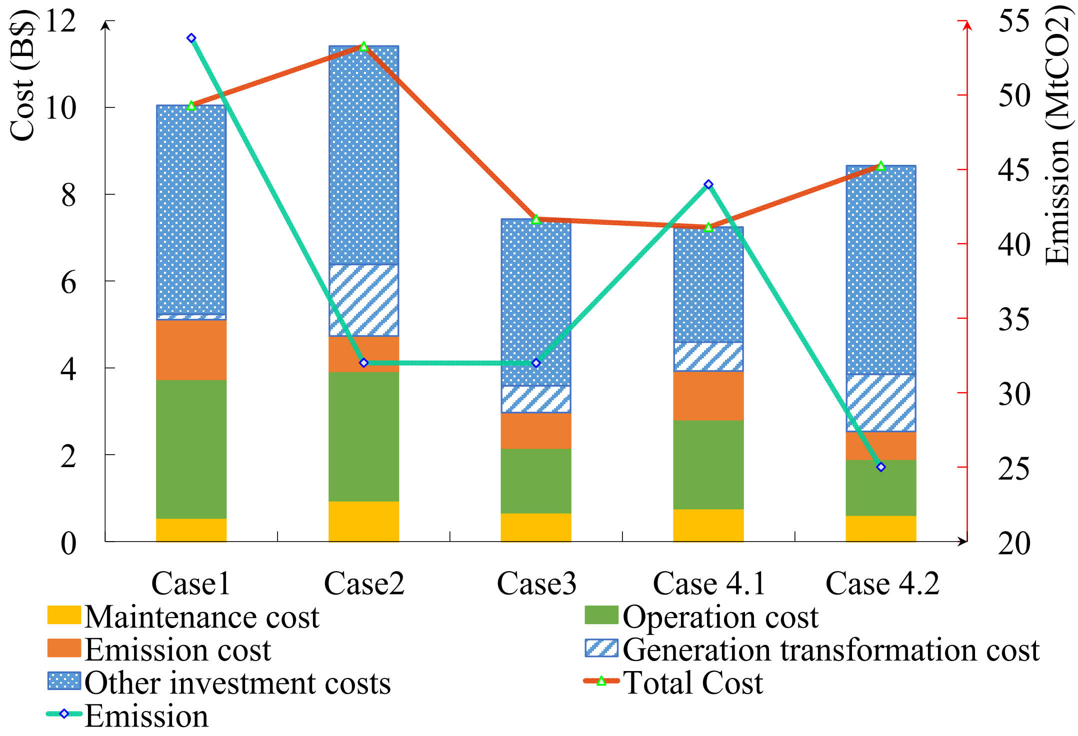

Figure 3-6 Comparison of system costs and emissions in each case

Figure 3-6 compares the cost and emissions results between the cases. It can be seen that the emission of Case 2 is essentially the same as that of Case 3, and both are much lower than that of Case 1. This indicates that both CCS retrofit and CtG conversion can effectively reduce system emissions. However, Case 2 is significantly higher than Case 3 when comparing costs. This is mainly because Case 2 has an exorbitant investment cost. Comparing the results of Case 3 with Cases 4.1 and 4.2, it can be found that the cost of Case 4.1 is only slightly lower than that of Case 3, but its emissions have increased by about 1.5 times. In Case 4.2, although the emission has been reduced to the preset target, the cost has also increased. It should be noted that the existing emission targets are set based on the circumstances of Case 1. If it is set according to the situation of Case 2 and Case 3, the emission target can be lower.

The above results show that since CtG conversion can achieve fewer emissions at a lower cost, it is very competitive during planning. However, there are few realistic examples of CtG conversion, and the investment costs in different regions may differ. Changes in prices may result in different planning results. It is necessary to verify the price-sensitive of this technology, which the result is shown in Figure 3-7.

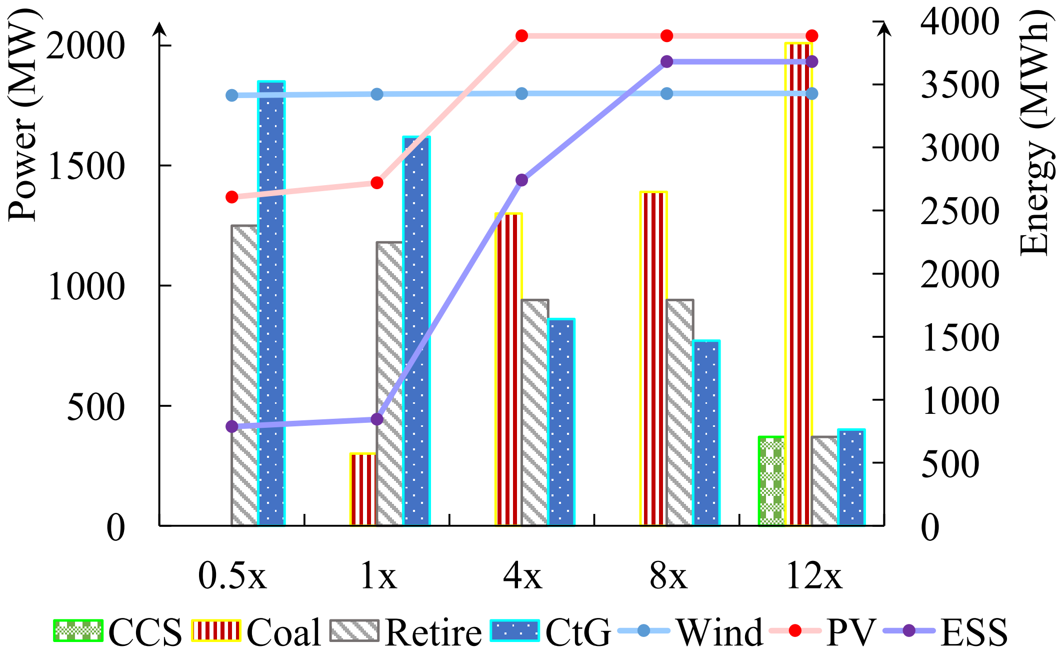

Figure 3-7 CtG Conversion Price Sensitivity Test

When the set price becomes half, more CFPPs prefer CtG conversion, while the number of PV installations decreases. As the price increases, the number of CFPPs who determine CtG conversion gradually decreases, and there is a significant decline when 4 and 12 times of current price, respectively. Meantime, the installed capacity of renewable energy and ESS will rise obviously.

TABLE 3-3 THE IMPACT OF ESSS INSTALLATION ON THE SYSTEM

Item	Case 1	Case 2	Case 3
	ESSs not installed		
Total Cost Change (M$)	+1006.766	+2617.642	+0.410
Emission Change ($MtCO_2$)	+36.565	+12.001	+0.007
	ESSs installed at maximum capacity		
Total Cost Change (M$)	+268.306	+248.423	+724.673
Emission Change ($MtCO_2$)	-0.012	-1.197	-6.991
Average Payback Period (years)	11.233	4.520	6.032

Table 3-3 compares the original results of Cases 1-3 and the scenarios of not installing ESSs at all and installing ESSs at their maximum capacity, which shows the impact of ESSs on system emission and cost. When ESSs are not installed, system emissions and costs will increase to varying degrees. Although not installing ESSs saves part of the investment cost, the increase in the operating cost of other equipment and the overall system emission cost leads to a rise in the total cost. Simultaneously, renewable energy resources cannot be fully utilized, increasing emissions. However, when ESSs are installed at their maximum capacity, the total cost still increases, but emissions are reduced to varying degrees. The results demonstrate that, firstly, the results obtained by the method proposed in this chapter provide the optimal economy for the system. The cost will increase whether ESSs are installed at maximum capacity or not installed at all. Secondly, large-scale installation of ESSs can better promote emission reduction, but the economic benefits of marginal emission reduction will diminish.

Additionally, when comparing the average payback period of ESSs with the maximum installed capacity, both Case 2 and Case 3 have shorter periods than Case 1. It's important to note that since the profitability of ESSs heavily relies on real-time bidding arbitrage in the market, advanced bidding strategies can increase profits. Therefore, the payback period in actual operation should be shorter than the results presented here. Furthermore, according to the U.S. Energy Information Administration's report [116], the estimated lifecycle of ESSs is ten years. The results of Case 2 and Case 3 are significantly shorter than this value, which validates their economic viability.

In the second stage, the flexibility test results of stage I planning schemes are presented in Table 3-4 and Figure 3-8. The probability of the additional investment cost of the system in each interval can be obtained by processing the adaptation cost of each system through the empirical cumulative distribution function (CDF). Table 3-4 shows that the adaptation cost possibility of Case 2 in each interval is the lowest among the three cases. Meanwhile, its maximum adaptation cost is also the smallest. This means that the planning results for Case 2 have the best system flexibility in these three cases. The outcome of Case 3 is slightly lower than that of Case 1 in each interval, and the maximum adaptation cost of Case 3 is also briefly smaller than that of Case 1.

TABLE 3-4 PROBABILITY AND VALUE OF ADAPTATION COST (BILLION $)

	1 B$	2 B$	4 B$	7 B$
Case1	56.7%	40.0%	18.3%	1.7%
Case2	21.7%	8.3%	0.0%	0.0%
Case3	50.0%	38.3%	16.7%	0.0%
	Maximum Adaptation Cost			
Case1	7.2 (B$)			
Case2	2.4 (B$)			
Case3	6.6 (B$)			

Figure 3-8 can intuitively obtain the results with the same trend. When the adaptation cost is the same in the figure, the larger the vertical axis, the better the system flexibility.

It can be seen from the results that the system flexibility of Case 2 has been much higher than that of the other two cases. The line of Case 3 and Case 1 only intersect when the adaptation cost is about 1.5, 3, 4B$. Case 3 is better than Case 1 in other intervals. This result is because there is no CFPP to be retired in Case 2, and a large amount of renewable energy and ESS is installed. The system has sufficient power generation capacity to cope with uncertainty prediction errors. Both the planning scheme of Case 3 and Case 1 have three CFPPs retired. The system flexibility results are basically the same and much lower than Case 2.

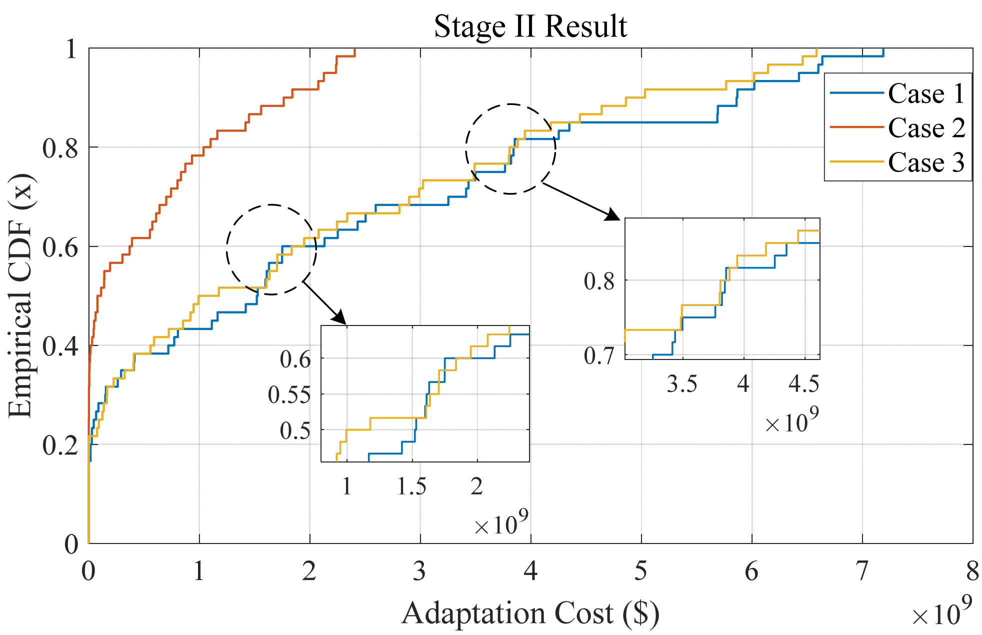

Figure 3-8 Empirical CDF of cases in stage II

3.5 Chapter Summary

This chapter proposes a novel two-stage generation expansion planning framework considering a CFPP low-carbon transition model including CtG conversion. Linear carbon targets can balance the system emissions and costs. Additionally, the adaptation cost of each CFPP transformation strategy under uncertain prediction deviations is intuitively measured through the flexibility test. Simulation results show that CtG conversion can effectively reduce system investment costs and reduce system emissions without adversely affecting system flexibility. Compared with other CFPP transformation technologies, CtG conversion can realize net zero transition more smoothly and achieve the emission reduction target at a lower cost. In future research, CtG conversion still has broad prospects, such as integrated planning with the gas network to maximize resource utilization efficiency and participating in the electricity and gas market as a GFPP. By studying these problems, the characteristics of CtG conversion can be fully utilized, and its value can be exerted.

Chapter 4 Fuzzy Inference-based Collaborative Supply-Demand Side Planning

To achieve the ambition of global emission reduction, a holistic framework for systemic emission reduction is required. The existing literature rarely considers the emission reduction methods of both the CCUS retrofit at the generation side and carbon response at the demand side. This chapter integrates the emission reduction methods of the demand and supply sides in the system and proposes a FIS-based two-stage system comprehensive emission reduction model. The proposed method has been validated on the IEEE 24-bus electricity system, confirming the effectiveness of the model.

4.1 Proposed System Decarbonization Framework

To achieve decarbonization of the power system, both supply-side and demand-side emission mitigation technologies are imperative. The emission reduction strategy of the system is depicted in Figure 4-1. On the supply side, this chapter considers the CCUS retrofit of CFPPs. Post-retrofit, the captured carbon dioxide can either be stored for other industry applications or reused through participation in P2G. Besides the conversion of existing power plants, the vigorous development of renewable energy sources can expedite emission reduction. In instances where wind and photovoltaic power generation surpasses demand, surplus power can be converted and stored in GESS via P2G technologies. Conversely, stored gas can be utilized for power generation during periods of high system demand.

On the demand side, considering the actual development of carbon markets in various countries around the world, carbon allowances have covered many industries such as steel and chemical. Large industrial factories can reduce emissions through temporal carbon response so that the remaining allowances can be traded in the emissions market for profit. In terms of IDCs, they are presently not within the ambit of emission mandatory management, thereby precluding them from cost reduction or profit generation through the sale of carbon quotas or similar mechanisms. Nevertheless, propelled by corporate environmental and sustainability image, many companies are willing to validate their environmental credentials by procuring green electricity, green certificates, and other carbon offset certificates. Consequently, employing spatial carbon response can effectively curtail the actual emissions and associated costs of companies.

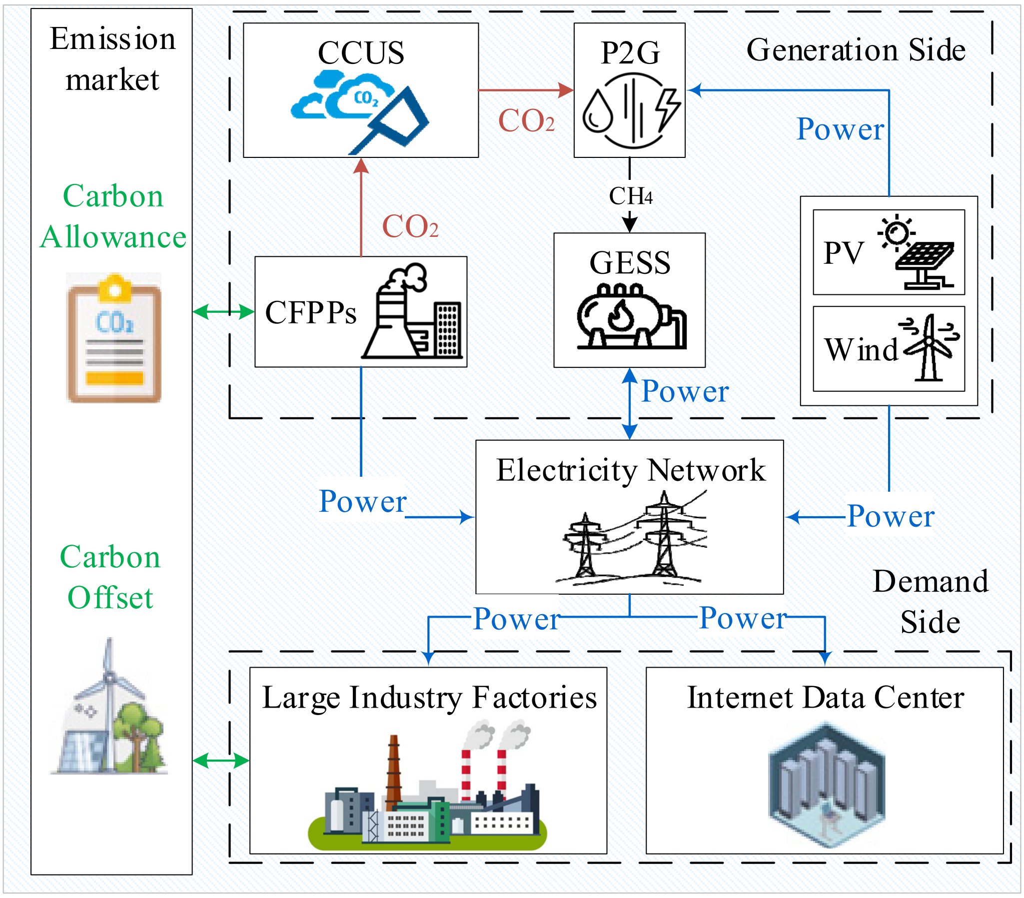

Figure 4-1 Joint supply-demand side emission mitigation approach.

The FIS-based two-stage system framework is illustrated in Figure 4-2. In terms of the two-stage system, in the first stage, the system focuses on decarbonization transition planning, incorporating the CCUS retrofit of CFPPs. Upon obtaining the planning outcomes, data such as generator power output and power flow are fed into the CEF model to determine nodal carbon intensity. Subsequently, in the second stage, large industrial load $D_{i,t}^{LIL}$ and IDC load $D_{i,t}^{IDC}$ adapt their power consumption plans in response to fluctuations in nodal carbon intensity, transmitting the revised results back to the first stage. During the system planning and operation process, not all system candidate nodes are equally amenable to the emission reduction approach mentioned above. Off-site factors such as climatic conditions, regional policy support, safety considerations, and economic viability significantly influence the feasibility of implementing these strategies in specific regions.

Using the CCUS retrofit of CFPPs as an illustration, it is observed that generators with higher rated capacities are typically more conducive to CCUS retrofitting, owing to higher economic viability. Moreover, the remaining operational lifespan of the CFPPs is a pivotal determinant of its retrofitting feasibility. The longer the remaining operational lifespan, the greater the value its modification can produce and the higher the possibility of being retrofitted. After retrofitting, the captured carbon dioxide necessitates subsequent processing or storage. Hence, the proximity between candidate generators and the storage facility emerges as a critical factor influencing the decision to retrofit. The shorter the distance, the easier it is to transport the captured carbon dioxide. On the demand side, analogous off-site factors play a significant role in determining the efficacy of large industrial loads in responding effectively. The level of automation, modularity, and intelligence in their production processes collectively dictate the facility's ability to adapt its production processes in accordance with variations in the system's carbon emission factors, thus enabling it to respond to the emission requirement. Additionally, the remaining off-site influencing factors encompass the effects of average temperature, average humidity, and environmental impact rate on the probability set of candidate nodes for P2G-coupled photovoltaic and wind turbine systems. Furthermore, the characteristics of latency sensitivity, partition tolerance, and data confidentiality play significant roles in determining whether a data center supports multi-region collaborative processing workflows.

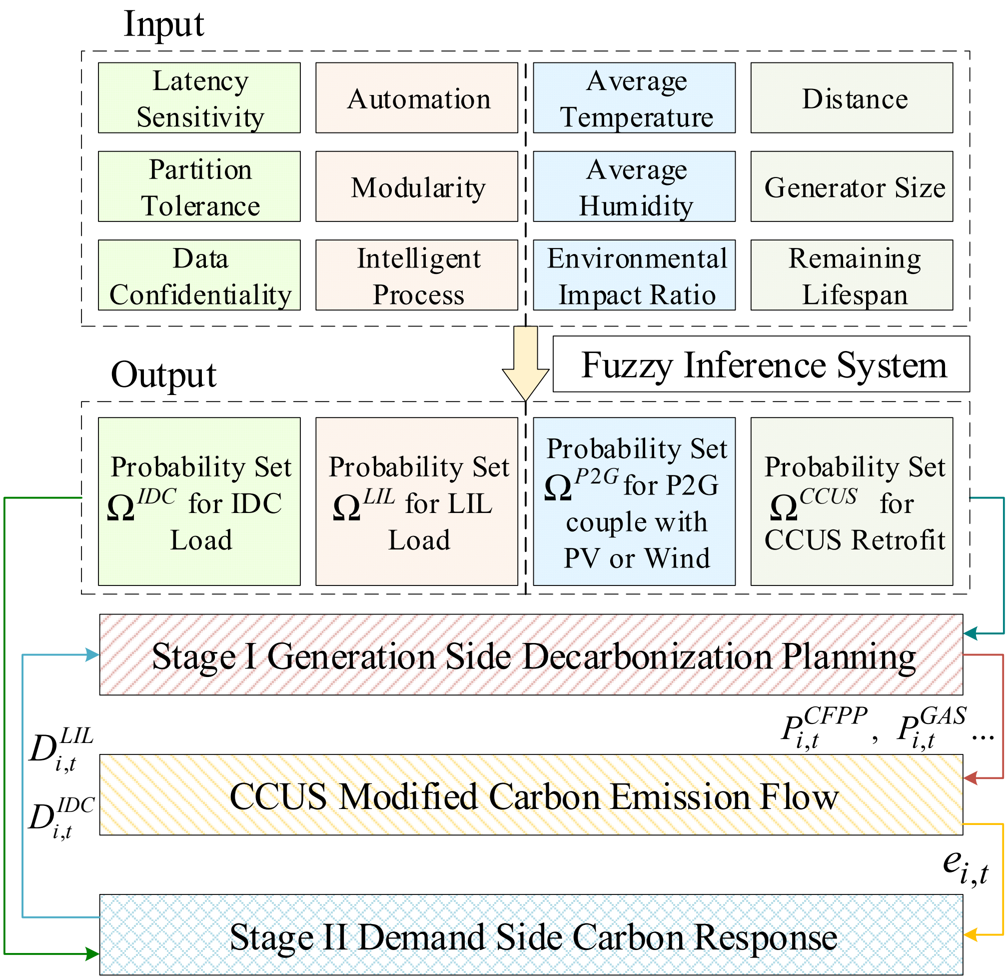

Figure 4-2 The proposed two-stage system framework.

To mitigate the influence of the aforementioned off-site factors on system planning and operational outcomes, this chapter introduces a novel three-input and one-output fuzzy inference system. This approach facilitates decision-making by considering the interplay of these non-mathematically modellable off-site factors, thereby computing pertinent sets of probabilities denoted as Ω^{τ}. These probability sets will be allocated to candidate nodes for each respective technology within the system while factoring in the trade-offs among the three pivotal factors.

4.2 Proposed FIS-Based Candidate Node Set Selection Method

FIS assesses inputs characterized by uncertain and imprecise factors using fuzzy logic and fuzzy rules, facilitating more reasoned decisions, particularly in the absence of precise data or deterministic relationships. Compared to the methods, including stochastic optimization and information gap decision theory, which model uncertain factors, FIS provides greater flexibility and adaptability in managing complex causal or nonlinear relationships. It does not require accurate numerical modeling of the relationships between inputs and outputs, making it well-suited for situations where these relationships are uncertain or imprecise.

The decision-making process in FIS comprises fuzzification, rule evaluation, and defuzzification. Fuzzification involves converting inputs into fuzzy sets, typically achieved through membership functions (MFs), which assign degrees of membership to each input variable, determining their contribution to the overall outcome. Subsequently, the Mamdani fuzzy inference algorithm is employed in this chapter, utilizing the obtained MFs to fuzzify the input variables based on a set of fuzzy rule tables. The fuzzy implication relationship is straightforwardly defined and obtained by taking the minimum value of the Cartesian product of fuzzy sets. Finally, defuzzification transforms the fuzzy output into specific values conducive to direct decision-making.

A. Fuzzy inference algorithm and rules table

In FIS, X^{τ}, Y^{τ}, and Z^{τ} represent three fuzzy inputs, where $\tau \in [CCUS, P2G, LIL, IDC]$ is determined by the subsystem to which each input belongs. The choice of τ specifies which subsystem each input pertains to within the FIS framework. Define X^{CCUS} {Distance}, Y^{CCUS} {Size}, Z^{CCUS} {Lifespan} are fuzzy variables of CCUS subsystem; X^{P2G} {Temperature}, Y^{P2G} {Humidity}, Z^{P2G} {Environmental Impact} are fuzzy variables of subsystem of P2G-PV or P2G-wind; X^{LIL} {Automation}, Y^{LIL} {Modularity}, Z^{LIL} {Intelligent} are fuzzy variables of LIL subsystem; and X^{IDC} {Latency Sensitivity}, Y^{IDC} {Partition Tolerance}, Z^{IDC} {Data Confidentiality} are fuzzy variables of IDC subsystem. The inputs X^{τ}, Y^{τ}, and Z^{τ} have fuzzy sets $\widetilde{F^{\tau}}^{*}$, $\widetilde{F_1^{\tau}}$, $\widetilde{F_2^{\tau}}$, …, $\widetilde{F_n^{\tau}}$, $\widetilde{G^{\tau}}^{*}$, $\widetilde{G_1^{\tau}}$, $\widetilde{G_2^{\tau}}$, …, $\widetilde{G_n^{\tau}}$, $\widetilde{H^{\tau}}^{*}$, $\widetilde{H_1^{\tau}}$, $\widetilde{H_2^{\tau}}$, …, $\widetilde{H_n^{\tau}}$ respectively. In here, $\widetilde{(\cdot)}^{*}$ means the real value, and $\widetilde{(\cdot)_{1-n}^{\tau}}$ means the pre-allocated value. O^{τ} {Probability} is the output variable with fuzzy sets $\widetilde{K^{\tau}}^{*}$, $\widetilde{K_1^{\tau}}$, $\widetilde{K_2^{\tau}}$, …, $\widetilde{K_n^{\tau}}$, which denotes the probability that these emission reduction methods are suitable for use in these candidate buses. In particular, they refer to determining the suitability degree of CCUS retrofits for candidate CFPPs and installing P2G-PV or P2G-wind at candidate buses. On the demand side, these values represent the maximum responsiveness of LIL and IDC loads. $\widetilde{R_n^\tau}(X^\tau, Y^\tau, Z^\tau, O^\tau)$ is the fuzzy rule that relates to the inputs X^τ, Y^τ, Z^τ and output O^τ, where n is the number of rules.

$$\mu_{\widetilde{R_n^\tau}}\left(x^\tau, y^\tau, z^\tau, o^\tau\right) = \begin{bmatrix} \mu_{\widetilde{F_n^\tau}}\left(x^\tau\right) \wedge \mu_{\widetilde{G_n^\tau}}\left(y^\tau\right) \\ \wedge \mu_{\widetilde{H_n^\tau}}\left(z^\tau\right) \wedge \mu_{\widetilde{K_n^\tau}}\left(o^\tau\right) \end{bmatrix} \tag{4.1}$$
$$\forall x^\tau \in X^\tau, \forall y^\tau \in Y^\tau, \forall z^\tau \in Z^\tau, \forall o^\tau \in O^\tau$$

where $\mu_{\widetilde{R_n^\tau}}(x^\tau, y^\tau, z^\tau, o^\tau)$, $\mu_{\widetilde{F_n^\tau}}(x^\tau)$, $\mu_{\widetilde{G_n^\tau}}(y^\tau)$, $\mu_{\widetilde{H_n^\tau}}(z^\tau)$, and $\mu_{\widetilde{K_n^\tau}}(o^\tau)$ present the selected MFs (Gaussian) of corresponding fuzzy sets under n th fuzzy rules. Subsequently, the fuzzy output sets {Probability} can be obtained by combining the fuzzy rules and input fuzzy variables, which detail shown as follows:

$$\begin{aligned}
\mu_{\widetilde{K^\tau}^*}\left(o^\tau\right) &= \begin{bmatrix} \mu_{\widetilde{F^\tau}^*}\left(x^\tau\right) \\ \wedge \mu_{\widetilde{G^\tau}^*}\left(y^\tau\right) \\ \wedge \mu_{\widetilde{H^\tau}^*}\left(z^\tau\right) \end{bmatrix} \wedge \begin{bmatrix} \mu_{\widetilde{R_1^\tau}}\left(x^\tau, y^\tau, z^\tau, o^\tau\right) \\ \vee \mu_{\widetilde{R_2^\tau}}\left(x^\tau, y^\tau, z^\tau, o^\tau\right) \vee \ldots \\ \ldots \vee \mu_{\widetilde{R_n^\tau}}\left(x^\tau, y^\tau, z^\tau, o^\tau\right) \end{bmatrix} \\
&= \left\{ \begin{matrix} \left[\mu_{\widetilde{F^\tau}^*}\left(x^\tau\right) \wedge \mu_{\widetilde{G^\tau}^*}\left(y^\tau\right) \wedge \mu_{\widetilde{H^\tau}^*}\left(z^\tau\right) \right] \\ \wedge \mu_{\widetilde{R_1^\tau}}\left(x^\tau, y^\tau, z^\tau, o^\tau\right) \end{matrix} \right\} \\
&\vee \left\{ \begin{matrix} \left[\mu_{\widetilde{F^\tau}^*}\left(x^\tau\right) \wedge \mu_{\widetilde{G^\tau}^*}\left(y^\tau\right) \wedge \mu_{\widetilde{H^\tau}^*}\left(z^\tau\right) \right] \\ \wedge \mu_{\widetilde{R_2^\tau}}\left(x^\tau, y^\tau, z^\tau, o^\tau\right) \end{matrix} \right\} \vee \ldots \\
&\ldots \vee \left\{ \begin{matrix} \left[\mu_{\widetilde{F^\tau}^*}\left(x^\tau\right) \wedge \mu_{\widetilde{G^\tau}^*}\left(y^\tau\right) \wedge \mu_{\widetilde{H^\tau}^*}\left(z^\tau\right) \right] \\ \wedge \mu_{\widetilde{R_n^\tau}}\left(x^\tau, y^\tau, z^\tau, o^\tau\right) \end{matrix} \right\} \\
&\forall x^\tau \in X^\tau, \forall y^\tau \in Y^\tau, \forall z^\tau \in Z^\tau, \forall o^\tau \in O^\tau
\end{aligned} \tag{4.2}$$

where $\mu_{\widetilde{K^\tau}^*}(o^\tau)$ is the output fuzzy sets obtained under n th fuzzy rule. The membership degree of o^τ in each fuzzy set is calculated using the minimum operator. Subsequently, the fuzzy output sets under each fuzzy rule are merged using the maximum operator to obtain the overall fuzzy output set, denoted as $\mu_{\widetilde{K^\tau}^*}(o^\tau)$. The overall fuzzy output can be also presented as:

$$\mu_{\widetilde{K^\tau}^*}\left(o^\tau\right) = \mu_{\widetilde{K_1^\tau}^*}\left(o^\tau\right) \vee \mu_{\widetilde{K_2^\tau}^*}\left(o^\tau\right) \vee \ldots \vee \mu_{\widetilde{K_n^\tau}^*}\left(o^\tau\right) \tag{4.3}$$
$$\forall x^\tau \in X^\tau, \forall y^\tau \in Y^\tau, \forall z^\tau \in Z^\tau, \forall o^\tau \in O^\tau$$

In equations (4.1)-(4.3), fuzzy rule $\widetilde{R_n^\tau}(X^\tau, Y^\tau, Z^\tau, O^\tau)$ can be expressed concretely, and the example is as follows. Note that the fuzzy rules shown in the table below are not a complete rule table due to the page limit.

TABLE 4-1 EXAMPLE OF FUZZY RULES

Distance	Generator Size	Remaining Lifespan	Probability of CCUS Retrofit
L	MH	M	H
M	ML	H	M
H	L	MH	ML
Temperature	Humidity	Environmental Impact	Probability of Install of P2G-PV or P2G-Wind
MH	H	ML	M
ML	H	MH	ML
H	M	L	MH
Automation	Modularity	Intelligent Process	Probability of LIL Load temporal dispatch
M	H	M	MH
L	M	L	ML
H	M	H	H
Latency Sensitivity	Partition Tolerance	Data Confidentiality	Probability of IDC Load spatial dispatch
H	H	M	ML
M	H	L	MH
L	H	M	H

Among them, fuzzy variables include generator size, remaining lifespan, temperature, environmental impact, and all fuzzy outputs are divided into five levels, namely low (L), medium-low (ML), medium (M), medium-high (MH), and high (H). All remaining variables are divided into three levels, namely, low (L), medium (M), and high (H).

B. Rank of Probability

The final probability sets at each candidate bus can be expressed in crisp value, as shown in (4.4)

$$o^{\tau*}(\text{Probability}) = \frac{\int o^\tau \cdot \mu(O^\tau) d(o^\tau)}{\int \mu(O^\tau) d(o^\tau)} = \frac{\sum_i o_i^\tau \mu(O_i^\tau)}{\sum_i \mu(O_i^\tau)} \tag{4.4}$$

where $o^{\tau*}$ is the probability of whether the emission reduction methods apply at the corresponding candidate bus; o_i^{τ} denotes the discrete value in the universe of discourse O_i^{τ}, which involves all probabilities; $\mu(O_i^{\tau})$ indicates the membership grade of the fuzzy set for the probability of ith bus. Equation (4.4) calculates the weighted average of the output variable corresponding to the membership degrees of the fuzzy set, delineating the gravity center of the fuzzy set as a crisp value.

To rank the probabilities from highest to lowest, select the required buses with the highest probability to form the candidate bus set Ω^{τ}, a pivotal variable passed to the subsequent optimization problem.

$$\begin{gathered}\Omega^{\tau} = Rank\left(o_1^{\tau*}, o_2^{\tau*}, o_3^{\tau*} \ldots, o_i^{\tau*}\right), \forall i \in \{candidate\ buses\} \\ \Omega^{\tau} \in [0,1]\end{gathered} \tag{4.5}$$

$$\delta_i^{CCUS\&P2G} = \begin{cases} 1 & if\ o_i^{CCUS\&P2G*} \geq 0.5 \\ 0 & else \end{cases}, \forall i \in \Omega^{\tau} \tag{4.6}$$

$$\delta_i^{LIL\&IDC} = o_i^{LIL\&IDC*}, \forall i \in \Omega^{\tau} \tag{4.7}$$

$$\begin{cases} 0 \leq \delta_{i,t}^{\Re f} \leq \delta_i^{CCUS} \\ 0 \leq \delta_{i,t}^{GESS} \leq \delta_{i,t}^{GESS,MAX} \cdot \delta_i^{P2G} \\ 0 \leq n_i^{W} \leq n_i^{W,MAX} \cdot \delta_i^{P2G} \\ 0 \leq \alpha_i^{S} \leq \alpha_i^{S,MAX} \cdot \delta_i^{P2G} \end{cases} \tag{4.8}$$

$$\begin{cases} \left|D_{i,t}^{LIL}\right| \leq \overline{D_{i,t}^{LIL}} \cdot \delta_i^{LIL} \\ \left|\sigma_{i,t}^{SDL}\right| \leq \varpi_{i,t}^{B} \cdot \delta_i^{IDC} \end{cases} \tag{4.9}$$

Equations (4.5)-(4.7) convert the probability values obtained in the fuzzy algorithm into explicit values that can be used in the planning process. Equations (4.6) and (4.8) stipulate that relevant investments in a particular bus for CCUS and P2G are only feasible when the application probability exceeds 0.5. Equations (4.7) and (4.9) establish the upper limit of the dispatchable load for IDC and LIL through probability calculations. Wherein, $\delta_i^{CCUS\&P2G}$ and $\delta_i^{LIL\&IDC}$ are the decision variables of CCUS, P2G, LIL and IDC; $\delta_{i,t}^{\Re f}$ is binary decision variables that indicate whether the generator is retrofitted at time t; $\delta_{i,t}^{GESS}$ is a GESS-related decision variable; and $\delta_{i,t}^{GESS,MAX}$ is the upper bound of GESS installation quantities; n_i^{W} and $n_i^{W,MAX}$, α_i^{S}

and $\alpha_i^{S,MAX}$ are the number and maximum quantities of wind turbines, and the area and maximum area of the solar power equipment; $D_{i,t}^{LIL}$ indicates time-shiftable large industry load, and $\sigma_{i,t}^{SDL}$ is the spatial-shiftable IDC load; $\overline{D_{i,t}^{LIL}}$ is the preset upper bound; $\varpi_{i,t}^{B}$ is the regulated power demand of IDC compared with set baseline.

4.3 Integrated Two-Stage System Emission Reduction Model

A. Stage I, Generation side decarbonization planning

Embedding the CCUS retrofit and P2G models into the planning process, an integrated system emission mitigation model can be obtained. The specific equation can be expressed as follows.

$$Min\ C^{total} = \frac{C^{\Re f} + C^{re} + C^{mt} + C^{cap} + C^{op}}{(1+\varsigma)^{Y}} \tag{4.10}$$

$$C^{\Re f} = \begin{cases} \underbrace{\rho_i^{\Re f} \cdot \delta_{i,t}^{\Re f} \cdot \overline{P_i^{CFPP}}}_{retrofit\ cost} \\ +\underbrace{\rho_i^{\Re f,mt} \cdot \delta_{i,t}^{\Re f} \cdot \overline{P_i^{CFPP}}}_{maintenance\ cost} \\ +\underbrace{\rho_i^{CCUS} \cdot \varepsilon_{i,t}^{CCUS}}_{operation\ cost} \end{cases} \tag{4.11}$$

$$C^{re} = \rho^{W} n_i^{W} + \rho^{S} \alpha_i^{S} + \rho^{GESS} E_{rate}^{GESS} \delta_{i,t}^{GESS} \tag{4.12}$$

$$C^{mt} = \begin{pmatrix} \rho_i^{mt} \cdot \overline{P_i^{CFPP}} + \rho^{W,mt} n_i^{W} \\ +\rho^{S,mt} \alpha_i^{S} + \rho^{GESS,mt} E_{rate}^{GESS} \delta_{i,t}^{GESS} \end{pmatrix} \tag{4.13}$$

$$C^{cap} = \sum_i \begin{bmatrix} \begin{pmatrix} \sum_t \begin{pmatrix} P_{i,t}^{CFPP} \cdot e_{i,t}^{CFPP} \\ -P_{i,t}^{CCUS} / \mu_i^{\Re f} \end{pmatrix} \cdot \Delta t \\ -Cap_i^{CFPP} \end{pmatrix} \\ +\left(\sum_t \left(P_{i,t}^{GAS} \right) \cdot e_{i,t}^{GAS} \cdot \Delta t - Cap_i^{GAS} \right) \end{bmatrix} \cdot \rho_i^{cap} \tag{4.14}$$

$$C^{op} = \begin{Bmatrix} \sum_{\theta \in CFPP\&GAS} \sum_i \sum_t \left[\alpha_i^{\theta} + \beta_i^{\theta} P_{i,t}^{\theta} + c_i^{\theta} \left(P_{i,t}^{\theta} \right)^2 \right] \\ +\sum_i \sum_t \left[\rho^{P2G} P_{i,t}^{P2G} + \rho^{CO_2,s} \varepsilon_{i,t}^{CO_2,s} \right] \end{Bmatrix} \tag{4.15}$$

where $C^{\Re f}$ denotes the total retrofit cost; C^{re} is the renewable energy capital cost, C^{cap} and C^{op} are total system emission and operation cost; ς is the cost discount rate and Y denotes the total operating years; $\rho_i^{\Re f}$ denotes the equipment installation cost coefficient at location i; $\rho_i^{\Re f,mt}$ denotes the maintenance cost coefficient of CCUS; $\overline{P_i^{CFPP}}$ denotes the rate power output of CFPP; ρ_i^{CCUS} and $\varepsilon_{i,t}^{CCUS}$ are the operation cost coefficient and captured emission; ρ^W, ρ^S and ρ^{GESS} are the investment cost coefficient of wind turbines, PV panels, and GESS; ρ_i^{mt}, $\rho^{W,mt}$, $\rho^{S,mt}$ and $\rho^{GESS,mt}$ are the cost coefficient of maintenance for each facility; $e_{i,t}^{CFPP}$, $e_{i,t}^{GAS}$ are the carbon intensity of coal and gas turbines, θ is a set of generator types including CFPP and GAS; Cap_i^{CFPP}, Cap_i^{GAS} denote the emission cap; ρ_i^{cap} is carbon allowance trading price; α_i^θ, β_i^θ, and c_i^θ are cost coefficients of CFPPs and gas generators; ρ^{P2G} and $\rho^{CO_2,s}$ are cost coefficient of P2G operation and supplementation. The system constraints are shown follows:

$$s.t.\ \begin{pmatrix} S_{ij,t} + P_{i,t}^{CFPP} + P_{i,t}^{W} + P_{i,t}^{S} \\ +P_{i,t}^{GAS} - P_{i,t}^{P2G} - P_{i,t}^{CCUS} \end{pmatrix} = D_{i,t}^{FL} + D_{i,t}^{LIL} + D_{i,t}^{IDC} \tag{4.16}$$

$$S_{ij,t} - B_{ij}\left(\vartheta_{i,t} - \vartheta_{j,t}\right) = 0 \tag{4.17}$$

$$\underline{S_{ij,t}} \le S_{ij,t} \le \overline{S_{ij,t}} \tag{4.18}$$

$$\underline{P_{i,t}^{CFPP}} \le P_{i,t}^{CFPP} \le \overline{P_{i,t}^{CFPP}} \tag{4.19}$$

$$P_{i,t}^{net} = P_{i,t}^{CFPP} - P_{i,t}^{CCUS} \tag{4.20}$$

$$P_{i,t}^{CCUS} = \mu_i^{\Re f} \varepsilon_{i,t}^{CCUS} \tag{4.21}$$

$$\varepsilon_{i,t}^{net} = \varepsilon_{i,t}^{CFPP} - \varepsilon_{i,t}^{CCUS}, \varepsilon_{i,t}^{CCUS} = \varepsilon_{i,t}^{CS} + \varepsilon_{i,t}^{CU} \tag{4.22}$$

$$0 \le \varepsilon_{i,t}^{CS} \le \varepsilon_{i,t}^{CCUS}, 0 \le \varepsilon_{i,t}^{CU} \le \varepsilon_{i,t}^{CCUS} \tag{4.23}$$

$$0 \le \varepsilon_{i,t}^{CCUS} \le \mu_{i,t}^{cap} \varepsilon_{i,t}^{CFPP} P_{i,t}^{CFPP} \delta_{i,t}^{\Re f} \tag{4.24}$$

$$\sum_i \mu^{CO_2}\left(\varepsilon_{i,t}^{CU} + \varepsilon_{i,t}^{CO_2,s}\right) = \sum_i \mu^{P2G} P_{i,t}^{P2G} \tag{4.25}$$

In equation (4.16), $D_{i,t}^{FL}$ and $D_{i,t}^{IDC}$ indicate the fix load and overall IDC load; and $S_{ij,t}$

represents the power flow at line $i-j$ which is restricted by power flow equation (4.17); B_{ij} and $\vartheta_{i,t}$ are the line susceptance and voltage phase angle; $\underline{(\cdot)}$ and $\overline{(\cdot)}$ denote the lower and upper bound. Equations (4.20)-(4.25) are constraints of CCUS, where $P_{i,t}^{net}$ is the net output power of CFPP after CCUS retrofit [109]; $P_{i,t}^{CFPP}$ and $P_{i,t}^{CCUS}$ are CFPP output power and CCUS consumption power, respectively; $\mu_{i}^{\Re f}$ represents the emission capture power coefficient; in equation (4.4), the net emission $\varepsilon_{i,t}^{net}$ is equal to the CFPP emission $\varepsilon_{i,t}^{CFPP}$ minus $\varepsilon_{i,t}^{CCUS}$; $\varepsilon_{i,t}^{CCUS}$ can be divided into two parts, CO_2 storage $\varepsilon_{i,t}^{CS}$ and utilization $\varepsilon_{i,t}^{CU}$; $\mu_{i,t}^{cap}$ represents the capture rate. μ^{CO_2}, μ^{P2G}, and $P_{i,t}^{P2G}$ are the amount of CO_2 consumed by P2G to generate CH_4, P2G conversion efficiency and P2G power consumption, respectively [38]; $\varepsilon_{i,t}^{CO_2,s}$ represents the supplementation from other sources when the amount of CO_2 captured by CCUS is insufficient.

P2G technology converts excess system electricity into grid-compatible gas in a two-step process. Initially, water is electrolyzed, resulting in the separation of hydrogen and oxygen. Subsequently, hydrogen catalyzes with carbon dioxide, leading to the formation of natural gas and water. The corresponding chemical equilibrium expression is presented below:

$$2H_2O \overset{electrolysis}{=} 2H_2 + O_2 \tag{4.26}$$

$$4H_2 + CO_2 \overset{catalysis}{=} CH_4 + 2H_2O \tag{4.27}$$

$$E_{i,t+1}^{GESS} = E_{i,t}^{GESS} + \left[P_{i,t}^{P2G}\mu^{c} - \left(P_{i,t}^{GAS} / \mu^{d} \right) \right]\Delta t \tag{4.28}$$

$$E_{rate}^{GESS} \cdot \underline{SoC} \le E_{i,t}^{GESS} \le E_{rate}^{GESS} \cdot \overline{SoC} \tag{4.29}$$

$$0 \le P_{i,t}^{P2G} \le \overline{P_{i,t}^{P2G}} \cdot \delta_{i,t}^{GESS} \tag{4.30}$$

$$0 \le P_{i,t}^{GAS} \le \overline{P_{i,t}^{GAS}} \cdot \delta_{i,t}^{GESS} \tag{4.31}$$

$$P_{i,t}^{W}\left(v_{i,t}^{W}\right)=\begin{cases}0 & v_{i,t}^{W}<v_{in}^{W}, v_{i,t}^{W}>v_{out}^{W}\\ n_{i}^{W}\cdot P_{i,rate}^{W}\cdot\dfrac{v_{i,t}^{W}-v_{in}^{W}}{v_{rate}^{W}-v_{in}^{W}} & v_{in}^{W}<v_{i,t}^{W}<v_{rate}^{W}\\ n_{i}^{W}\cdot P_{i,rate}^{W} & v_{rate}^{W}<v_{i,t}^{W}<v_{out}^{W}\end{cases} \tag{4.32}$$

$$P_{i,t}^{S}\left(H_{i,t}\right)=H_{i,t}\cdot\alpha_{i}^{S}\cdot\mu_{i}^{S} \tag{4.33}$$

where equation (4.28)-(4.31) is the mathematical models of GESS, E_{rate}^{GESS}, $E_{i,t}^{GESS}$, and $P_{i,t}^{GAS}$ denote the rate energy, stored energy, and GESS discharging power; u^{c} and u^{d} are the efficiency of GESS charge and discharge; Δt is the time interval. Equation (4.32)-(4.33) represent the output power constraints of wind energy and solar power, respectively; $v_{i,t}^{W}$ denotes the wind speed, and $P_{i,t}^{W}$ is the wind turbine output power; v_{in}^{W}, v_{rate}^{W}, v_{out}^{W} present the cut-in, rated, and cut-out speed, respectively; $P_{i,rate}^{W}$ is the rated power; $P_{i,t}^{S}$ represents the solar output power; $H_{i,t}$ and μ_{i}^{S} are the solar radiation and the conversion efficiency of PV panels. Considering that regions have different natural conditions, such as solar exposure, temperatures, and wind speed, the site selection of renewable energy will tremendously affect the output of devices. Therefore, the aforementioned fuzzy methods can be applied to maximize the utilization efficiency of the equipment. Additionally, regarding the uncertainty of parameters such as wind, light, and load, the processing method in this chapter is referred to [61]. That is, an approach based on GANs is adopted to construct a set of future scenarios based on historical data.

After stage I planning is completed, the system can calculate the carbon intensity of each bus in the current system condition. Large-scale industrial loads on the demand side need to adjust their loads in real-time according to the nodal carbon intensity at different times for carbon response.

B. Stage II, Demand side carbon response

It is common sense that most carbon emissions in the power system are related to suppliers rather than consumers. However, from the point of view of economics, “consumption furnishes the impulse to produce”, that is, the demand preferences of consumers will affect the production behavior of enterprises [117]. Thus, consumers’ low-carbon consumption concepts and behaviors can dominate the value orientation of the energy market. To accurately demand side carbon response according to the nodal carbon intensity, it is necessary to deploy the CEF method to calculate [118]. The specific CEF model based on CCUS is as follows:

$$e_{i,t} = \frac{\left\{ \begin{array}{l} P_{i,t}^{CFPP} e_{i,t}^{CFPP} - P_{i,t}^{CCUS} / \mu_i^{\Re f} \\ + P_{i,t}^{GAS} e_{i,t}^{GAS} + \sum\limits_{j \in S^+} \left(S_{ij,t} e_{ij,t} \right) \end{array} \right\}}{\left\{ P_{i,t}^{CFPP} + P_{i,t}^{W} + P_{i,t}^{S} + P_{i,t}^{GAS} + \sum\limits_{j \in S^+} S_{ij,t} \right\}} \tag{4.34}$$

$$e_{ij,t} = \begin{cases} e_{i,t},\ if\ S_{ij,t} \geq 0 \\ e_{j,t},\ if\ S_{ij,t} \leq 0 \end{cases} \tag{4.35}$$

where S^+ represents the power flowing into the bus j; $e_{i,t}$, and $e_{ij,t}$ represent the nodal carbon intensity at bus i and the branch carbon intensity of line $i-j$.

After calculating the carbon intensity, their respective carbon response costs can be obtained through the following model. It should be noted that since the cost function and benefits function of various industries are difficult to unify, whether the production cost and market benefit will be affected by the carbon response still needs further verification. This chapter assumes an ideal situation in which the carbon response does not affect its costs and benefits, and the process of carbon response is independent. Based on this assumption, the carbon response cost and constraint models of IDC Loads and LILs in the emissions market are as follows:

$$Min\ C_i^{CR} = \frac{1}{(1+\varsigma)^Y} \left[\begin{array}{l} \left(\sum\limits_t D_{i,t}^{LIL} \cdot e_{i,t} \cdot \Delta t - Cap_i^{LIL} \right) \cdot \rho_i^{cap} \\ + \left(\sum\limits_t D_{i,t}^{IDC} \cdot e_{i,t} \cdot \Delta t \right) \cdot \rho_i^{green} \end{array} \right] \tag{4.36}$$

$$\sum_{t \in T} D_{i,t}^{LIL} = 0 \tag{4.37}$$

$$\underline{D_t^{LIL,total}} \leq \sum_i D_{i,t}^{LIL} \leq \overline{D_t^{LIL,total}} \tag{4.38}$$

$$D_{i,t}^{IDC} = \sigma_{i,t}^{base} + \sigma_{i,t}^{SDL} + \Lambda_{1i} \sigma_{i,t}^{HQoS} \tag{4.39}$$

$$\sum_{i \in \Omega^{IDC,bus}} \left(\sigma_{i,t}^{SDL} / \Lambda_{2i} \right) = 0 \tag{4.40}$$

$$-\sigma_{i,t}^{SDL} / \Lambda_{3i} \leq \varpi_{1i,t} \tag{4.41}$$

$$-\sigma_{i,t}^{SDL}/\Lambda_{1i}+\sigma_{i,t}^{HQoS}\le\varpi_{2i,t} \tag{4.42}$$

$$\Lambda_{1i}=\left(1+e_{1i}\right) \tag{4.43}$$

$$\Lambda_{2i}=\Lambda_{1i}\cdot\left[\frac{\left(\frac{NE_iEE_i+NA_iEA_i+NC_iEC_i}{NS_i}+EI_i\right)}{\left(u_i-\frac{1}{w}\right)+\left(\frac{EP_i-EI_i}{u_i}\right)}\right] \tag{4.44}$$

$$\Lambda_{3i}=\Lambda_{2i}\cdot\left(u_i-\frac{1}{w}\right) \tag{4.45}$$

$$\sigma_{i,t}^{base}=\varpi_{i,t}^{B}+\left(e_{1i}/e_{3i}\right)\left(q_{i,t}^{O}-q_{i,t}^{I}\right)+\left(1+e_{1i}\right)o_{i,t}+e_{2i} \tag{4.46}$$

$$\varpi_{1i,t}=NS_i-\varpi_{i,t}^{B}/\Lambda_{3i} \tag{4.47}$$

$$\varpi_{2i,t}=NS_iEP_i-\varpi_{i,t}^{B}/\Lambda_{1i} \tag{4.48}$$

where C_i^{CR} denotes the emission cost of large industrial factories; Cap_i^{LIL}represents the emission cap; $\overline{D_t^{LIL,total}}$ and $\underline{D_t^{LIL,total}}$ represents the upper bounds and lower limits of the load that can be dispatched per unit time. Equation (4.37) ensures that the total load remains unchanged for a certain period which will not affect the production schedule. Equation (4.38) ensures that there will be no other peak power consumption due to the centralized shifting of loads. Another relevant constraint is shown in (4.9) before.

Equations (4.39)-(4.48) represent the IDC load constraints, which are casted based on the models proposed in [119]. In (4.39), the load of IDCs is composed of the baseline power consumption with the minimum quality of service (QoS) $\sigma_{i,t}^{base}$, the shiftable IDC load $\sigma_{i,t}^{SDL}$, and power consumption of IT equipment for high QoS in IDCs $\sigma_{i,t}^{HQoS}$. Λ_{1i} is the increased power consumption when a unit amount of IT equipment power consumption is introduced. In (4.40)-(4.48), Λ_{2i} presents the increased power consumption in IDC when processing a unit amount of workload with the minimum QoS, $\Lambda_{3i}$is the increased power load of an active server in IDC handling the maximum workload with the minimum QoS; $\varpi_{1i,t}$ indicates the number of inactive servers in IDC; $\varpi_{2i,t}$ denotes the margin of the IT equipment power consumption in IDC; in (4.44), NS_i is the number of servers in each IDC; EI_i, EP_i are idle and peak power of each server; NA_i, NE_i, and NC_i are the quantities of aggregate, edge, and core switch, and EA_i, EE_i, and EC_i are the corresponding rated power loads; u_i is the average service rate servers and w is tolerant service delay of workload; e_{1i} and e_{2i} denote the empirical constants of cooling system; e_{3i} represents the equivalent thermal resistance of IDC; $q^I_{i,t,y}$, $q^O_{i,t,y}$ are preset indoor and outdoor temperature; $o_{i,t,y}$ is the load of lighting and other equipment. Equation (4.40) illustrates the spatial load regulation potential among various IDCs. Equation (4.41) denotes load regulation limits under constrained computing resources, while equations (4.44)-(4.47) delineate the constraints on IDC power consumption associated with factors such as servers, workload, and environmental conditions. For a thorough proof and derivation process, further details can be found in [119].

4.4 Chapter Case Study

The proposed power system decarbonization transition approach is simulated on a modified IEEE 24-bus benchmark system. Within the proposed FIS framework, the supply side includes the retrofit of CCUS and the installation of P2G-PV and P2G-wind. In contrast, the demand side assesses the load dispatchability probability of LIL and IDC. Four sets of FIS models with three inputs and one output each were developed by incorporating the respective off-site factors and their potential influences. In two-stage system, stage I considers the generation expansion planning, especially the CCUS retrofit. Stage II studies the low carbon demand side response considering the carbon allowance and offsets trading of LILs and IDCs. Both stage I and II are mix-integer linear programming. The fuzzy algorithm and two-stage optimization programs are simulated on the MATLAB® platform, using a laptop equipped with a 3.4GHz Intel® Core i7-1260P and 16GB RAM. The solver in this chapter is Gurobi within the YALMIP toolbox. To streamline computations, this chapter combines five years as a single stage in case study. The basic parameters involving the transmission line susceptance of the IEEE 24-bus network are quoted from [32]. The system topology and main parameters of each FIS, involving the location, distance between CFPP and CO_2 storage location, capacity, remaining lifespan, average temperature, etc., are shown in the figure below. For remaining system parameters, this chapter derives historical data such as wind speed and solar radiation from the Australian Bureau of Meteorology

(BOM). The basic system load data can be obtained from AEMO. This chapter validates the proposed model and method using three cases:

Case 1: Base case, do not consider CCUS retrofit and carbon response on the demand side.

Case 2: The system considers supply-side investment only, which includes CCUS retrofit of CFPPs and installation of P2F-PV and P2G-Wind.

Case 3: The system simultaneously considers emission reduction modification on the supply side and active carbon response on the demand side.

Among cases 1-3, case 1 employs as the base case, and the primary function is to calculate essential system emissions and costs. The simulation results of Cases 2 and 3 can be utilized to verify the positive impact of CCUS retrofit and demand-side carbon response on emission reduction. The effectiveness of proposed model could be confirmed by comparing the outcomes of three cases.

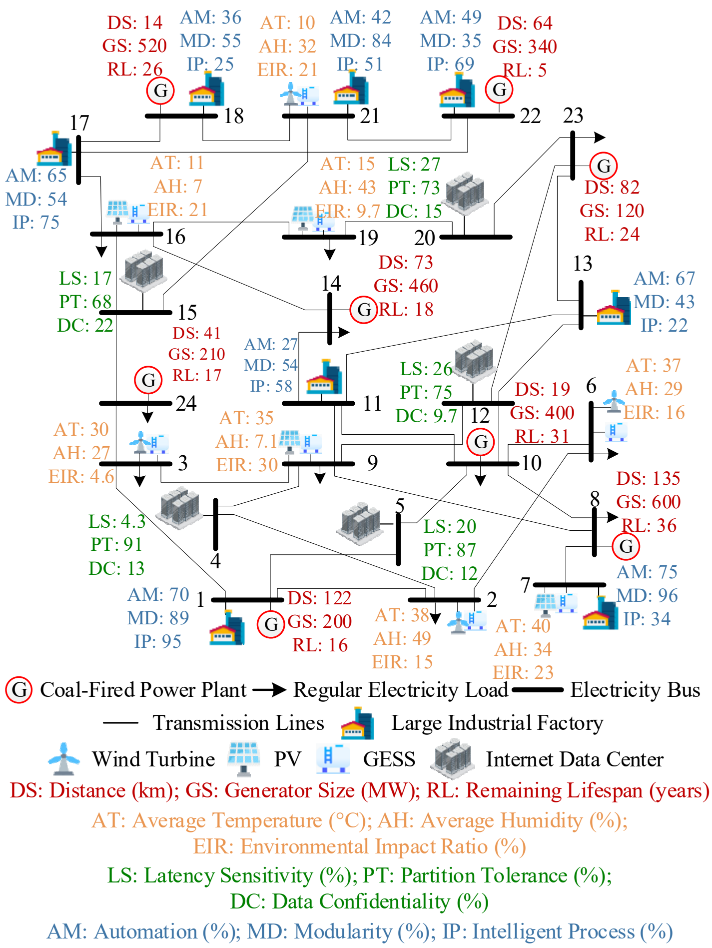

Figure 4-3 The system topology and main parameters

The output results of the fuzzy inference system are presented in Table 2. Concerning the installation and retrofitting of equipment, those with results lower than 0.5 are excluded from the candidate set. This implies that CFPPs situated in buses 1, 22, 23, and 24 are deemed unsuitable for CCUS retrofit. As for demand-side dispatchable loads, the obtained possibility necessitates multiplication by the traditional dispatchable upper limit to further limit its feasible range, thereby enhancing feasibility under real operating conditions.

TABLE 4-2 FUZZY RESULTS

Probability of CCUS Retrofit			
Bus 1	0.212	Bus 18	0.782
Bus 8	0.786	Bus 22	0.210
Bus 10	0.707	Bus 23	0.309
Bus 14	0.529	Bus 24	0.362
Probability of Install of P2G-PV or P2G-Wind			
P2G-PV		P2G-Wind	
Bus 7	0.673	Bus 2	0.620
Bus 9	0.563	Bus 3	0.789
Bus 16	0.689	Bus 6	0.741
Bus 19	0.724	Bus 21	0.778
Probability of LIL Load temporal dispatch			
Bus 1	0.791	Bus 17	0.648
Bus 7	0.722	Bus 18	0.465
Bus 11	0.509	Bus 21	0.678
Bus 13	0.551	Bus 22	0.577
Probability of IDC Load spatial dispatch			
Bus 4	0.827	Bus 15	0.694
Bus 5	0.807	Bus 20	0.689
Bus 12	0.720		

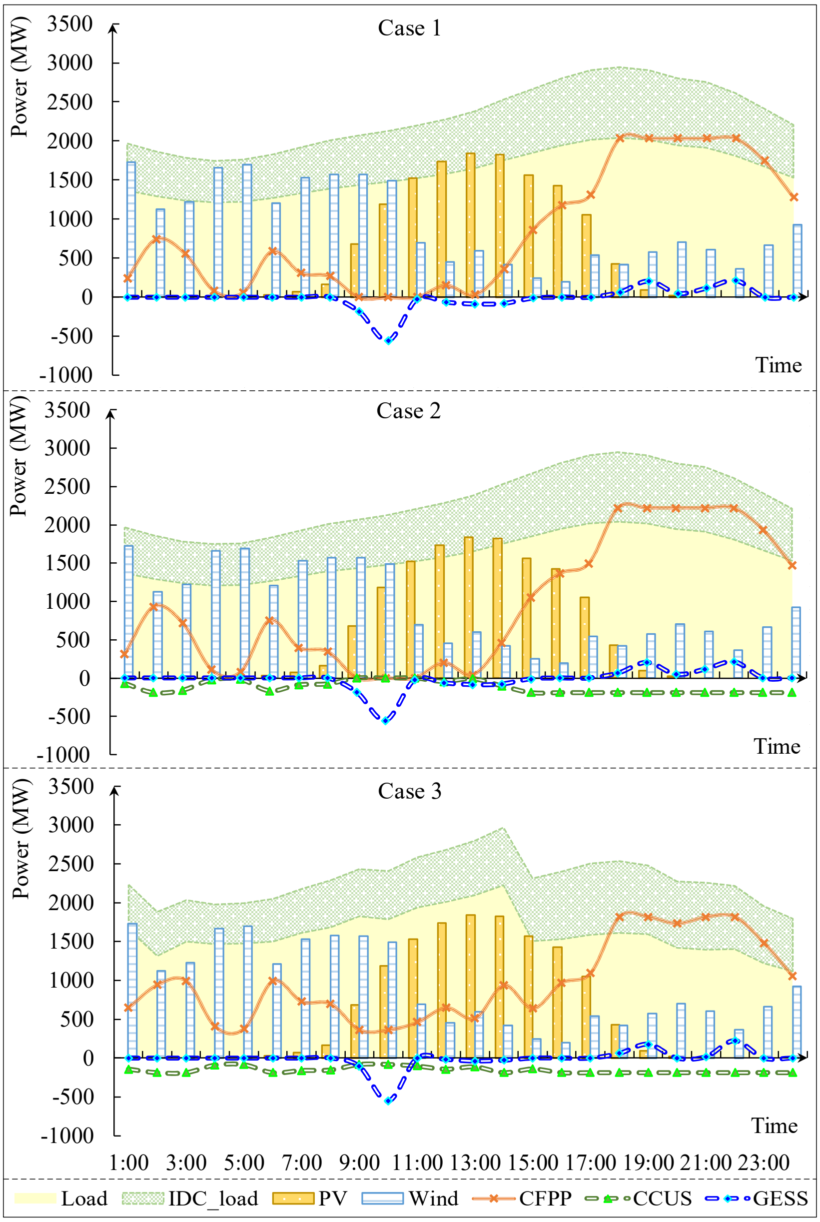

Figure 4-4 The system operating result.

The system operation results of Case 1-3 are illustrated in Figure 4-4. A comparison between Case 1 and Case 2 reveals that following CCUS retrofit of some CFPPs in Case 2, the power output of CFPPs increased due to reduced emission costs. Furthermore, before the demand-side carbon response in Case 3, the system peak load is mainly concentrated between 17:00 and 21:00, while renewable energy output peaks during the early morning and noon. This indicates that if the demand side can be flexibly adjusted based on carbon intensity, the system can effectively enhance renewable energy utilization and mitigate the output of high-emission power generation such as CFPPs.

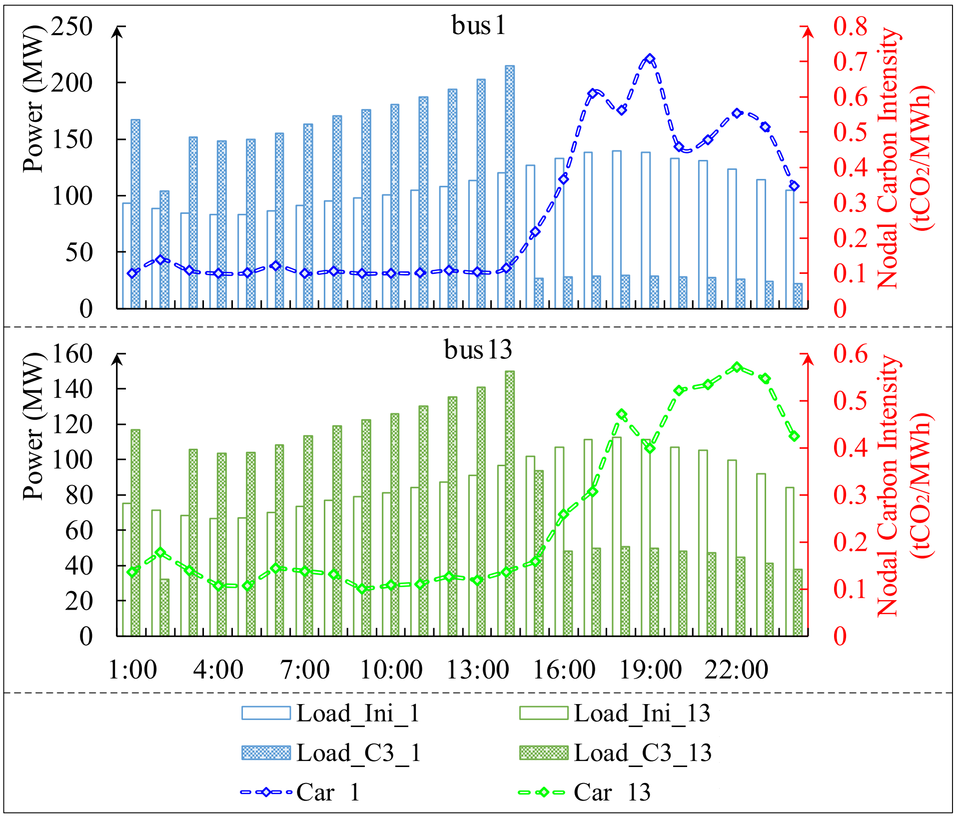

Figure 4-5 The LIL temporal carbon response result of Case 3.

The detailed low carbon demand response results are presented in Figures 4-5 and 4-6. Figure 4-5 displays the temporal carbon response of LIL, whereas Figure 4-6 shows the spatial carbon response of IDC load. In Figure 4-5, it's evident that the node carbon intensity is significantly higher in the evening period compared to the daytime. Consequently, LILs located on buses 1 and 13 in Case 3 opt to shift the load from evening to morning to respond to the real-time carbon intensity.

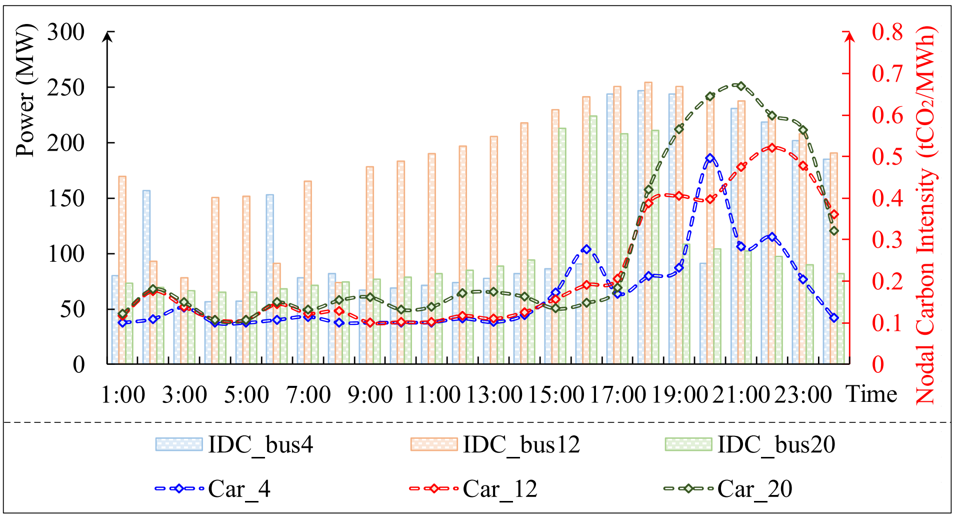

Figure 4-6 The IDC spatial carbon response result of Case 3.

Figure 4-6 highlights the IDC load located on three distinct buses and the carbon intensity of the corresponding buses. The difference from LIL is that the load scheduling of IDC does not occupy the transmission capacity of the power grid but balances the load between multiple IDCs in real time through virtual data flow to achieve spatial load scheduling. It can be found that during the evening period, when the carbon emission intensity of bus 20 is high, the IDC load of this bus is re-dispatched to other buses with lower carbon intensity. This effectively achieves carbon response in the spatial dimension. It should be noted that the average carbon intensity of the system tends to be higher during the night compared to the day. This elevated average carbon intensity during nighttime may lead to a less effective spatial carbon response from the IDC.

In Figure 4-7, a comparison of the CFPP emissions in each case reveals that the emissions of each CFPP in Case 1 are the highest among all cases. In Case 2, where CCUS is installed in the third and fourth CFPPs, the emissions of these two CFPPs are significantly reduced. Furthermore, the output of other CFPPs is also partially transferred to these two CFPPs, resulting in a slight reduction in emissions for all remaining CFPPs. Compared with the previous two cases, Case 3 shows that both the total emissions and the emissions of each CFPP have been further reduced. Therefore, it can be concluded that the method proposed in this chapter can effectively help the system to minimize emissions.

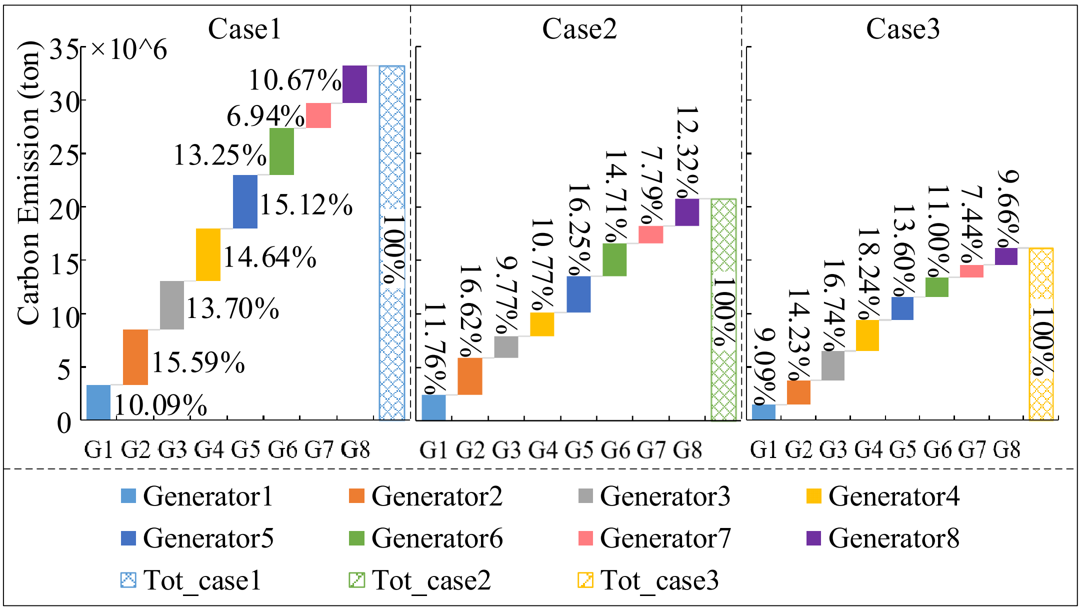

Figure 4-7 The carbon emission of CFPPs.

Combining the above results, Figure 4-8 compares the total system cost and emissions of each case. It can be seen that although Cases 2 and 3 increase the related costs of

CCUS retrofit, the significant reduction in emission costs can effectively help the system achieve a lower total cost. Therefore, it can be concluded that incorporating CCUS retrofit can effectively lower the total system emissions and decrease the overall system cost. Furthermore, integrating supply and demand-side emission reduction strategies can significantly enhance the overall system resource utilization efficiency while concurrently further reducing system emissions and costs.

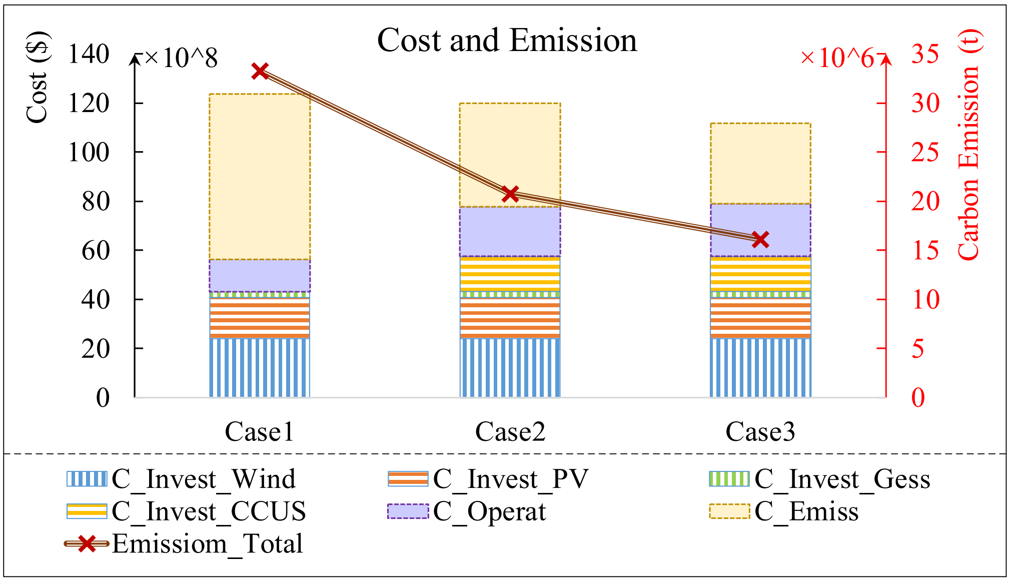

Figure 4-8 The comparison of total system cost and emission.

4.5 Chapter Summary

This chapter proposes a FIS-based integrated system decarbonization framework in two stages that consider CCUS retrofit and installation of P2G-PV and P2G-Wind on the generation side and active low-carbon response of LIL and IDC load on the demand side. In this framework, the four FISs respectively consider multiple off-site factors and obtain the corresponding narrowed candidate node set in the system. These factors jointly determine the optimal planning results. The experimental analysis demonstrates that the comprehensive consideration of both supply and demand-side emission reduction methods can effectively reduce system emissions while avoiding excessive costs. Collaboration between multiple sides can accelerate the realization of a clean, low-carbon power system. Moreover, the proposed FIS method can be used to pre-screen the candidate node set, which not only simplifies the optimization problem but also ensures that the obtained results are more practical. Since the proposed framework also mentions the trading aspect of the carbon market, in the future research, the power generation and demand sides can participate in the allowance bidding transaction in the carbon market rather than just being price takers. The bidding process can further improve the benefits of both parties and accelerate emission reduction while promoting market activity.

Chapter 5 Distribution Network Planning: A Spatial-temporal Carbon Response Method

In the above literature, it can be found that the existing studies may lack a planning approach that can consider both the emission reduction targets and the economic benefits of the system. When exclusively considering the carbon cost, the system's emission abatement outcome is easily affected by price signals, and it is also difficult to quantify the emission reduction amount explicitly. When only considering carbon target constraints, the system flexibility would be compromised, and excessive system planning costs may be elicited to achieve the emission reduction goal. Therefore, this chapter proposes a method based on an exterior point barrier function to embed traditional carbon constraints into objective function by penalizing solutions that violate the bounds of the constraints. This approach differs from the big-M method in that it can relax the relevant carbon constraints, effectively replacing the constrained problem with an unconstrained problem. Moreover, low carbon dispatch of distribution-side GDLs containing DDCs and MESSs is rarely studied, which can further reduce system emissions via its spatial-temporal carbon response features. To fill the existing research gaps, this chapter proposes a two-stage distribution network planning model incorporating both well-defined emission reduction targets and the spatial-temporal carbon response of GDLs.

5.1 Proposed Two-Stage System Framework

To specify the planning emission reduction targets while fully utilizing the system GDLs resources, this chapter establishes a two-stage low-carbon system planning framework, which is shown in Figure 5-1.

In the first stage, resembling our previous work [61], the uncertain parameters such as solar radiation intensity, the regular load of each bus, and the initial DDC load are predicted by a machine learning method GANs with an hourly resolution. In the following planning process, the important operating variables of the system such as whether the MESS is installed Ψ_m^{MESS}, the amount of charge $P_{m,i,t,y}^{MESS,ch}$ and discharge

$P_{m,i,t,y}^{MESS,dis}$, the number and location of photovoltaic (PV) installations Ψ_i^{re}, the output of various types of generators $P_{g,i,t,y}^{G}$, and the system power flow $P_{ij,t,y}$ can be obtained, and those values will be delivered to the CEF model and stage II. At this stage, an explicit emission reduction target ε is formulated through the exterior point method and embedded in the objective function, targeting emission mitigations to the maximum extent without affecting actual system costs. During the first iteration of the stage I model, the default position of the MESSs and the load of the DDCs do not move between different buses, so they can be regarded as fixed-position loads at that moment.

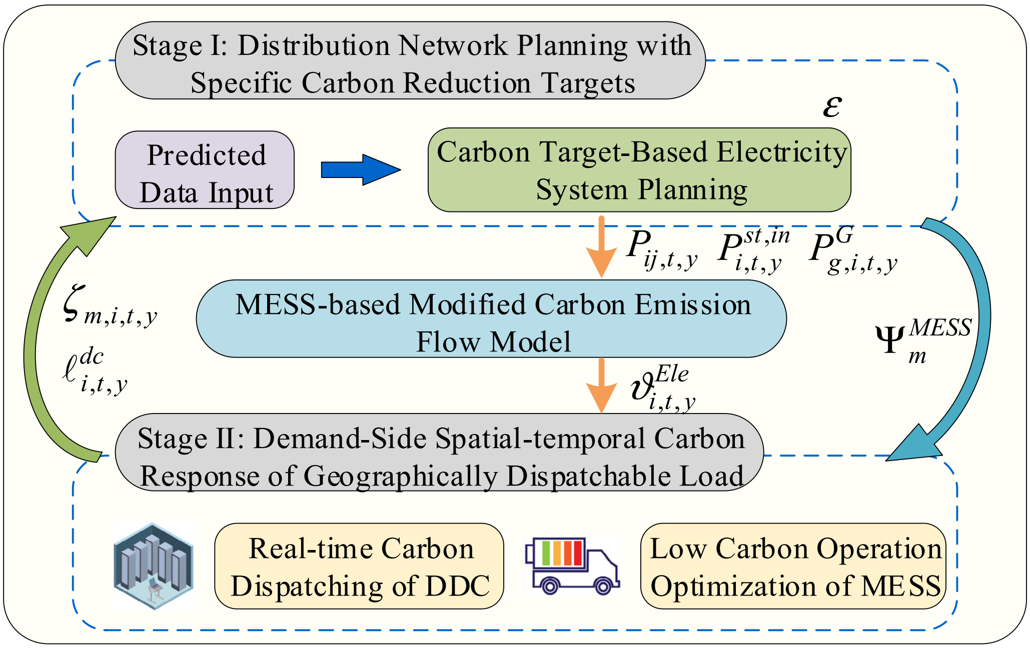

Figure 5-1 The two-stage low-carbon system planning framework

When the planning of the first stage is completed, it entails calculating the nodal carbon intensity $\vartheta_{i,t,y}^{Ele}$ through the MESS-based modified CEF model and substituting these values into the second stage. In the second stage, two categories of GDLs are mainly considered, namely MESSs and DDCs. Demand-side spatial-temporal carbon response can be achieved by shifting the GDLs from buses with high carbon intensity to buses with low carbon intensity. Wherein, MESSs optimize their charge and discharge position $\zeta_{m,i,t,y}$ in this stage according to the charge and discharge power figured out in the first stage. For DDCs, the load proportion of each DDC is adjusted via the data flow. After finalizing the second stage optimization, the information of each DDC load and the MESS location will be sent back to the first stage to complete an iteration.

The two-stage optimization framework proposed in this chapter integrates system planning and operation problems. In the first stage of planning, this chapter adopts the method of partitioning time into periods, wherein multiple typical daily data are selected as continuous periods for simulation during the total planning period of y years. The second stage simulates the spatial-temporal dispatch of GDLs on these typical days, ensuring that the time scales of the two stages are consistent.

5.2 The Proposed Mathematical Model

A. Carbon Targets-Based Planning Model

1) Conventional planning model considering carbon emissions

The planning problem considering carbon emissions is typically modelled as follows:

$$Min\, f = C^{in} + C^{car} \tag{5.1}$$

$$C^{car} = \begin{cases} \pi^{car} \cdot E^{car} & if\, \Psi^{car} = 1 \\ \pi^{cap}\left(E^{car} - CAP\right) & else \end{cases} \tag{5.2}$$

$$s.t.\; A^T P_{ij} + P^G = P^D \tag{5.3}$$

$$P_{ij} - B_{ij}\left(\theta_i - \theta_j\right) = 0 \tag{5.4}$$

$$\left|P_{ij}\right| \le \overline{P_{ij}}, 0 \le P^G \le \overline{P^G} \tag{5.5}$$

$$E^{car} = P^G \vartheta^G, \sum E^{car} \le e^{target} \tag{5.6}$$

where C^{in} and C^{car} are the investment cost and carbon cost in the system; C^{in} usually consists of line investment and generators installation cost; Ψ^{car} is a binary variable, when Ψ^{car} is equal to 1 or 0, C^{car} is composed of the carbon tax or carbon allowance cost, respectively; E^{car}, CAP, π^{car}, π^{cap} separately represent the generator emission, generator carbon allowance, carbon tax price, and carbon allowance trading price. In the constraints part, equation (5.3) is the nodal balance constraints; A, P_{ij}, P^G, P^D are vectors of node-branch incidence, power flow, power generation, and load, respectively. Equation (5.4) is power flow constraint, where B_{ij} is the susceptance between bus $i-j$, θ_i, θ_j are voltage angles of bus i and j. Equation (5.5) restricts variables cannot exceed the limit, and $\overline{(\bullet)}$ means the rated capacity, namely the upper limit. Equation (5.6) is the carbon target constraint, where

E^{car} is calculated by power generation times generation carbon intensity ϑ^G, and the total generator emission should be less than an emission target e^{target}.

From the aforementioned models, the conventional method in regard to carbon emissions reduction is mainly divided into two threads, i.e., considering emission costs or carbon target constraints. If only the emission cost is considered, the setting of the cost coefficient will greatly affect the result of system emission reduction. Each planning scheme has its own maximum emission reduction limit, and the carbon cost factor cannot guarantee that the current planning results can successfully achieve the emission reduction target. Inconsistent with considering the carbon cost, if the emission constraints are taken into account, although the planning result will definitely fulfill the emission reduction requirements, excess system costs will be paid in order to achieve the emission mitigation target, which is not conducive to the system's economic benefits. Moreover, as mentioned earlier, there are countries such as Germany that have modified their net-zero emissions grid plan, and such policy changes can cause unnecessary economic damage to the system.

2) Proposed carbon targets-based planning model

Due to the vast aspects of uncertainties during the planning process, the investment and operation costs may be enormous to guarantee the achievement of the emission target under all scenarios. With a specific emission reduction target, it is more practical to obtain the optimal planning scheme that has an acceptable system emission upper bound.

$$\left(\sum P^G \vartheta^G\right) \leq e^{target} \tag{5.7}$$

$$f(e) = \sum P^G \vartheta^G - e^{target} \leq 0 \tag{5.8}$$

where this specific emission reduction target is incorporated into the objective function by the exterior point method [108]. This method is essentially adding a penalty to violated constraints (or infeasible solution points), without penalty at feasible points. The entire iterative process is to search the outside region solutions (i.e., exterior point). Subsequently, the barrier function regarding the emission target can be defined.

$$\varepsilon = \left[\max\left\{0, f(e)\right\}\right]^2 \tag{5.9}$$

The quadratic form of the barrier function is a consensus express method in the exterior point method [108]. When $f(e) \leq 0$, the value of ε is equal to 0, and the emission target has been achieved. Otherwise $\varepsilon = [f(e)]^2$. So far, the objective function (5.1) can be modified as follow:

$$C^{in}+C^{car}+\Lambda_{\varepsilon}\varepsilon \tag{5.10}$$

From carbon targets-based objective functions (5.7)-(5.10), it can be found that when the system's total emissions are less than the preset carbon target (that is, the variable in feasible point), the carbon target penalty coefficient $\Lambda_\varepsilon$will be invalid. However, when the emissions are greater than the carbon target (infeasible point), according to the different Λ_ε values, the penalty item will urge the system to curb emissions to the maximum extent. It should be noted that the penalty term will not be included in the actual system cost during the cost settlement. Meanwhile, when Λ_ε is set to an enormous value, the effect of the penalty term will be similar to the carbon target constraint.

B. MESS-based modified CEF model

In general, the nodal carbon intensity of different buses is related to two factors, namely the incoming power from other buses and the local generator power injection of the current bus [17]. However, as ESS has been considered, the nodal carbon intensity will be further changed as the charge and discharge of ESS [118] since that ESS is different from other types of loads. The ESS does not directly consume the power during the charging process but stores it. Therefore, a certain amount of carbon intensity will be stored inside the ESS during this period. The change of carbon intensity inside the ESS during charging and discharging is shown in Figure 5-2.

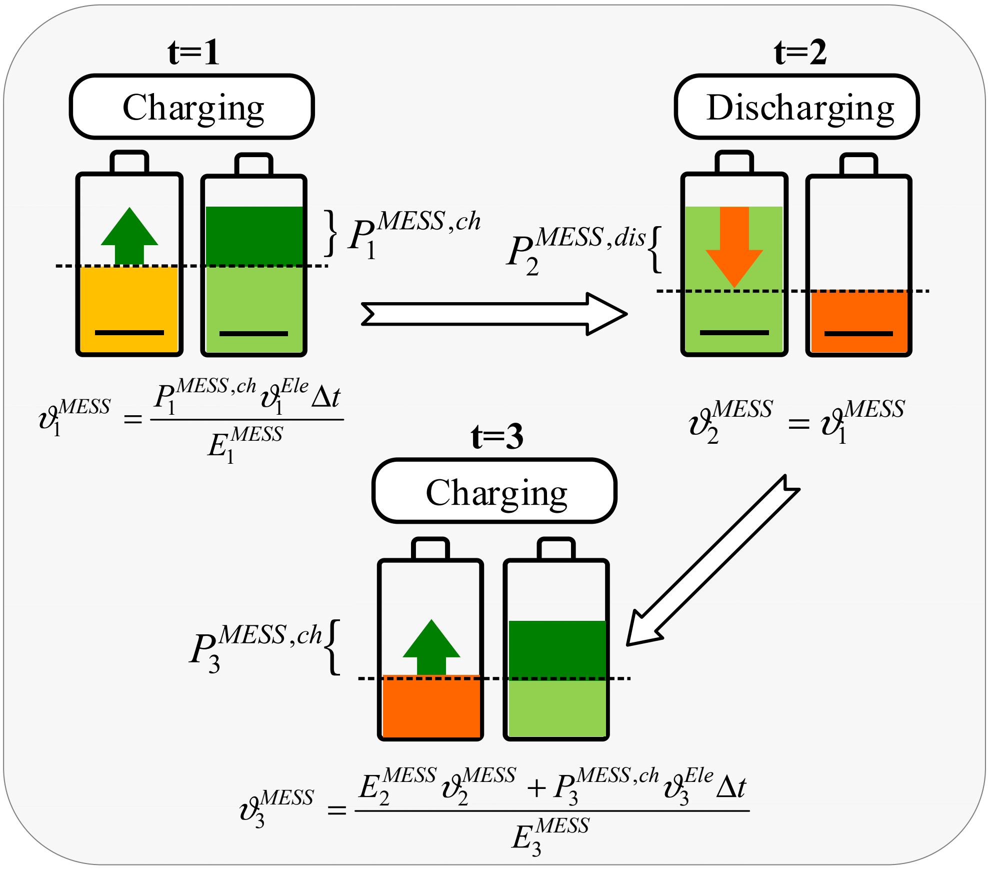

Figure 5-2 The change of carbon intensity inside the ESS

The ESS can be interpreted as a container, in which the internal electricity can be regarded as clean water [118]. As shown in Figure 5-2, when the ESS is charging, it can be understood as supplementing new liquid (e.g., saline) to the container. This process certainly changes the salt concentration of the liquid in the container. However, during the discharge process, its internal carbon intensity will not be changed. Mathematically, this process can be expressed as:

$$e_{m,i,t,y}^{MESS} = \begin{Bmatrix} \left(E_{m,i,t-1,y}^{MESS} \cdot \vartheta_{m,t-1,y}^{MESS}\right) \\ + \sum_{i \in \Omega^{M,bus}} \left(P_{m,i,t,y}^{MESS,ch} \cdot \vartheta_{i,t,y}^{Ele} \cdot \Delta t\right) \end{Bmatrix} \tag{5.11}$$

$$\vartheta_{m,t,y}^{MESS} = \begin{cases} \vartheta_{m,t-1,y}^{MESS}, & if \ P_{m,i,t,y}^{MESS,ch} = 0 \\ \dfrac{e_{m,i,t,y}^{MESS}}{E_{m,i,t,y}^{MESS}}, & else \end{cases} \tag{5.12}$$

where $e_{m,i,t,y}^{MESS}$ is the virtual emission volume of mth MESS at bus i, time t, year y; $E_{m,i,t-1,y}^{MESS}$ and $\vartheta_{m,t-1,y}^{MESS}$ denote the energy storage and internal carbon intensity of

MESS at $t-1$ time; $P_{m,i,t,y}^{MESS,ch}$ is the charging power and $\vartheta_{i,t,y}^{Ele}$ is the nodal carbon intensity at the corresponding bus; $\Omega^{M,bus}$ is the set of bus locations of MESS; Δt represents the time step. Equation (5.12) indicates that when the charging power $P_{m,i,t,y}^{MESS,ch}$ is equal to 0 at time t, the internal carbon intensity of the MESS is equal to its value at the previous time. Otherwise, it is the quotient of $e_{m,i,t,y}^{MESS}$ and $E_{m,i,t,y}^{MESS}$.

Different from stationary ESS, MESS can move between different buses, the schematic diagram is shown in figure 5-3:

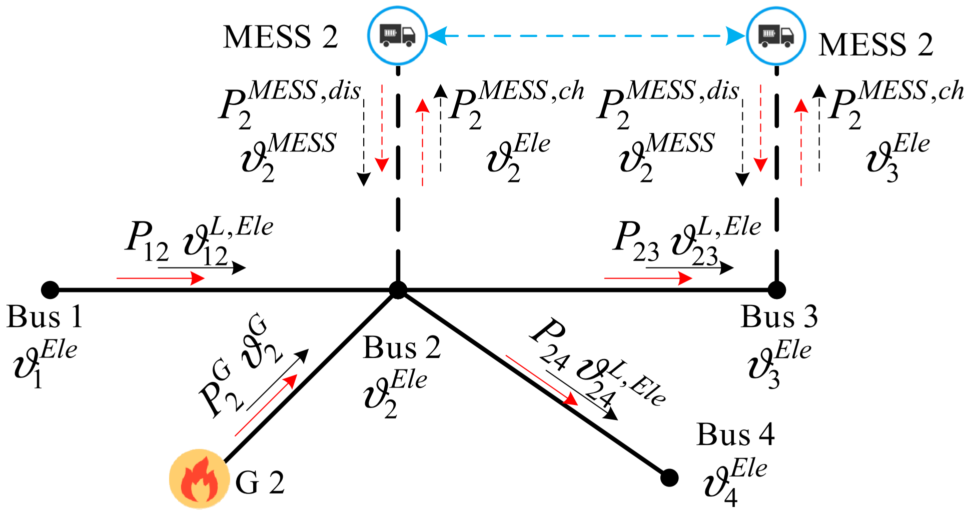

Figure 5-3 The core idea of CEF model with MESS

As can be seen from the Figure 5-3, the difference from the conventional CEF is that when the MESS is located in bus 2 and bus 3, the corresponding carbon intensities of the charging power are ϑ_2^{Ele} and ϑ_3^{Ele}, which will affect the internal carbon intensity ϑ_2^{MESS} of the MESS. This will further affect the system's carbon intensity during discharge. The mathematical model of the MESS-based CEF can be formulated as follows:

$$\vartheta_{i,t,y}^{Ele} = \frac{\left\{ \begin{array}{l} P_{g,i,t,y}^{G}\vartheta_{g,i,t,y}^{G} + P_{m,i,t,y}^{MESS,dis}\vartheta_{m,t,y}^{MESS} \\ + \sum\limits_{j\in P^{+}} \left(P_{ij,t,y}\vartheta_{ij,t,y}^{L,Ele} \right) \end{array} \right\}}{\left\{ \begin{array}{l} P_{g,i,t,y}^{G} + P_{i,t,y}^{re} + P_{m,i,t,y}^{MESS,dis} \\ + \sum\limits_{j\in P^{+}} \left(P_{ij,t,y} \right) \end{array} \right\}} \tag{5.13}$$

$$\vartheta_{ij,t,y}^{L,Ele} = \begin{cases} \vartheta_{i,t,y}^{Ele}, & if\ P_{ij,t,y} \geq 0 \\ \vartheta_{j,t,y}^{Ele}, & if\ P_{ij,t,y} \leq 0 \end{cases} \tag{5.14}$$

where $P^{G}_{g,i,t,y}$, $\vartheta^{G}_{g,i,t,y}$ are active power output of gth type of generator and its generation carbon intensity; $P^{MESS,dis}_{m,i,t,y}$ is the discharging power of MESS; P^{+} denotes the power inflowing into bus j; $\vartheta^{L,Ele}_{ij,t,y}$ represents the branch carbon intensity between bus i and j; $P^{re}_{i,t,y}$ is the active renewable energy power output.

Based on the above equations, it can be seen that the charging and discharging of MESS will affect the nodal carbon intensity of different buses. Hence, the spatial-temporal carbon response can be applied by dispatching MESS.

5.3Stage I, Distribution Network Planning with A Specific Emission Reduction Target

The objective of the first stage is to minimize the total system cost while limiting system carbon emission in a certain range. In objective function, the aforementioned equation in Section III can be embedded, and a specific emission reduction target can be considered in the proposed model, which is formulated as follows:

$$Min\ J=\left\{\frac{\left(C^{in}+\Lambda_{\varepsilon}\varepsilon\right)}{\left(1+\lambda\right)^{Y}}+\sum_{y=1}^{Y}\frac{\left(C^{op}_{y}+C^{mt}_{y}+C^{car}_{y}\right)}{\left(1+\lambda\right)^{y}}\right\} \tag{5.15}$$

where λ and Y are the discount rate and total planning years; C^{in}, C^{op}_{y}, C^{mt}_{y}, and C^{car}_{y} indicate the investment cost, operating cost, maintenance cost, and environmental cost, respectively; $\Lambda_{\varepsilon}\varepsilon$ represents the carbon target penalty.

The investment-related cost can be divided into four parts, namely, the expansion cost of substation capacity C^{ep}_{ST}, the investment cost of renewable energy devices C^{in}_{re} and MESSs C^{in}_{MESS}, and the retirement cost of generators C^{retire}_{G}.

$$C^{in} = C_{ST}^{ep} + C_{re}^{in} + C_{MESS}^{in} + C_{G}^{retire}$$
$$= \left\{ \begin{array}{l} \sum_{i \in \Omega^{ST,bus}} \left(\pi_i^{st,ep} \cdot \overline{P_i^{st}} \cdot \Psi_i^{st} \right) \\ + \sum_{i \in \Omega^{R,bus}} \left(\pi_i^{re} \cdot \overline{P_i^{re}} \cdot \Psi_i^{re} \right) \\ + \sum_{m \in \Omega^{MESS}} \left(\pi_m^{MESS} \cdot \overline{E_m^{MESS}} \cdot \Psi_m^{MESS} \right) \\ + \sum_{g \in \Omega^{G}} \sum_{i \in \Omega^{G,bus}} \left(\tau_g - \varsigma_g \right) \Psi_{g,i}^{retire} \end{array} \right\} \tag{5.16}$$

where $\Omega^{ST,bus}$, $\Omega^{R,bus}$, Ω^{MESS}, Ω^{G}, $\Omega^{G,bus}$ denote the set of bus locations of substations, bus locations of renewable energy devices, MESSs, types of generators, and bus locations of generators, respectively; $\pi_i^{st,ep}$, π_i^{re}, π_m^{MESS} are the per-unit cost of substation, renewable energy devices, and MESSs; τ_g and ς_g represent the uninstallation and salvage cost of generators; Ψ_i^{st}, Ψ_i^{re} are integer variables, which decide to expand the substation and install the renewable energy devices at bus i; Ψ_m^{MESS} and $\Psi_{g,i}^{retire}$ are decision variables that determine whether the mth MESS should be installed and the gth type of generators should be retired.

The system operation cost is formulated as follows, which includes the operating cost of generators C_G^{op}, substation C_{ST}^{op}, and MESSs C_{MESS}^{op}.

$$C_y^{op} = C_G^{op} + C_{ST}^{op} + C_{MESS}^{op}$$
$$= \sum_{k \in K} \sum_{t \in T} \left\{ \begin{array}{l} \omega_k \times \\ \left[\begin{array}{l} \sum_{g \in \Omega^{G}} \sum_{i \in \Omega^{G,bus}} \left[\begin{array}{l} a_g \left(P_{g,i,t,y}^{G} \right)^2 \\ + b_g P_{g,i,t,y}^{G} + c_g \end{array} \right] \\ + \sum_{i \in \Omega^{ST,bus}} \left(\pi_{i,t,y}^{st,in} P_{i,t,y}^{st,in} + \pi_{i,t,y}^{st,out} P_{i,t,y}^{st,out} \right) \\ + \sum_{m \in \Omega^{MESS}} \pi_{m,y}^{op,MESS} \left(1 - \sum_{ij \in \Omega^{M,bus}} \tau_{m,ij,t,y}^{MESS} \right) \end{array} \right] \end{array} \right\} \tag{5.17}$$

where a_g, b_g, and c_g denote the cost coefficient of generators; ω_k is the probability weight of the kth scenario appearance in the set of all scenarios K; $P_{i,t,y}^{st,in}$, $P_{i,t,y}^{st,out}$, $\pi_{i,t,y}^{st,in}$ and $\pi_{i,t,y}^{st,out}$ are the active power inflow and outflow from the substation and the corresponding price, respectively; $\pi_{m,y}^{op,MESS}$ represents the unit distance movement cost of MESSs; $\tau_{m,ij,t,y}^{MESS}$ means whether mth MESS travels from bus i to j at time t.

The total maintenance cost consists of that for generators C_G^{mt}, renewable energy devices C_{re}^{mt}, and MESSs C_{MESS}^{mt}. The variable of $\pi_{g,y}^{mt}$, $\pi_{i,y}^{mt,re}$, $\pi_{i,y}^{mt,st}$, and $\pi_{m,y}^{mt,MESS}$ represent the maintenance cost of corresponding devices. Their values are assumed to be 3%-10% of their investment cost empirically.

$$\begin{aligned} C_y^{mt} &= C_G^{mt} + C_{re}^{mt} + C_{MESS}^{mt} \\ &= \sum_{k\in K} \left\{ \begin{aligned} &\omega_k \times \\ &\left[\begin{aligned} &\sum_{g\in\Omega^G} \sum_{i\in\Omega^{G,bus}} \left[\pi_{g,y}^{mt} \cdot \left(1-\Psi_{g,i}^{retire}\right) \right] \\ &+ \sum_{i\in\Omega^{R,bus}} \left(\pi_{i,y}^{mt,re} \cdot \overline{P_i^{re}} \cdot \Psi_i^{re} \right) \\ &+ \sum_{i\in\Omega^{ST,bus}} \left(\pi_{i,y}^{mt,st} \cdot \overline{P_i^{st}} \right) \left(1+\Psi_i^{st}\right) \\ &+ \sum_{m\in\Omega^{MESS}} \left(\pi_{m,y}^{mt,MESS} \cdot \overline{E_m^{MESS}} \cdot \Psi_m^{MESS} \right) \end{aligned} \right] \end{aligned} \right\} \end{aligned} \tag{5.18}$$

The environmental cost in this chapter is determined by the carbon tax. It should be noted that although MESS affects the system's carbon flow, it does not generate emissions by itself. System emissions are ejected from substations and various types of generators.

$$C_y^{car} = \sum_{k\in K} \sum_{t\in T} \left\{ \begin{aligned} &\omega_k \times \\ &\left[\begin{aligned} &\sum_{g\in\Omega^G} \sum_{i\in\Omega^{G,bus}} \left(\pi_{g,y}^{car} \cdot P_{g,i,t,y}^G \cdot \vartheta_{g,i,t,y}^G \right) \\ &+ \sum_{i\in\Omega^{ST,bus}} \left(\pi_{i,y}^{car} \cdot P_{i,t,y}^{st,in} \cdot \vartheta_{i,t,y}^{st} \right) \end{aligned} \right] \end{aligned} \right\} \tag{5.19}$$

where $\pi_{g,y}^{car}$ and $\pi_{i,y}^{car}$ are the carbon tax price of generators and the substation; $\vartheta_{i,t,y}^{st}$ denotes the carbon intensity of the substation, the value of which mainly depends on the upstream main grid.

Similar to equations (5.8)-(5.9), in equation (5.20), $f(e)$ is the barrier function with regard to the system carbon target. The modeling process of equations (5.20)-(5.21) has been discussed in detail in Section III.

$$f\left(e\right)=\sum_{t\in T}\left(\begin{array}{l}\sum_{g\in\Omega^{G}}\sum_{i\in\Omega^{G,bus}}P_{g,i,t,y}^{G}\cdot\vartheta_{g,i,t,y}^{G}\\+\sum_{i\in\Omega^{ST,bus}}P_{i,t,y}^{st,in}\cdot\vartheta_{i,t,y}^{st}\end{array}\right)-e_{y}^{target}\leq 0 \tag{5.20}$$

$$\varepsilon=\left[\max\left\{0,f\left(e\right)\right\}\right]^{2} \tag{5.21}$$

The constraints of the stage I objective function are expressed below:

$$\left(\begin{array}{l}P_{i,t,y}^{st,in}-P_{i,t,y}^{st,out}+\sum_{g\in\Omega^{G}}P_{g,i,t,y}^{G}+P_{i,t,y}^{re}\\+P_{m,i,t,y}^{MESS,dis}-P_{m,i,t,y}^{MESS,ch}-P_{i,t,y}^{D}-\ell_{i,t,y}^{ddc}\end{array}\right)=\left[\begin{array}{l}\sum_{zi\in\Omega^{bus}}P_{zi,t,y}\\-\sum_{ij\in\Omega^{bus}}P_{ij,t,y}\end{array}\right] \tag{5.22}$$

$$Q_{i,t,y}^{st,in}-Q_{i,t,y}^{st,out}+Q_{i,t,y}^{re}-\mathrm{Q}_{i,t,y}^{D}=\sum_{zi\in\Omega^{bus}}Q_{zi,t,y}-\sum_{ij\in\Omega^{bus}}Q_{ij,t,y} \tag{5.23}$$

$$V_{j,t,y}=V_{i,t,y}+\frac{P_{ij,t,y}R_{ij}+Q_{ij,t,y}X_{ij}}{V_{0}} \tag{5.24}$$

$$\begin{cases}\underline{V}\leq V_{i,t,y}\leq\overline{V}\\0\leq P_{ij,t,y}^{2}+Q_{ij,t,y}^{2}\leq\overline{S_{ij}}^{2}\end{cases} \tag{5.25}$$

$$\left|Q_{i,t,y}^{re}\right|\leq P_{i,t,y}^{re}\cdot\tan\theta \tag{5.26}$$

$$E_{m,i,t+1,y}^{MESS}=\left\{\begin{array}{l}E_{m,i,t,y}^{MESS}+\sum_{i\in\Omega^{M,bus}}\left(P_{m,i,t,y}^{MESS,ch}\cdot u_{m}^{eff,ch}\right)\Delta t\\-\sum_{i\in\Omega^{M,bus}}\left(P_{m,i,t,y}^{MESS,dis}/u_{m}^{eff,dis}\right)\Delta t\end{array}\right\} \tag{5.27}$$

$$0\leq E_{m,i,t,y}^{MESS}\leq\overline{E_{m}^{MESS}}\cdot\Psi_{m}^{MESS} \tag{5.28}$$

$$\begin{cases}0\leq P_{m,i,t,y}^{MESS,ch}\leq\overline{P_{m,i,t,y}^{MESS,ch}}\cdot\zeta_{m,i,t,y}\\0\leq P_{m,i,t,y}^{MESS,dis}\leq\overline{P_{m,i,t,y}^{MESS,dis}}\cdot\zeta_{m,i,t,y}\end{cases} \tag{5.29}$$

$$0\leq P_{g,i,t,y}^{G}\leq\overline{P_{g,i}^{G}}\cdot\left(1-\Psi_{g,i}^{retire}\right) \tag{5.30}$$

$$P_{i,t,y}^{re}=g_{i,t,y}^{re}\cdot\Psi_{i}^{re} \tag{5.31}$$

$$\begin{cases}0\leq {P_{i,t,y}^{st,in}}^{2}+{Q_{i,t,y}^{st,in}}^{2}\leq\overline{S_{i}^{st}}^{2}\cdot\left(1+\Psi_{i}^{st}\right)\\0\leq {P_{i,t,y}^{st,out}}^{2}+{Q_{i,t,y}^{st,out}}^{2}\leq\overline{S_{i}^{st}}^{2}\cdot\left(1+\Psi_{i}^{st}\right)\end{cases} \tag{5.32}$$

$$\begin{cases}0\leq\Psi_{m}^{MESS}\leq\overline{\Psi_{m}^{MESS}}\\0\leq\Psi_{i}^{re}\leq\overline{\Psi_{i}^{re}}\\0\leq\Psi_{g,i}^{retire}\leq\overline{\Psi_{g,i}^{retire}}\\0\leq\Psi_{i}^{st}\leq\overline{\Psi_{i}^{st}}\end{cases} \tag{5.33}$$

Equations (5.22)-(5.24) are the branch power flow model in linearized Distflow format, while equations (5.22) and (5.23) denote the active and reactive power balance of each bus; where $\ell_{i,t,y}^{ddc}$ indicates the DDC load, which can be obtained from stage II results; $P_{zi,t,y}$ and $P_{ij,t,y}$ represent the active inflow and outflow power at bus i, when $i = 1$, $P_{zi,t,y} = 0$; Ω^{bus} is the set of bus location; $Q_{i,t,y}^{re}$ and $Q_{i,t,y}^{D}$ are the reactive power output and load; $Q_{zi,t,y}$ and $Q_{ij,t,y}$ are the reactive power flow, when $i = 1$, $Q_{zi,t,y} = 0$; $Q_{i,t,y}^{st,in}$, $Q_{i,t,y}^{st,out}$ are the reactive power inflow and outflow from the substation. Equation (5.24) describes the relationship between node voltage and power inflow (active and reactive), where $V_{j,t,y}$, $V_{i,t,y}$ and V_0 denote the node voltage magnitude at each bus and the slack bus voltage; R_{ij} and X_{ij} indicate the resistance and reactance of branch ij. Equation (5.25) is the upper and lower bound of bus voltage and feeder complex power, where $\underline{(\bullet)}$ means the lower bound of variables, $\overline{S_{ij}}$ is the rated complex power capacity of feeder. The power factor constraint of the renewable energy devices is shown in (5.26), where $tan\,\theta$ =0.48 means that the power factor is always between 0.9 leading or lagging. Equations (5.27)-(5.29) indicate the process of MESS charging and discharging, where $u_m^{eff,ch}$ and $u_m^{eff,dis}$ are the charging and discharging efficiency of MESS; $\zeta_{m,i,t,y}$ represents whether mth MESS parks at bus i at time t, which can be derived from stage II results. Equation (5.30) reflects the generator power limit when it has not been retired. In (5.31), $g_{i,t,y}^{re}$ denotes the power output function of renewable energy devices. Equations (5.32) and (5.33) indicate the maximum power of the substation and the upper bound of each decision variable, where $\overline{S_i^{st}}$ indicates the rated complex power of substation.

Compared with the original planning method, i.e., equations (5.1)-(5.6), a penalty function term associated with carbon targets is introduced in the proposed planning model and the carbon cost is considered jointly as well. Meanwhile, the proposed MESS and DDC loads further improve the system's flexibility. After this stage, variables such as power flow, and generator output will be substituted into the optimization process of CEF and the second stage as parameters.

5.4Stage II, Low Carbon Operating with The Spatial-Temporal Carbon Response Model of GDLs

A. MESS-based modified CEF model

Before the second-stage optimization, the node carbon intensity of each bus entails to be calculated, the model of which is formulated as follows:

(5.11)-(5.14)

After solving the nodal carbon intensity $\vartheta_{i,t,y}^{Ele}$ of each bus, the second stage optimization process will be conducted as follows.

B. Low Carbon Spatial-Temporal Schedule of Geographical Dispatchable Loads

The objective function of stage II is to minimize the total emission of GDLs, which is shown below:

$$Min \sum_{\kappa\in K}\sum_{y=1}^{Y}\sum_{t\in T}\left\{\begin{aligned}&\omega_k\times\\&\left[\begin{aligned}&\sum_{i\in\Omega^{D,bus}}\vartheta_{i,t,y}^{Ele}\cdot\ell_{i,t,y}^{ddc}\\&+\sum_{i\in\Omega^{M,bus}}\vartheta_{i,t,y}^{Ele}\cdot P_{m,i,t,y}^{MESS,ch}\cdot\zeta_{m,i,t,y}\\&-\sum_{i\in\Omega^{M,bus}}\vartheta_{i,t,y}^{Ele}\cdot P_{m,i,t,y}^{MESS,dis}\cdot\zeta_{m,i,t,y}\end{aligned}\right]\end{aligned}\right\} \tag{5.34}$$

where $\Omega^{D,bus}$ is the set of bus locations of DDCs.

The constraints of dispatching of DDCs and MESSs are formulated as follows:

$$\ell_{i,t,y}^{ddc}=\ell_{i,t,y}^{base}+\ell_{i,t,y}^{GLB} \tag{5.35}$$

$$\sum_{i\in\Omega^{D,bus}}\left(\ell_{i,t,y}^{GLB}/\varphi_{1i}\right)=0 \tag{5.36}$$

$$\ell_{i,t,y}^{GLB}\le\varphi_{i,t,y}^{B} \tag{5.37}$$

$$-\ell_{i,t,y}^{GLB}/\varphi_{2i}\le\Gamma_{1i,t,y} \tag{5.38}$$

$$\varphi_{1i}=\left(1+e_{1i}\right)\left[\frac{\left(\dfrac{NE_iEE_i+NA_iEA_i+NC_iEC_i}{NS_i}+EI_i\right)}{\left(u_i-\dfrac{1}{w}\right)+\left(\dfrac{EP_i-EI_i}{u_i}\right)}\right] \tag{5.39}$$

$$\varphi_{2i} = \varphi_{1i} \cdot \left(u_i - \frac{1}{w} \right) \tag{5.40}$$

$$\ell_{i,t,y}^{base} = \varphi_{i,t,y}^{B} + \left(e_{1i} / e_{3i} \right) \left(q_{i,t,y}^{O} - q_{i,t,y}^{I} \right) + \left(1 + e_{1i} \right) o_{i,t,y} + e_{2i} \tag{5.41}$$

$$\Gamma_{1i,t,y} = NS_i - \varphi_{i,t,y}^{B} / \varphi_{2i} \tag{5.42}$$

$$\zeta_{m,i,t,y} \le 1 - \sum_{i \in \Omega^{M,bus}} \sum_{j \in \Omega^{M,bus}} \tau_{m,ij,t,y}^{MESS} \tag{5.43}$$

$$\sum_{m \in \Omega^{MESS}} \sum_{i \in \Omega^{M,bus}} \zeta_{m,i,t,y} \le 1 \tag{5.44}$$

$$\alpha_{m,i,t,y} - \delta_{m,i,t,y} = \zeta_{m,i,t,y} - \zeta_{m,i,t-1,y} \tag{5.45}$$

$$\sum_{i \in \Omega^{M,bus}} \left(\alpha_{m,i,t,y} + \delta_{m,i,t,y} \right) \le 1 \tag{5.46}$$

$$\sum_{j \in \Omega^{M,bus}} \tau_{m,ij,t,y}^{MESS} \ge \delta_{m,i,t,y} \tag{5.47}$$

$$\alpha_{m,i,t,y} - \lambda_{m,i,t,y} = \sum_{i \in \Omega^{M,bus}} \left(\tau_{m,ij,t,y}^{MESS} - \tau_{m,ij,t-1,y}^{MESS} \right) \tag{5.48}$$

$$\sum_{i \in \Omega^{M,bus}} \left(\alpha_{m,i,t,y} + \lambda_{m,i,t,y} \right) \le 1 \tag{5.49}$$

$$\tau_{m,ij,t,y}^{MESS} \ge \tau_{m,ij,t-1,y}^{MESS} - \tau_{m,ij,t-TD,y}^{MESS} \tag{5.50}$$

Equations (5.35)-(5.42) are the DDC load constraints, which are casted based on the models proposed in [120]. In (5.35), the DDC load is composed of the baseline power consumption with the minimum quality of service (QoS) $\ell_{i,t,y}^{base}$ and regulated power load $\ell_{i,t,y}^{GLB}$. Equation (5.36) indicates the spatial coupling of load regulation potential between different DDCs. Equations (5.37) and (5.38) are DDCs' maximum dispatchable load, and load regulation limits under limited computing resources, where φ_{1i} and φ_{2i} are the increased power consumption in DDC when processing a unit amount of workload with the minimum QoS, and the increased power load of an active server in DDC handling the maximum workload with the minimum QoS; $\varphi_{i,t,y}^{B}$ and $\Gamma_{1i,t,y}$ are the increased power consumption of DDC when processing a baseline amount of workload with the minimum QoS, and the number of inactive servers in DDC. Equations (5.39)-(5.42) describe the limitations of DDC power consumption related to factors such as server, workload, and environment. Detailed proof and derivation process can be sought out in [120] and [119]; where e_{1i} and e_{2i} are the empirical constants of cooling system; e_{3i} is the equivalent thermal resistance of DDC;

$q_{i,t,y}^{O}$, $q_{i,t,y}^{I}$ are preset outdoor and indoor temperature; $o_{i,t,y}$ is the load of lighting and other equipment; NE_i, NA_i, and NC_i are the numbers of edge, aggregate, and core switch in DDC, and EE_i, EA_i, EC_i are the corresponding rated power loads; NS_i is the number of servers in DDC, and EP_i, EI_i are peak and idle power of each server; u_i and w are the average service rate servers and tolerant service delay of workload.

Equations (5.43)-(5.50) are the constraints of MESS, which refer to [121]. In (5.43), each MESS can only park at one bus simultaneously, and cannot be parked during traveling. Equation (5.44) restricts different MESSs cannot park on the same bus. Equations (5.45)-(5.47) enforce that the arrival and departure of MESS will not happen at the same time and place, where $\alpha_{m,i,t,y}$ and $\delta_{m,i,t,y}$ indicate whether mth MESS arrives at or depart from bus i. In (5.48)-(5.49), the change of $\tau_{m,ij,t,y}^{MESS}$ is physically consistent with that of $\alpha_{m,i,t,y}$, and $\lambda_{m,i,t,y}$ is an auxiliary binary variable. Equation (5.50) means the travel time limit, and TD is the time intervals required for driving of MESS from bus i to j.

5.5 Chapter Case Study

A. Test System and Parameters Settings

In the proposed optimization problem, the distribution network planning in stage I is the mixed-integer quadratic programming, and the low carbon system operating in stage II is the mix-integer linear programming. The simulation programs have been programmed on a laptop with a 3.3 GHz AMD Ryzen 9 5900HX and 16GB RAM. The optimization models are solved on the Gurobi solver within the YALMIP toolbox in MATLAB. The proposed two-stage model is simulated on the modified IEEE 33-bus distribution system. Moreover, the scalability and feasibility of the proposed model are verified on the modified IEEE 123-bus distribution system. In the first stage, the 33-bus distribution system planning problem has 8293 variables and 13093 constraints. The proposed stage I 33-bus system planning problem can be solved within approximately 70 seconds per single iteration, with the stage II carbon response portion being solvable within 20 seconds. These results are deemed acceptable for both long-term planning problems and short-term operational problems. For uncertainty prediction, this chapter deploys the same method as in the previous work [61], i.e., using GANs to predict data including solar radiation intensity, electricity load, and DDC regular load distribution. GANs is a machine learning method that can be trained with historical data to generate future scenarios, the detailed theory of which refers to [49]. To verify the effectiveness of the proposed planning and operating methods, the following cases are established:

Case 1: The system is planned with a specific emission reduction target, and GDLs can be spatial-temporal dispatch.

Case 2: The system conditions are similar to case 1 but have a large carbon target penalty coefficient.

Case 3: The system is planned with a specific emission reduction target, but GDLs cannot be spatial-temporal dispatch.

Case 4: The system is planned without a specific emission reduction target, GDLs can be spatial-temporal dispatch.

Case 5: The system is planned without a specific emission reduction target, GDLs cannot be spatial-temporal dispatch.

In the above cases, Case 1 is selected as the base case to verify whether the system can reasonably select a trade-off approach between emission mitigation and economic benefits and whether the spatial-temporal carbon response of GDLs can further reduce emissions. Cases 2-5 are utilized as comparative cases to prove the utility of the proposed methods and models from another aspect. Wherein, Case 2 and Case 1 are the same except for the carbon target penalty coefficient. In Case 2, an enormous penalty coefficient is used to model the influence of carbon target constraints. Case 3 verifies the effect of the spatial-temporal carbon response of GDLs on system emissions. Cases 4 and 5 are to prove the superiority of the proposed emission reduction targets planning model for emission reduction. Before the simulation results analysis, some basic system parameters are shown in Table 5-1 and Table 5-2.

TABLE 5-1 MAIN PARAMETERS OF STAGE I

Parameter	Value	Parameter	Value
π_i^{re}	883 (\$/kW)	π_m^{MESS}	650 (\$/kWh)
$\pi_{g,y}^{car}$	25.53 (\$/ton)	$\overline{E_m^{MESS}}$	2 (MW)

$\vartheta^{G}_{g,i,t,y}$	0.875 (tCO_2/MWh)	$u_m^{eff,ch}$	0.95
$\vartheta^{G}_{g,i,t,y}$	0.385 (tCO_2/MWh)	$u_m^{eff,dis}$	0.95
$\vartheta^{st}_{i,t,y}$	0.467 (tCO_2/MWh)	e_y^{target}	50000 (ton)

For the parameters in stage one, the MESS investment cost refers to the data in [28], and its operating cost is about 5%-10% of its investment cost. The setting value of its rated capacity is based on real MESS manufacturers such as Power Edison and Nomad Transportable Power Systems. The value of Emission Target e_y^{target} is set at about 50% of Case 5 emissions. The emission coefficient of the unit is 0.875 (tCO2/MWh) for coal-fired generators and 0.385 (tCO2/MWh) for gas-fired generators according to different types of units. Since the substation is connected to the main grid, the type and proportion of generators in the main grid are uncertain, the value of carbon intensity takes the average value.

TABLE 5-2 MAIN PARAMETERS OF STAGE II

Parameter	Value	Parameter	Value
EP_i	0.2 (kW)	EI_i	0.1 (kW)
EE_i	0.2 (kW)	EA_i	0.35 (kW)
EC_i	19 (kW)	w	0.1 (s)
e_{1i}	0.5	e_{3i}	1.4 (°C/kW)

The parameters of DDCs in Stage II mainly refer to server and switch industry suppliers and papers [119]. In this system, the maximum dispatchable capacity $\varphi^{B}_{i,t,y}$ of a single DDC is about 0.3MW, and the rated capacity $\overline{E_m^{MESS}}$ of MESS is 2MWh. Moreover, the remaining basic system parameters are quoted from [61], and various historical data come from AEMO and BOM.

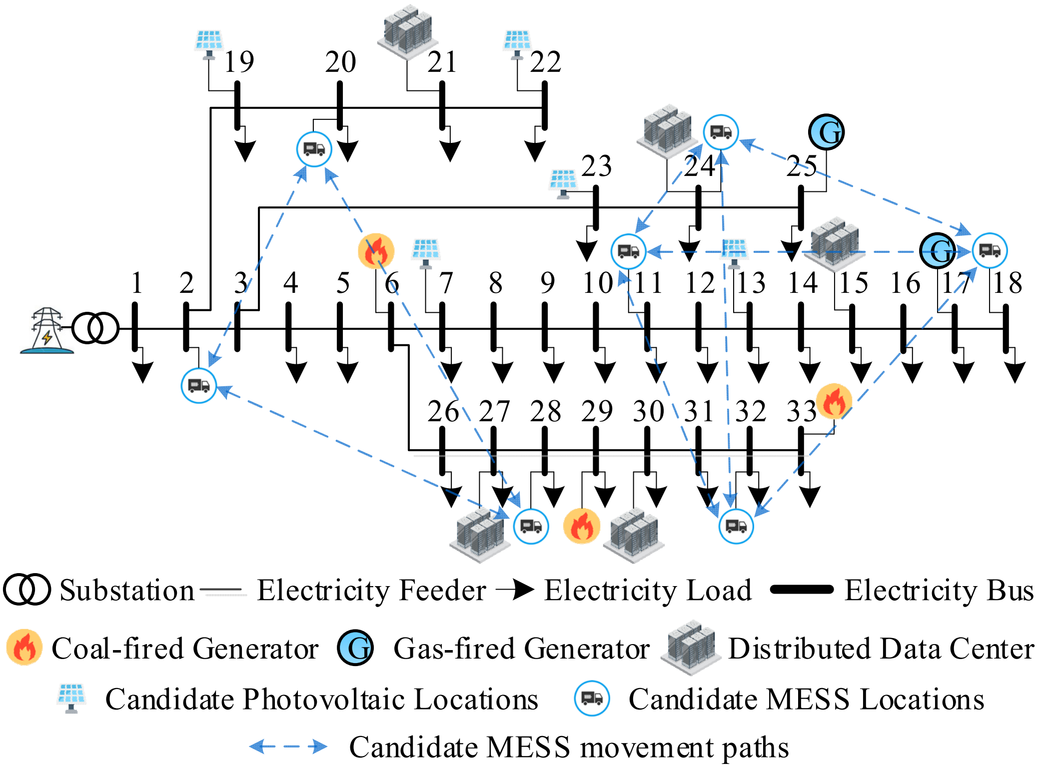

Figure 5-4 Network topology diagram of modified IEEE 33-bus system

B. Numerical Analysis of IEEE 33-bus simulation results

The model and method proposed in this chapter are simulated in a modified IEEE 33-bus power distribution network, which includes GDLs such as DDCs and MESSs, as well as power generation equipment such as PV, coal-fired generators, and gas-fired generators. The network structure diagram is shown in Figure 5-4. In the system, up to two MESSs are expected to be installed, and their candidate movement paths are shown in blue dotted lines in the figure.

In case 1, the MESS operation results are shown in Figure 5-5. The bars in the figure represent the MESS charge and discharge power, and the lines represent the real-time carbon intensity at different candidate path end-buses. The color change of the bars in the figure indicates that the MESS moves to the corresponding bus for charging and discharging. It can be seen from the figure MESS1 chooses to charge at bus 20 with the lowest carbon intensity during the afternoon period and discharge at bus 28 with the highest carbon intensity during the night period. The charging and discharging movement path of MESS2 also obey the same principle, which selects the candidate bus with the lowest carbon intensity (bus 18) to charge, and the highest carbon intensity (32) to discharge. The charge-discharge curve demonstrates that the proposed MESS-related model is capable of achieving not only carbon response on a traditional time scale, but also flexible spatial carbon response based on the carbon intensity of different nodes.

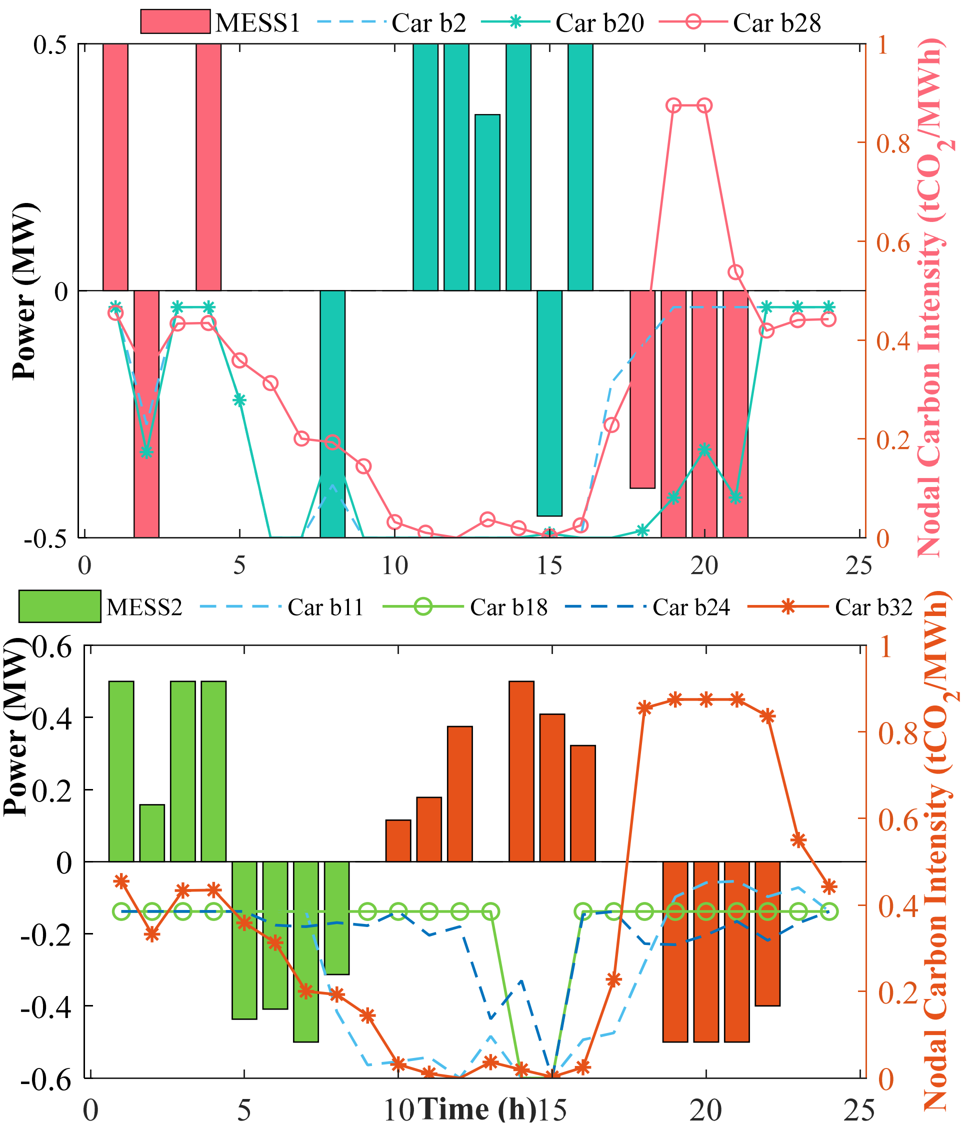

Figure 5-5 MESS operation and the carbon intensity of the corresponding bus

The spatial-temporal carbon response results of DDCs' load are shown in Figure 5-6. The difference compared with MESS is that DDC cannot realize the spatial dispatch of load by its own movement. The load of the DDC is re-dispatched in real time through the data flow. The DDC loads and corresponding bus carbon intensities shown in the figure are located on bus 15, bus 21, and bus 30, respectively.

When the carbon intensity of buses 21 and 30 is low during the afternoon period, the load is mainly concentrated on the relevant DDCs. As the carbon intensity of bus 30 increases during the night, the load shifts accordingly, transferring from the DDC on bus 30 to the DDC on bus 15. It is important to note that the overall system load is high during the night period, leading to higher carbon intensities on each corresponding bus compared to the noon period. This higher average bus carbon intensity may result in reduced effectiveness of the GDLs' spatial carbon response.

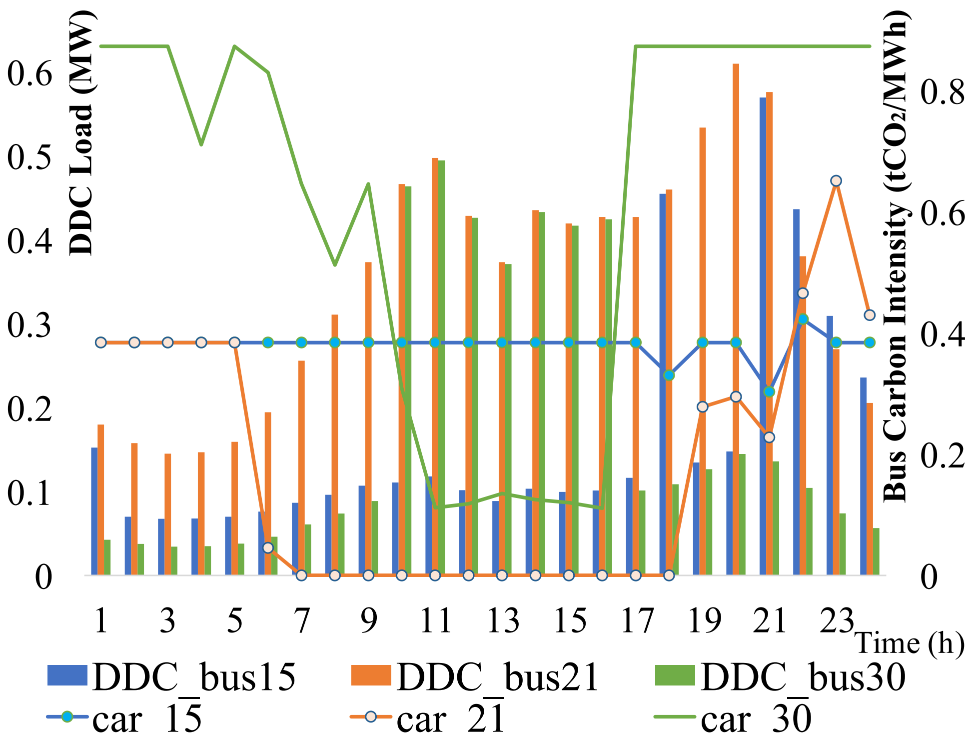

Figure 5-6 The spatial-temporal carbon response results of DDCs

Through the spatial-temporal carbon responses of DDC and MESS, the overall carbon intensity changes of the system are shown in Figure 5-7.

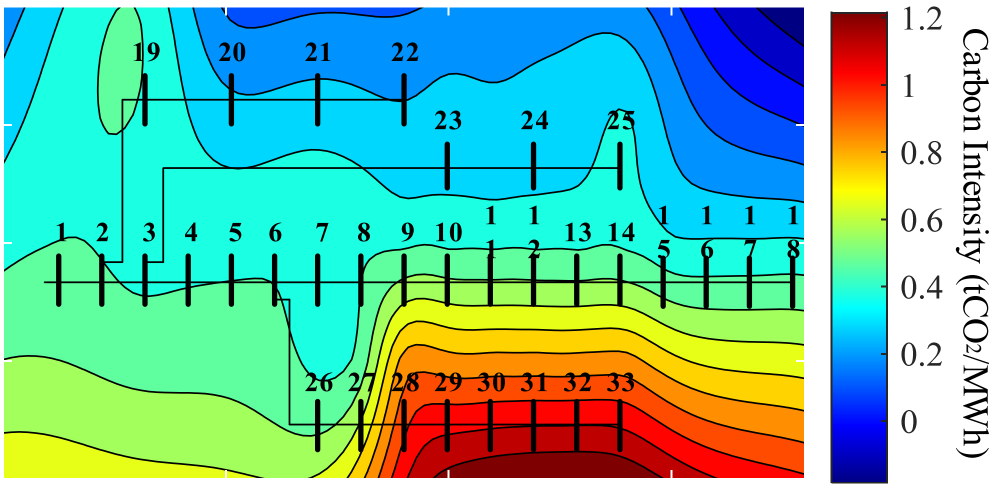

(a) System carbon intensity distribution without the spatial-temporal carbon response of GDLs

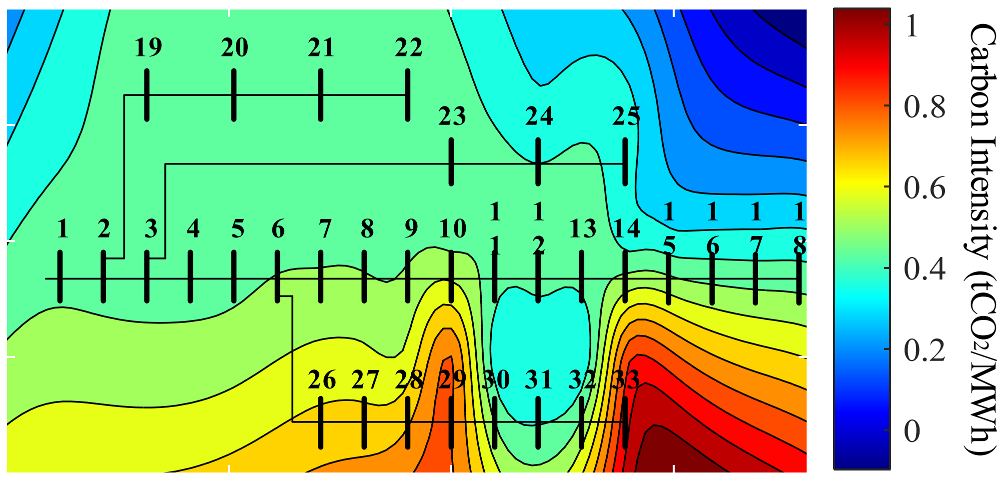

(b) System carbon intensity distribution with the spatial-temporal carbon response of GDLs

Figure 5-7 System carbon intensity distribution with and without the spatial-temporal carbon response at 20:00

Since in this system, high-emission coal-fired generators are mainly located in buses 26 to 33, the carbon intensity of this area is generally higher than that of the rest of the system. Under the spatial-temporal carbon response of GDLs, as shown in Fig.7 (b), the carbon intensities of buses 30-32 have an obvious reduction at 8 p.m. Simultaneously, the maximum carbon intensity of the system is also reduced in this situation, from 1.2 to 1 (tCO2/MWh).

In this case, the emission comparison of various types of generators and substations in the system is shown in Figure 5-8.

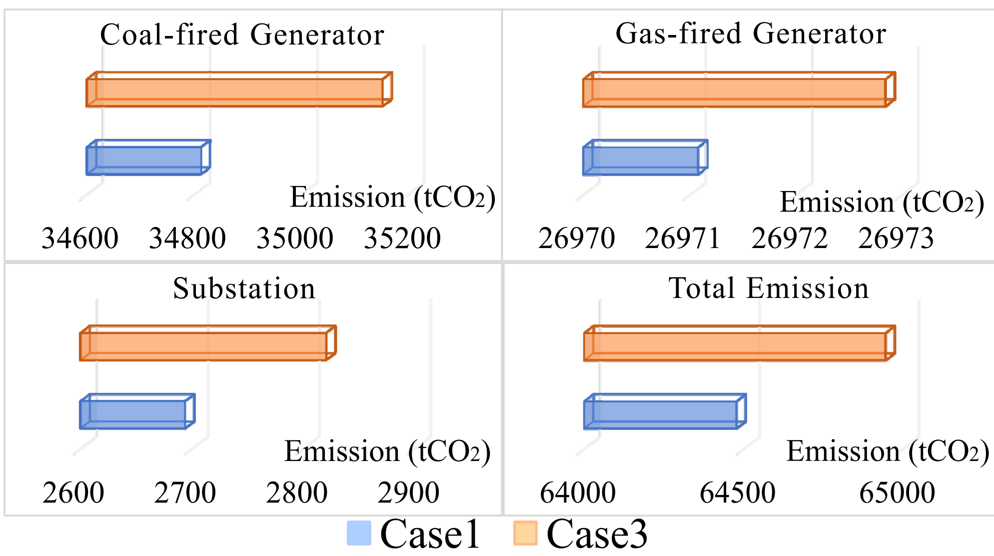

Figure 5-8 System emission comparison of Case 1 and 3

In Case 3, since that MESS and DDC cannot adjust their loads and positions according to real-time carbon intensity, the overall system emissions are higher than that in Case 1. Moreover, in Case 3, coal-fired generators, gas-fired generators, and substation all have higher emissions.

The above case analyses compare the effects of the spatial-temporal carbon responses of GDLs on system emissions. Regarding the proposed carbon target-based objective function, its impact on the system is shown in figure 5-9 and Table 5-3.

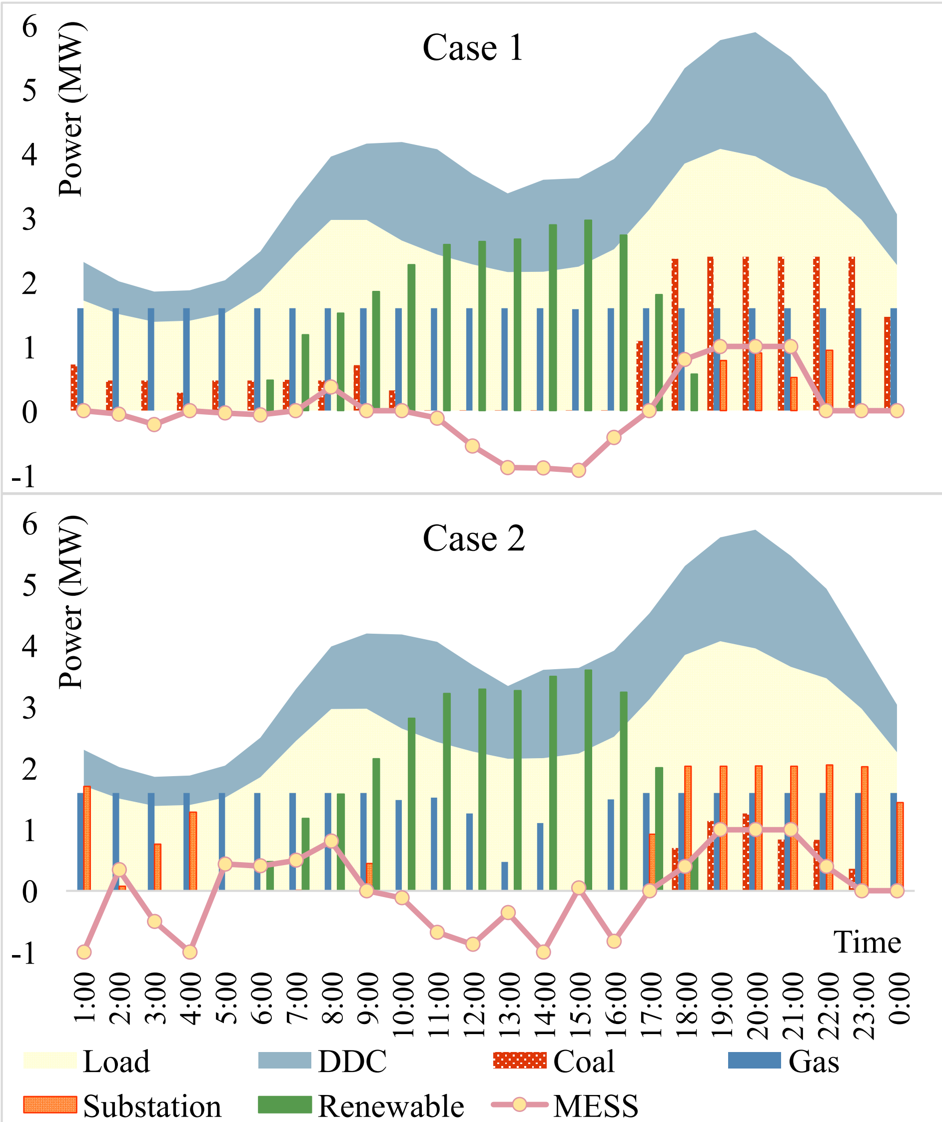

Figure 5-9 The system output comparison between Case 1 and 2

After comparing Case 1 and Case 2 in Figure 5-9, it is evident that with a large carbon target penalty coefficient, there is a significant increase in renewable energy output. In contrast, there is a clear decrease in the power output of coal-fired generators. Furthermore, the effect of Case 2 on MESS is primarily manifested in the charge-discharge curve having some fluctuations due to the increase in the output ratio of renewable and low-emission generators, but the overall trend remains unaffected.

TABLE 5-3 SIMULATION RESULTS OF EACH CASE

Item	Case 1 Value	Case 2 Value	Case 4 Value
The penalty coefficient Λ_{ε} ($)	46	5000	0
PV Quantity (unit)	407	500	115
PV Location (bus)	7,13,19,22, 23	7,13,19,22, 23	19,22
Investment cost PV (M$)	2.44	2.99	0.69
Total investment cost (M$)	5.04	5.59	3.29
Total maintenance cost (M$)	0.55	0.57	0.46
Total operating cost (M$)	3.11	7.03	3.77
Total carbon cost (M$)	1.65	1.24	2.39

From the results in this table, in each case, different carbon target penalty coefficients mainly affect the number of PV installations. In Case 4, the system has fewer PV installations to avoid high investment costs. However, the consequence of the reduction in PV output is a substantial increase in the cost of carbon emissions. In Case 2, due to the large penalty coefficient, the installation quantity of PV and the system investment cost is the highest among all cases. Meantime, to maximize emission reduction, the system reduces the utilization of low-cost coal-fired generators but raises the usage of high-cost low-emission gas-fired generators and substation. The operating cost of this case has been significantly increased.

A comprehensive comparison in terms of system costs and emissions for all cases is shown in Figure 5-10.

From the comparison results, in Cases 4 and 5, since there is no carbon target penalty coefficient, the system emission reduction only depends on the carbon tax price. System emissions were the highest in each case, and emission reduction targets could not be achieved. The emission reduction target was achieved in Case 2, but the system cost increased significantly, much higher than that in the other cases. In case 1, an appropriate penalty coefficient can lead to a large reduction in system emissions with only a slight increase in cost. Compared with Case 4, Case 1 reduced emissions by about 31.1%, while costs only increased by 4.4%. In contrast, compared with Case 4, the emission of Case 2 decreased by 48.1%, but the cost increased by 45.7%.

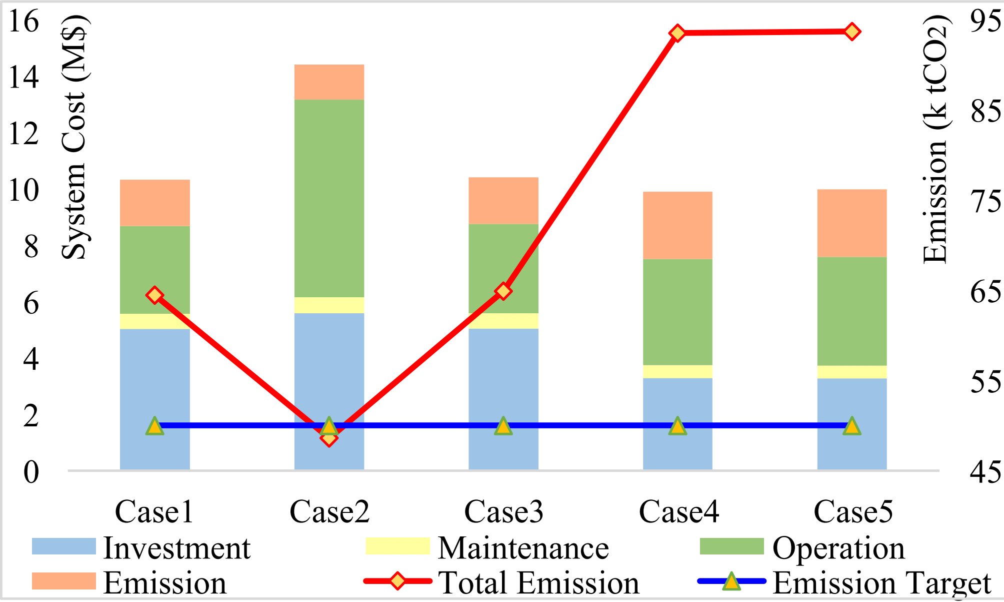

Figure 5-10 The comprehensive result comparison of system costs and emissions

C. Scalability of the Proposed Method

To further verify the scalability and applicability of the proposed model and method, simulations are performed on a modified IEEE 123-bus distribution system. The network topology and basic system parameters can be found in [122], and the case settings follow the previous cases 1, 2, and 5. In such a large test system, the generators, PVs, MESSs, and DDCs will also be clustered into different zones to improve the efficiency of spatial-temporal carbon response based on system partition results. Table 5-4 provides detailed information about the configuration of the 123-bus system, including the location of GDLs and generators.

TABLE 5-4 CANDIDATE LOCATION OF DEVICES IN THE 123-BUS SYSTEM

Devices	Candidate Location (bus)
Substation	1
Coal-fired Generators	4, 20, 27, 35, 65, 73, 82, 97
Gas-fired Generators	54, 109
MESS1	11, 28, 46
MESS2	68, 92, 99, 120
Renewable (PV)	13, 19, 39, 45, 49, 59, 69, 105, 116, 121
Distributed Data Centers	13, 30, 34, 47, 52, 62, 87, 95, 113, 118

The hourly emissions of the 123-bus system in a single day are presented in Figure 5-11. By comparing the results of Case 1 and Case 3, it can be concluded that the proposed GDLs spatial-temporal dispatching method can effectively reduce the emission of each bus and the total system emission during the PV peak output hours, which occur around

10 am. Moreover, although the emission has also shifted between buses at night, the overall emission reduction effect is weaker than during the daytime.

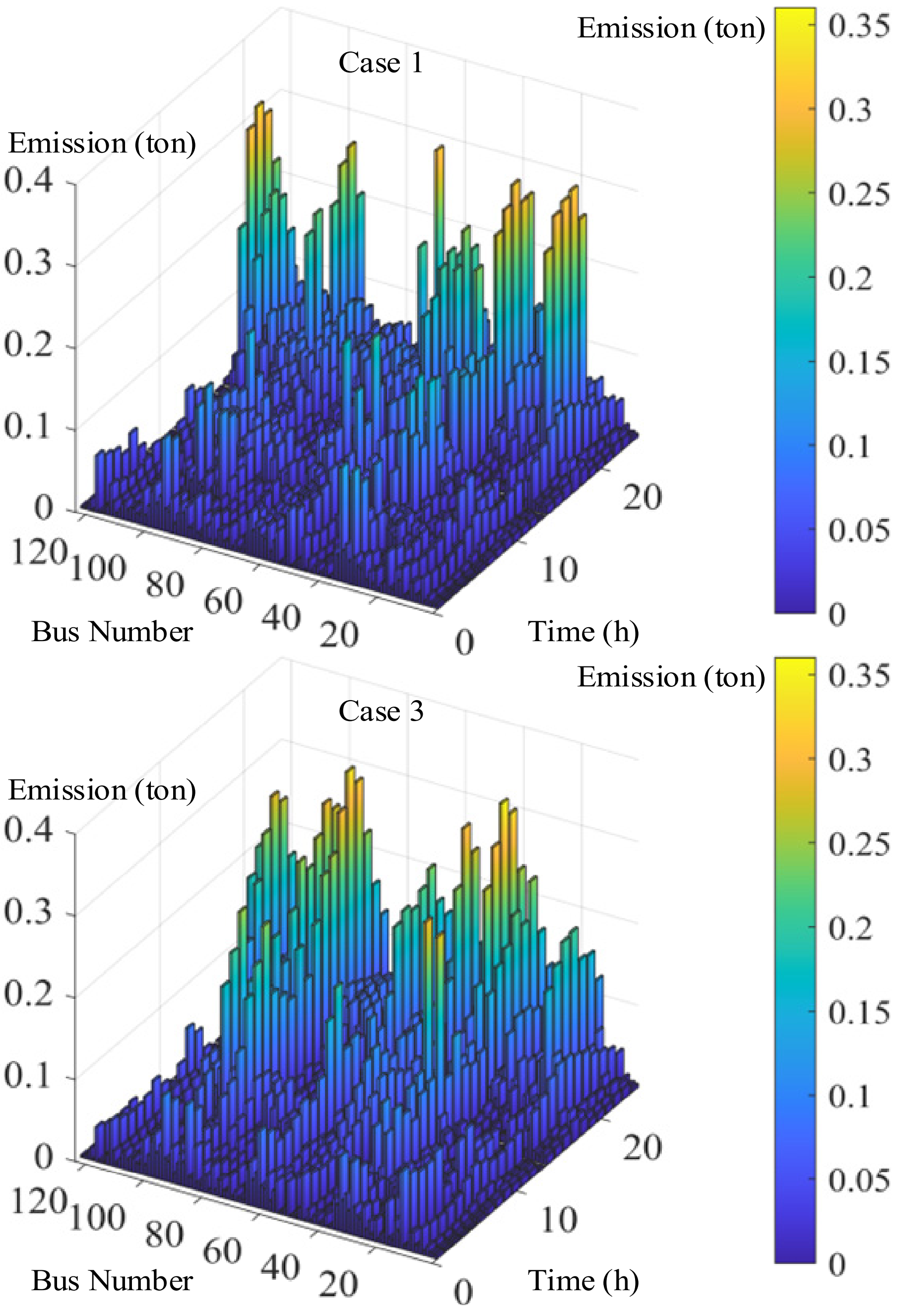

Figure 5-11 123-bus system carbon emission distribution in a single day

Figure 5-12 compares the hourly emissions of the 123-bus system under Case 1 and Case 5. The results show that the combination of spatial-temporal carbon response and carbon target can effectively reduce system emissions, especially when the system load is low, as shown before 5 pm in the figure. During peak times, due to heavy loads, coal-fired generators must be used to ensure the system's power supply, leading to high levels of average system carbon emission at each bus. Although the proposed method can shift part of the load to areas with lower emissions intensity, the effect is slightly insignificant under current system conditions.

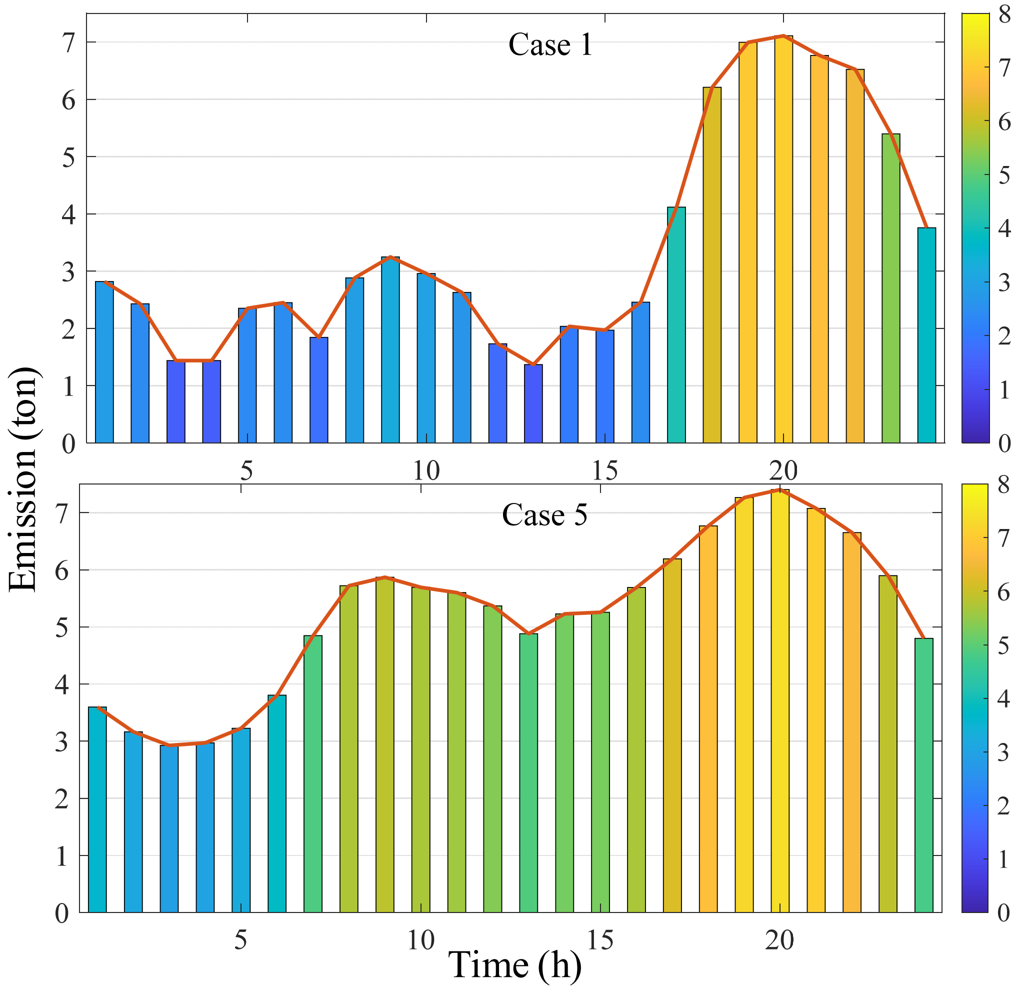

Figure 5-12 123-bus system hourly total carbon emission distribution

5.6 Chapter Summary

This chapter introduces a two-stage carbon target-based distribution network planning method that maximizes emissions reductions while suppressing cost growth. Furthermore, a spatial-temporal carbon response model based on GDLs, including MESSs and DDCs, is proposed in this chapter. According to the system carbon intensity, The GDLs can be real-time scheduled via the cooperation between the spatial-temporal carbon response model and the MESS-based CEF model. Through the simulation of the modified IEEE 33-bus and the scalability verification of IEEE 123-bus distribution systems, the following conclusion can be obtained.

(1) The proposed carbon target-based planning method can effectively suppress system

emissions. Specifically, the approach results in further emission reductions of at least 30% compared to the scenario without a carbon target. The cost increase associated with this reduction does not exceed 5%.

(2) The current system resources are still not fully utilized, and the experimental results prove that the spatial-temporal carbon response of GDLs can further reduce system emissions by 500 tons in a 33-bus system, thereby maximizing resource utilization efficiency.

(3) Inflexible carbon target setting may result in excessive cost growth. In the IEEE 33-bus system, when the preset carbon target is fully achieved, meaning that the emission reduction ratio reaches 48.1%, the associated cost increase can be as high as 45.7%.

The simulation results fully prove the effectiveness of the proposed carbon target-based planning model and the spatial-temporal carbon response model. However, there are still challenges that need to be addressed in future research. Firstly, traffic uncertainty during the MESS moving process needs to be further studied, as it may impact its timely arrival to the candidate location, leading to reduce the contribution of emission mitigation. Secondly, the impact of the capacity change of DDCs and ESSs on the effectiveness of carbon response requires investigation in more detail. Finally, the effect of different types of renewable energy on spatial-temporal carbon response, such as wind power and tidal energy, needs to be verified to explore further opportunities for emission reduction.

Chapter 6 Echelon Utilization of Second-Life of Used Electric Vehicle Batteries

In the existing research, it is generally assumed that BESS is composed of fresh batteries, and a few studies that consider SLBs have generally compared and analyzed the differences in cost and system economy. However, there is no planning method currently that can flexibly choose different types of BESS according to the present operating conditions of the system. To address the existing research gaps, in this chapter, a novel integrated network planning method is proposed, aiming to realize the echelon utilization of SLBs. The main contribution of this chapter is that the proposed model can select the optimal BESS planning options according to the existing system conditions, thereby further reducing system cost. This chapter proposes a two-stage system planning strategy for the long-term scale. In the first stage, the electrical and transportation networks are comprehensively considered, and the situations of equipment installation and system operation are determined. In the second stage, according to the operating results of the previous stage, the flexibility of the system is analyzed through transmission and sub-station expansion planning. Moreover, multiple life cycles are considered, BESS with a low state of health (SOH) value will be retired to ensure that the lifespan of the BESS in the system is maintained in an appropriate range.

6.1Proposed Two-Stage System Framework

Reassembling and reusing the retired battery into low battery performance requirement scenarios is a useful method to make full use of their remaining value. As shown in Figure 6-1, due to the uneven remaining SOH of retired batteries, they need to be tested, sorted, and reassembled.

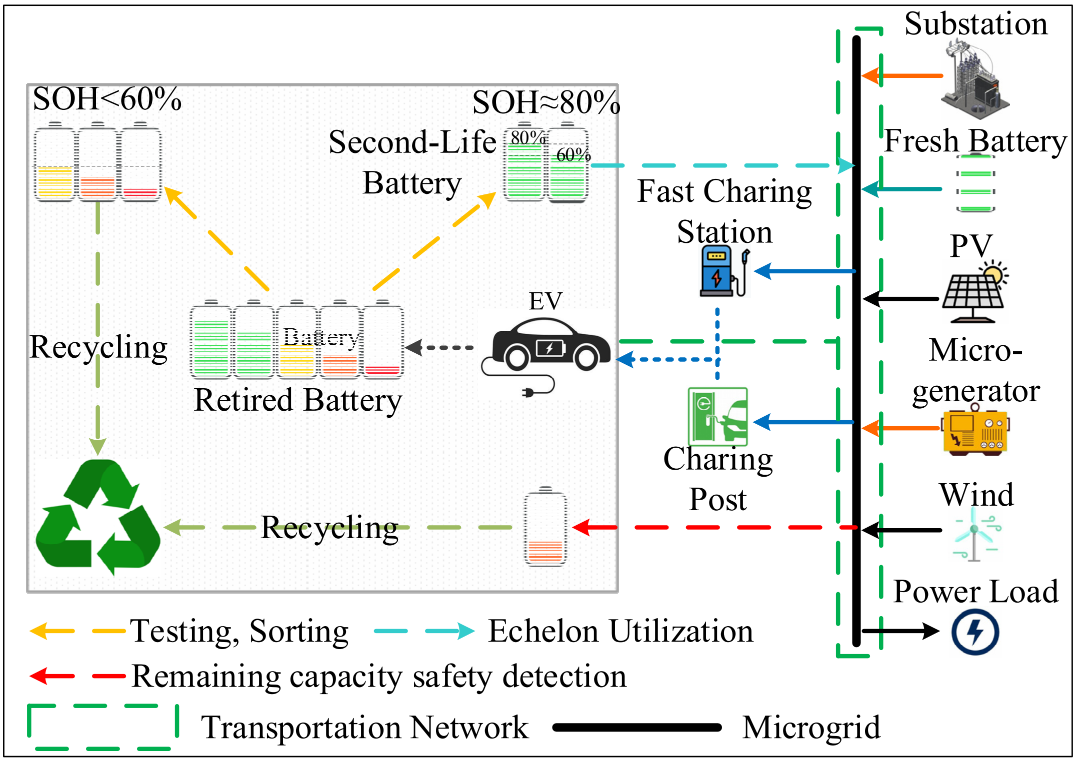

Figure 6-1 Retired battery processing and system operation architecture

For retired batteries with low SOH, because of the problems such as unstable power output and rapid decline in SOH, they are not suitable for secondary use and need to be directly recycled. For those retired batteries that retain considerable SOH, they can still be used as SLBs for microgrid operation again after reassembly. In this study, we consider the initial SOH value of all SLBs used in the system to be 80%. Besides, we assume that the SLBs used have undergone strict quality testing. In the proposed BESS model, the parameters of SLBs and fresh batteries are different in terms of charge and discharge efficiency, rated energy capacity, initial SOH value, and the BESS total number of cycles at 100%-DOD. In this integrated system, fresh batteries are also considered, and the selection of candidate battery types will be determined by the optimization program.

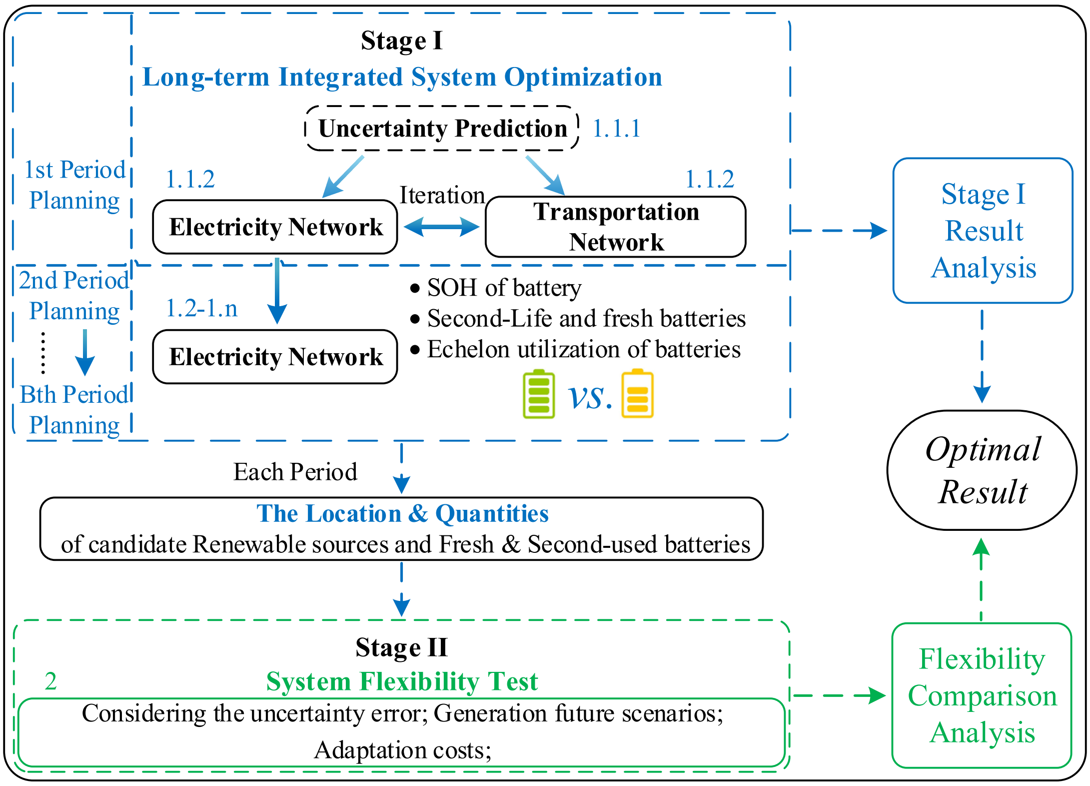

Figure 6-2 The proposed two-stage system framework

This chapter proposes a two-stage system framework for collaborative planning of the electricity microgrid and the transportation network. The structure of the framework is shown in Figure 6-2, and the sequence of system operation is marked. At the beginning of the first stage, the system obtains values such as traffic flow, load, and wind speed from the results of the uncertainty prediction and brings these values into the planning of the transportation network and power network. In the first stage, the total duration of system planning is up to several decades, of which Y years is a period, divided into B period blocks in total. In the first period of stage I, the two networks iterate with each other. The transportation network obtains the traffic flow of each node and line through traffic flow simulation and selects some nodes with the largest flow as the location of FCSs and charging posts (CPs). Therefore, the buses' load in the corresponding microgrid increases by $P_{i,t,y,b}^{CP}$ and $P_{i,t,y,b}^{FCS}$ respectively. Subsequently, the microgrid considers the impact of the added load and planned the location of the BESS. Since this chapter assumes that BESS, renewable energies, and EV charging facilities are all at the same bus, the decision variable $\delta_{k,i,y,b}^{BESS}$ of BESS will also affect the results of traffic flow. After iteration in the first period, the candidate installation locations of these facilities are finally determined, and these locations will remain unchanged in the subsequent periods of microgrid planning. In microgrid planning, the optimization results of the previous period will be passed to the next period as initial conditions, such as the quantities and locations of installed candidate renewable energy facilities, installed BESS, and retired BESS. When all periods within the total planned duration of the system are completed, the sum of the costs of each period is the optimization result of stage I.

In the second stage, the system is tested for flexibility according to the overall planning scheme of the previous stage. We compare the differences in system flexibility between different cases, combine the cost of the first stage, analyze and obtain the optimal system planning results.

6.2 Traditional Model of BESS Life Cycle and Operation

In this section, the traditional BESS life cycle and operating model will be introduced. The service life of the BESS $T_{service}$. can usually be expressed by the cycle life T_{cycle} or the float life T_{float} [101]. Among them, the float life of BESS usually corresponds to the corrosion processes, which is regarded as a constant [98]. This chapter assumes that the influence of float life and temperature on BESS life has been considered, and the cycle life is mainly discussed. The cycle life of a BESS usually depends on its charging and discharging behavior within the cycle. The equations are as follows:

$$T_{cycle} = \frac{N_d^{fail}}{W \cdot n_d^{day}} \tag{6.1}$$

$$N_d^{fail} = N_{100}^{fail} \cdot d^{kp} \tag{6.2}$$

$$Loss(\%) = \frac{n_d}{N_d^{fail}} \times 100\% \tag{6.3}$$

$$n_{100}^{eq} = n_d \cdot d^{kp} \tag{6.4}$$

where N_d^{fail} denotes the maximum number of battery life cycles at a certain d (DOD); n_d^{day} represents the number of cycles per day at this DOD value; W is the average number of operating days in a year. In this chapter, Peukert Lifetime Energy Throughput (PLET) model [100] is to estimate the battery life cycle based on its usage, as shown in (6.2), where N_{100}^{fail} is the number of cycles with 100%-DOD before it is retired; kp is the Peukert Lifetime constant ranging from 0.8 to 2.1 [98]. Equation (6.3) shows the loss of battery life cycle $Loss(\%)$ at each cycle n_d under d DOD. By keeping the loss constant, the equivalent 100%-DOD cycle number n_{100}^{eq} for the n_d cycle can be expressed as (6.4).

The life cycle of the battery is to describe its charge and discharge behavior essentially. In the BESS system, its specific charge and discharge equation can be expressed as

$$E_{k,i,t+1,y,b}^{BESS} = E_{k,i,t,y,b}^{BESS} + \left(\begin{array}{l} P_{k,i,t,y,b}^{BESS,ch} \left(\sum\limits_{k \in \Omega^{f\&s}} \left(u_k^{eff,ch} \delta_{k,i,y,b}^{BESS} \right) \right) \Delta t \\ - \left[P_{k,i,t,y,b}^{BESS,dis} \Big/ \sum\limits_{k \in \Omega^{f\&s}} \left(u_k^{eff,dis} \delta_{k,i,y,b}^{BESS} \right) \right] \Delta t \end{array} \right) \tag{6.5}$$

where $E_{k,i,t,y,b}^{BESS}$, $P_{k,i,t,y,b}^{BESS,ch}$ and $P_{k,i,t,y,b}^{BESS,dis}$ represent the stored energy, charging power and discharging power of the kth type BESS at the ith candidate bus, tth time, yth year, and bth period block, respectively; $\Omega^{f\&s}$ is the set of BESS, which including fresh and second-life batteries; $u_k^{eff,ch}$ and $u_k^{eff,dis}$ indicate the charge and discharge efficiency of their corresponding types of BESS; their values are constrained by the decision variable $\delta_{k,i,y,b}^{BESS}$, that is, $\delta_{k,i,y,b}^{BESS}$ decides whether to install kth type BESS; Δt denotes the time interval between time t and $t+1$. Note that the fresh batteries and SLBs are planned simultaneously. Therefore, the difference from the traditional BESS model is that this model is nonlinear and uses different parameters including efficiency and rated capacity for different types of batteries.

6.3 Stage I, Comprehensive System Planning Based on Echelon Utilization of BESS

In this section, the model of uncertainty prediction, traffic flow, and electricity network planning involved in the first stage will be introduced. In stage I, the overall planning time scale is subdivided into several periods. The uncertainty prediction model is initially run, and the results of its operation will be used as parameters in the subsequent planning process. In the first period, the electricity and transportation networks iterate with each other to determine the candidate locations for BESS. Subsequently, the power system planning will operate sequentially over time to obtain the optimized results of the first stage. The purpose of stage I is to find an optimal system planning scheme to minimize system costs.

A. Stochastic Scenarios Uncertainty Prediction

GANs is a machine learning method that uses historical data to train and directly generate future scenarios. The advantage is that there is no need to specify the model or probability distribution in advance, and it has excellent prediction accuracy [49]. The core of GANs is based on game theory, which establishes a minimax two-player game between the generator and the discriminator. As shown in Figure 6-3, the input of the generator usually adopts the noise signals with Gaussian distribution, and the generator converts the input signal into an output (fake historical data) with the same characteristics as the real historical data through the learning of historical data. The discriminator tries to distinguish the difference between real historical data and fake historical data. Each training iteration, the generator will update the data to generate fake samples to "fool" the discriminator. Theoretically, the final output data of the generator can be almost completely consistent with the real historical data, so that the overall network training is completed.

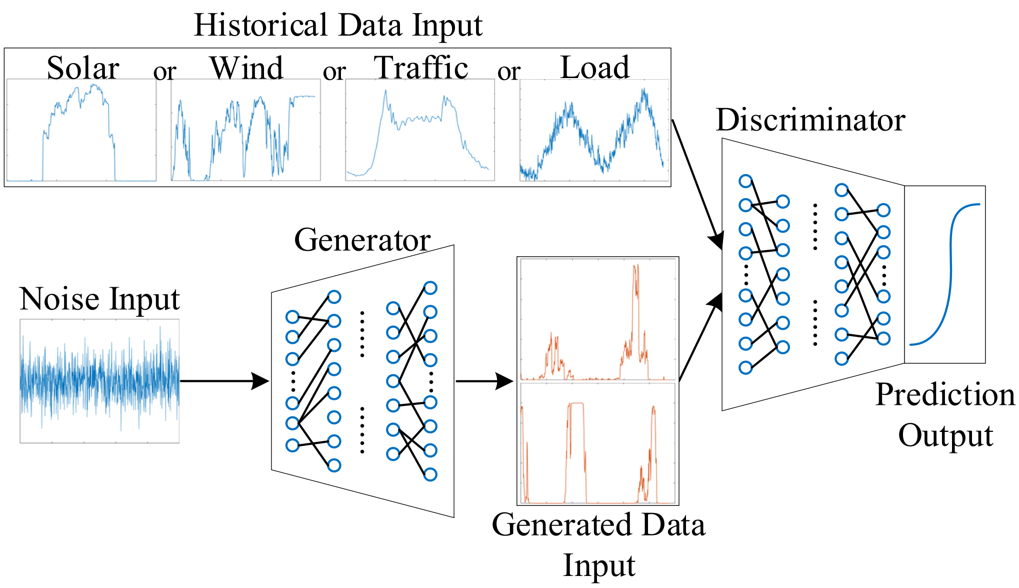

Figure 6-3 The architecture diagram of GANs

The models of GANs are as follow [49]:

$$L_G = -E_Z\left[D\left(G(Z)\right)\right] \tag{6.6}$$

$$L_D = -E_X\left[D\left(X\right)\right] + E_Z\left[D\left(G(Z)\right)\right] \tag{6.7}$$

$$\min_G \max_D V\left(G,D\right) = E_X\left[D\left(X\right)\right] - E_Z\left[D\left(G(Z)\right)\right] \tag{6.8}$$

assuming that X is a set of real historical data, for the mth historical data, the observation values X_t^m at time t, $t \in T$ can be obtained. Let P_X represents the true distribution of the observation. Assume that the distribution of a set of noise vector input z follows $Z \sim P_Z$. The goal of GANs is to train the generator network $G(\bullet)$ to make the distribution of z approach P_X as much as possible. The discriminator network $D(\bullet)$ is trained simultaneously with the generator. L_G, L_D are the loss functions of the generator and discriminator, respectively. For the generator, the smaller L_G means that the output is closer to the real value. The smaller the L_D means the distinguishing ability of the discriminator is stronger. $E_{\bullet}[\bullet]$ represents its mathematical expectation. Combining (6.6) and (6.7), the two-player minimax game function (6.8) can be obtained, where the $V(G,D)$ is the negative of L_D. It should be noted that the time-series data prediction obtained by GANs usually considers the delay in the input data. However, because the problem proposed in this chapter is long-term planning, the delay has little effect on this type of problem, so it will not affect the planning result.

For the scenarios generated by GANs, the K-medoids clustering algorithm is used to reduce the number, which is shown below. The reason why we use K-medoids in this part is that there are some outliers in the uncertainty prediction results. After simply comparing the effects of K-medoids and K-means, we find that K-medoids has better performance in dealing with this problem.

$$Min \sum_{\substack{u_s \in S \\ u_s \notin S_0}} w_{syb} \max_{u_{S_0} \in S_0} d\left(u_s, u_{s_0}\right) \tag{6.9}$$

$$d\left(u_s, u_{s_0}\right) = \| u_s - u_{s_0} \| = \sum_{t=1}^{T} \left| u_s^t - u_{s_0}^t \right| \tag{6.10}$$

where S and S_0 are the set of all scenarios and the optimal subset after reduction; w_{syb} is the probability of sth scenario appearance; u_s, u_{s_0} are the data value of sth and s_0th scenarios; $d(u_s, u_{s_0})$ is the distance between sth and s_0th scenarios. In this chapter, all variables have different values in different scenarios, so s is not displayed in the subscript of other variables.

B. Charing Demand and Traffic Flow Determination Models

The charging methods of EVs are divided into CP and FCS according to different powers. According to [58] and [77], the charging demand model can be established as:

$$P_{i,t,y,b}^{CP} = C_{i,y,b} h \frac{v_{i,t,y,b}}{\sum_{s \in S} \sum_{t \in T} \left(w_{syb} v_{i,t,y,b} \right)} P_i^{CP} \tag{6.11}$$

$$C_{i,y,b} = \frac{C_{y,b} \cdot \beta \sum_{s \in S} \sum_{t \in T} \left(w_{syb} v_{i,t,y,b} \right)}{\sum_{i \in \Omega^{bus}} \sum_{s \in S} \sum_{t \in T} \left(w_{syb} v_{i,t,y,b} \right)} \tag{6.12}$$

$$P_{i,t,y,b}^{FCS} = C_{y,b} \left(1 - \beta \right) \frac{f_{i,t,y,b}^{trip}}{\sum_{s \in S} \sum_{t \in T} f_{i,t,y,b}^{trip}} \cdot \frac{f_{i,t,y,b}}{\sum_{i \in \Omega^{bus}} f_{i,t,y,b}} P_{i,t}^{FCS} \tag{6.13}$$

where $C_{i,y,b}$ and $C_{y,b}$ are the charging demand of ith charging facility and total charging demand in the yth year bth period block; h is the average charging duration; $v_{i,t,y,b}$ denotes the average number of EVs parked at ith charging post; β indicates the choosing ratio of CP; P_i^{CP}, $P_{i,t}^{FCS}$ represent the rate charging power of CP and FCS; Ω^{bus}, T indicate the set of bus location and time; $f_{i,t,y,b}^{trip}$ is the travel ratio; $f_{i,t,y,b}$ is the traffic flow captured by the FCS, which can be calculated through the user equilibrium-based traffic assignment model (UETAM) [123]-[124]. This model is nonlinear programming. The variables in the model are continuous.

$$Min\ j = \sum_{a \in \Omega^A} \int_0^{x_a} t_a(\omega) d\omega \tag{6.14}$$

$$s.t. \sum_{p \in \Omega_{rs}^p} f_p^{rs} = q^{rs} \tag{6.15}$$

$$f_p^{rs} \geq 0 \tag{6.16}$$

$$x_a = \sum_{p \in \Omega_{rs}^p} \left(f_p^{rs} \cdot \delta_{p,a}^{rs} \right) \tag{6.17}$$

where $t_a(\omega)$ represents the road impedance function, also known as the link performance function; Ω^A is the set of road section; x_a denotes the traffic flow on ath road section; Ω_{rs}^p is the set of the link of the OD section from r to s; f_p^{rs} and

q^{rs} are the traffic flow of pth path of OD section and traffic demand from r to s; $\delta_{p,a}^{rs}$ indicates ath road is on pth path of OD section from r to s. In the analysis of transportation systems, it is more common to use road impedance function (6.18) developed by the U.S. Bureau of Public Roads as an alternative to (6.14) [77].

$$t_a\left(x_a\right)=t_a^0\cdot(\xi)^{\delta_{k,i,y,b}^{BESS}}\left[1+\alpha^m\left(\frac{x_a}{c_a}\right)^L\right] \tag{6.18}$$

where t_a^0 is the free travel time, which is affected by the results of microgrid planning, when the decision variable $\delta_{k,i,y,b}^{BESS}$ is equal to 1, it needs to be multiplied by the coefficient ξ, and ξ is equal to 0.9 in this chapter; x_a and c_a are traffic flow on the link a and capacity of the link a; α^m and L are the pre-determined parameters, their values are usually 0.15 and 4, and can be changed according to different regions. After the optimization problem is solved, the traffic flow on each road x_a can be obtained. Subsequently, the traffic flow captured by the fast-charging station can be calculated by (6.19):

$$f_{i,t,y,b}=\sum_{a\in\Omega^A}\left(x_a\cdot u_{i,a}\right) \tag{6.19}$$

where $u_{i,a}$ represents whether the FCS of the ith bus is connected to the ath road.

C. Multi-Period Electricity System Planning Based on Echelon Utilization of BESS

The objective of the first stage is to solve an integrated network planning problem including transportation networks, which focuses on planning the installation and retirement for different types of BESS. After linearizing equation (6.5), the model proposed in this part is transformed into mixed-integer quadratic programming. The variables in the model are mixed types. Among them, there are 5 types of decision variables, which are binary variables to determine the installation of renewable energy, the installation and retirement of BESS, and the constraints of simultaneous charging and discharging. At this stage, the main input parameters include network topology, various cost coefficients of different facilities, and uncertain parameters. The objective function of the first stage is to minimize the total cost of the system, which is as follows:

$$Min\ J=\left\{\sum_{b=1}^{B}\frac{1}{(1+\sigma)^b}\left[\begin{array}{l}\left(C^{Re\&BESS}\right)\\+\sum_{y=1}^{Y}\frac{1}{(1+\sigma)^y}\left(C_y^{O\&M}+C_y^{Car}\right)\end{array}\right]\right\} \tag{6.20}$$

where σ indicate the discount rate; $C^{Re\&BESS}$ is the total cost of renewable energy and BESS; $C_y^{O\&M}$ represents the system operating and maintenance cost; C_y^{Car} denotes the system environmental cost; Y, B are the set of the year and total planning horizon respectively.

The cost of renewable energy and BESS is divided into three parts, namely, the cost of renewable energy investment, BESS investment, and BESS retirement.

$$\begin{aligned}
&C^{Re\&BESS} = C^{(Re,In)} + C^{(BESS,In)} + C^{(BESS,Retirement)} \\
&= \sum_{r\in\Omega^R}\sum_{i\in\Omega^{bus}}\left(\pi_{r,b}^{Re}\cdot\delta_{r,i,b}^{Re}\right) \\
&+ \sum_{k\in\Omega^{f\&s}}\sum_{i\in\Omega^{bus}}\left(\pi_{k,y,b}^{BESS}\cdot\overline{E_{k,i,t,y,b}^{BESS}}\cdot\delta_{k,i,y,b}^{BESS}\right) \\
&+ \sum_{k\in\Omega^{f\&s}}\sum_{i\in\Omega^{bus}}\left[\left(\tau_{i,y,b}-\varsigma_{i,y,b}\right)\cdot\left(\begin{array}{l}\overline{E_{k,i,t,y,b}^{BESS}}\delta_{k,i,y,b}^{BESS,retire} \\ +\overline{E_{k,i,t,y,b-1}^{BESS}}\delta_{k,i,y,b-1}^{BESS,retire}\end{array}\right)\right]
\end{aligned} \tag{6.21}$$

where Ω^R indicates the set of renewable energy device types; $\pi_{r,b}^{Re}$ and $\pi_{k,y,b}^{BESS}$ represent the per-unit cost of rth type renewable energy devices and kth type BESS; $\tau_{i,y,b}$ and $\varsigma_{i,y,b}$ are uninstallation cost and salvage cost of BESS when its lifespan cycle is completely over; $\overline{(\bullet)}$ indicates the upper bound of that value; $\delta_{r,i,b}^{Re}$ is an integer variable, which decides to install the rth type renewable energy facilities at the ith bus in bth period block; $\delta_{k,i,y,b}^{BESS,retire}$ is a decision variable that determines whether the kth type BESS should be retired.

The cost of system operation and maintenance can be expressed as below, which includes the operating cost of the micro-thermal generator, the operating and maintenance cost of the substation, and the maintenance cost of renewable energy devices and BESS.

$$
\begin{aligned}
C_y^{O\&M} &= C_y^{Op,G} + C_y^{Op\&Mt,ST} + C_y^{Mt,Re} + C_y^{Mt,BESS} \\
&= \sum_{s\in S}\sum_{t\in T}\left\{\begin{array}{l} w_{syb} \times \\ \left[\begin{array}{l} \sum\limits_{i\in\Omega^{bus}} \left(a_{i,y,b}\left(P_{i,t,y,b}^{G}\right)^2 + b_{i,y,b}P_{i,t,y,b}^{G} + c_{i,y,b}\right)\Delta t \\ +\left(\left(\pi_{y,b}^{Mt} + \pi_{t,y,b}^{buy}\right)P_{t,y,b}^{ST,buy} - \pi_{t,y,b}^{sell}P_{t,y,b}^{ST,sell}\right)\Delta t \\ +\sum\limits_{r\in\Omega^{R}}\sum\limits_{i\in\Omega^{bus}} \delta_{r,i,b}^{Re}\cdot\pi_{r,y,b}^{Mt,Re} \\ +\sum\limits_{k\in\Omega^{f\&s}}\sum\limits_{i\in\Omega^{bus}} \left(\delta_{k,i,y,b}^{BESS} - \delta_{k,i,y,b}^{BESS,retire}\right)\cdot\pi_{k,y,b}^{Mt,BESS} \end{array}\right] \end{array}\right\}
\end{aligned}
\tag{6.22}
$$

where $P_{i,t,y,b}^{G}$ is the output power of micro-thermal generator; $a_{i,y,b}$, $b_{i,y,b}$, $c_{i,y,b}$ are the cost coefficient of the generator; $\pi_{y,b}^{Mt}$, $\pi_{t,y,b}^{buy}$, and $\pi_{t,y,b}^{sell}$ represent the cost of substation maintenance, purchase electricity, and feed-in tariff; $P_{t,y,b}^{ST,buy}$, $P_{t,y,b}^{ST,sell}$ are the electricity purchased from and sold to the transmission network by the substation; $\pi_{r,y,b}^{Mt,Re}$ and $\pi_{k,y,b}^{Mt,BESS}$ denote the maintenance cost of renewable energy devices and different types of BESS, its value is assumed to be 3.5-10% of the investing cost depending on the equipment.

The environmental cost of the system is to limit excessive carbon emissions during system operation. In addition to the generator and the substation, this chapter assumes that some emissions will also be generated in the process of disposal of retired batteries. Therefore, the equation is as follows:

$$
\begin{aligned}
C_y^{Car} &= C_y^{Car,G} + C_y^{Car,ST} + C_y^{Car,BESS,retire} \\
&= \sum_{s\in S}\sum_{t\in T}\left\{\begin{array}{l} w_{syb} \times \\ \left[\begin{array}{l} \sum\limits_{i\in\Omega^{bus}} \left(P_{i,t,y,b}^{G}\xi_{i,y,b}^{G}\Delta t\right) \\ +\left(P_{t,y,b}^{ST,buy}\xi_{y,b}^{ST}\Delta t\right) \\ +\sum\limits_{k\in\Omega^{f\&s}}\sum\limits_{i\in\Omega^{bus}} \delta_{k,i,y,b}^{BESS,retire}\xi_{y,b}^{BESS} \end{array}\right]\pi_{y,b}^{Carbon} \end{array}\right\}
\end{aligned}
\tag{6.23}
$$

where $\xi_{i,y,b}^{G}$, $\xi_{y,b}^{ST}$ and $\xi_{y,b}^{BESS}$ indicate the carbon emission intensity of the generator, the substation, and the retirement of BESS, respectively; $\pi_{y,b}^{Carbon}$ is the cost coefficient of the carbon tax.

The constraints of the objective function are expressed below:

$$\begin{Bmatrix} S_{ij,t,y,b} + P_{t,y,b}^{ST,buy} - P_{t,y,b}^{ST,sell} + P_{i,t,y,b}^{G} \\ + \sum_{r \in \Omega^R} P_{r,i,t,y,b}^{Re} + P_{k,i,t,y,b}^{BESS,dis} - P_{k,i,t,y,b}^{BESS,ch} \end{Bmatrix} = \begin{Bmatrix} P_{i,t,y,b}^{D} \\ +P_{i,t,y,b}^{CP} + P_{i,t,y,b}^{FCS} \end{Bmatrix} \tag{6.24}$$

$$S_{ij,t,y,b} - B_{ij}\left(\theta_{i,t,y,b} - \theta_{j,t,y,b}\right) = 0 \tag{6.25}$$

$$\underline{S_{ij,t,y,b}} \le S_{ij,t,y,b} \le \overline{S_{ij,t,y,b}} \tag{6.26}$$

$$\underline{P_{i,t,y,b}^{G}} \le P_{i,t,y,b}^{G} \le \overline{P_{i,t,y,b}^{G}} \tag{6.27}$$

$$\begin{cases} 0 \le P_{t,y,b}^{ST,buy} \le \overline{P_{t,y,b}^{ST,buy}} \\ 0 \le P_{t,y,b}^{ST,sell} \le \overline{P_{t,y,b}^{ST,sell}} \end{cases} \tag{6.28}$$

$$P_{r,i,t,y,b}^{Re} = g_{r,i,t,y,b}^{Re} \times \delta_{r,i,b}^{Re} \tag{6.29}$$

Equations (6.24)-(6.25) express nodal power balance and power flow constraints, where $S_{ij,t,y,b}$ is the power flow from bus i to bus j at time t; $P_{r,i,t,y,b}^{Re}$ indicates the power output from renewable energy devices; $P_{i,t,y,b}^{D}$ denotes the load of bus i; B_{ij}, $\theta_{i,t,y,b}$ and $\theta_{j,t,y,b}$ are the line susceptance at branch $i-j$, and voltage phase angle of bus i and bus j, respectively. Equations (6.26)-(6.28) indicate the upper bounds and lower bounds $\underline{(\bullet)}$ of $S_{ij,t,y,b}$, $P_{i,t,y,b}^{G}$, $P_{t,y,b}^{ST,buy}$ and $P_{t,y,b}^{ST,sell}$. In (6.29), $g_{r,i,t,y,b}^{Re}$ is the power output function of rth type of renewable energy device.

$$E_{k,i,t+1,y,b}^{BESS} = \sum_{k \in \Omega^{f\&s}} \begin{Bmatrix} E_{k,i,t,y,b}^{BESS} + \left(P_{k,i,t,y,b}^{BESS,ch} u_k^{eff,ch}\right)\Delta t \\ -\left(P_{k,i,t,y,b}^{BESS,dis} / u_k^{eff,dis}\right)\Delta t \end{Bmatrix} \tag{6.30}$$

$$0 \le E_{k,i,t,y,b}^{BESS} \le \overline{E_{k,i,t,y,b}^{BESS}}\left(\delta_{k,i,y,b}^{BESS} - \delta_{k,i,y,b}^{BESS,retire}\right) \tag{6.31}$$

$$0 \le P_{k,i,t,y,b}^{BESS,ch} \le \overline{P_{k,i,t,y,b}^{BESS,ch}} \times \delta_{k,i,t,y,b}^{c} \tag{6.32}$$

$$0 \le P_{k,i,t,y,b}^{BESS,dis} \le \overline{P_{k,i,t,y,b}^{BESS,dis}} \times \delta_{k,i,t,y,b}^{d} \tag{6.33}$$

$$\delta_{k,i,y,b}^{BESS} \le \delta_{k,i,y+1,b}^{BESS} \tag{6.34}$$

$$\delta_{k,i,y,b}^{BESS,retire} \le \delta_{k,i,y+1,b}^{BESS,retire} \tag{6.35}$$

$$\delta_{k,i,y,b}^{BESS,retire} \leq \delta_{k,i,y,b}^{BESS} \tag{6.36}$$

$$0 \leq \sum_{k \in \Omega^{f\&s}} \delta_{k,i,y,b}^{BESS} \leq 1 \tag{6.37}$$

$$\delta_{k,i,t,y,b}^{c} + \delta_{k,i,t,y,b}^{d} \leq 1 \tag{6.38}$$

$$\Delta d_{k,i,t,y,b} = \left| \frac{E_{k,i,t,y,b}^{BESS} - E_{k,i,t-1,y,b}^{BESS}}{\overline{E_{k,i,t,y,b}^{BESS}}} \right| \tag{6.39}$$

$$n_{100,k,i,y,b}^{eq,day} = \sum_{t \in T} N_0 \left(\Delta d_{k,i,t,y,b} \right)^{kp} \tag{6.40}$$

$$T_{cycle,k,i,b}^{remaining} = \frac{N_{100,k,i,b}^{fail}}{\sum_{y \in Y} \sum_{b \in B} W \cdot n_{100,k,i,y,b}^{eq,day}} \tag{6.41}$$

$$Loss_{k,i,b}^{cycle}(\%) = \frac{1}{T_{cycle,k,i,b}^{remaining}} \times 100\% \tag{6.42}$$

$$SOH_{k,i,b}(\%) = SOH_{k,i,b}^{initial}(\%) - Loss_{k,i,b}^{cycle}(\%) \tag{6.43}$$

$$\underline{SOH_{k,i,b}(\%)} \leq SOH_{k,i,b}(\%) \leq \overline{SOH_{k,i,b}(\%)} \tag{6.44}$$

$$\delta_{k,i,y,b-1}^{BESS,retire} = \begin{cases} 1; & if\ SOH_{k,i,b-1}(\%) < SOH_{k,i}^{safety}(\%) \\ \delta_{k,i,y,b-1}^{BESS,retire}; & otherwise \end{cases} \tag{6.45}$$

Equations (6.30)-(6.45) express the constraints related to BESS echelon utilization. To reduce the computational difficulty, this chapter linearizes the nonlinear part of (6.5), as shown in (6.30). This method is to achieve the same constraint effect as the original equation by adding the number of constraints. In (6.31)-(6.33), $\delta_{k,i,t,y,b}^{c}$ and $\delta_{k,i,t,y,b}^{d}$ are the decision variables of BESS to restrict BESS simultaneous charging and discharging, which is explained in (6.38). The above decision variables need to satisfy the constraints from (6.34) to (6.38). Equations (6.34)-(6.36) respectively indicate that in the same period block, BESS is not allowed to be repeatedly installed and dismantled, and retirement can only be performed after installation. Equation (6.37) denotes that the system can only install one type (fresh or second life) of BESS at the same candidate bus.

Combined with the above BESS model, for the life cycle calculation method of specific DOD, because BESS may not be able to complete a full charging and discharging behavior in each operation cycle. Therefore, the change in DOD is expressed in time series and can be obtained in (6.39), where $\Delta d_{k,i,t,y,b}$ represents the amount of DOD change in adjacent times. According to (6.1) and (6.4), the 100%-DOD equivalent BESS daily cycle number $n_{100,k,i,y,b}^{eq,day}$ and the total remaining cycles of BESS $T_{cycle,k,i,b}^{remaining}$ are calculated from (6.40), (6.41), respectively. N_0 is a battery cycle parameter, usually 0.5 or 1; $N_{100,k,i,b}^{fail}$ represents the BESS total number of cycles at 100%-DOD. Then, the loss and SOH of BESS can be obtained from (6.42), (6.43), where $Loss_{k,i,b}^{cycle}(\%)$ denotes the loss of BESS life cycles, and its value is equal to the reciprocal of $T_{cycle,k,i,b}^{remaining}$; $SOH_{k,i,b}(\%)$, $SOH_{k,i,b}^{initial}(\%)$ are the real-time remaining health status and initial SOH value of kth type BESS at ith bus in a period block. Combining equations (6.39)-(6.41), and (6.30)-(6.33), it can be seen that the main difference in the operation of fresh batteries and SLBs is the charging and discharging efficiency, the rated energy capacity, and the upper limit of the charging and discharging power. Since this chapter assumes that the SLBs used are strictly tested, the remaining parameters of the SLBs are consistent with fresh batteries.

To ensure the safe operation of the system and increase the overall service life of the BESS, it is necessary to limit the safety margin of BESS energy storage during the operation process, as shown in (6.44). This constraint can ensure that the charging and discharging behavior of BESS are limited when the SOH value is low. Generally speaking, it is believed that the charge and discharge efficiency of SLBs is lower than that of fresh batteries. Because of this, BESS composed of SLBs will have more power loss during charging and discharging. Therefore, without the restriction of equation (6.44), the capacity reduction of SLBs will be faster than that of fresh batteries. As shown in (6.45), before the start of the planning of each period block, the system will check the SOH value of each currently installed BESS. If $SOH_{k,i,b-1}(\%)$is lower than the set safety value $SOH_{k,i}^{safety}(\%)$, the system will force it to retire, and $\delta_{k,i,y,b-1}^{BESS,retire}$ will become 1. The retirement cost will be added to the total cost of the system. Subsequently, in the bth period block, the variables $\delta_{k,i,y,b}^{BESS}$, $\delta_{k,i,y,b}^{BESS,retire}$, and $SOH_{k,i,b}(\%)$ will be restored to their initial values. Otherwise, these values from the $b-1$th block are retained until the bth block. This process is the multiple life cycles of BESS.

6.4 Stage II, The Flexibility Analysis of Planned Network

In this section, the analysis approach of system flexibility in stage II and the models of adaptation cost are introduced. Among them, the results of each period of the first stage will be input as parameters into the second stage. After obtaining the results of stage II, we comprehensively analyze and compare the results of the two stages to obtain the optimal results. The purpose of stage II is to assess the flexibility of the system in the face of uncertain prediction errors.

A. Overview of System Flexibility Analysis Method

The implementation of planning usually takes many years. During this period, uncertainty errors may also cause major changes in the result. For example, it may lead to failure to achieve the original objectives after the planning is completed and cause a sharp rising in the overall system cost [125]. Therefore, before the implementation of the planning, it is necessary to consider the flexibility of the system in advance.

The flexibility of the system can be determined by comparing the adaptation cost of each system in possible future scenarios [126]. The main process of the system flexibility assessment method adopted in this chapter is shown below. Firstly, according to the system planning results of each period block in the first stage, combined with previously inapplicable uncertainty prediction errors, N future scenarios are randomly generated in the bth period block. Secondly, calculate whether the planning scheme of the first stage can meet the operating constraints in the nth scenario. If not, it is necessary to re-expansion the system to meet the constraints and calculate the adaptation cost. If yes, evaluate the next case. Finally, by repeating the process $N \times B$ times, the adaptation cost of all scenarios can be obtained.

The Main Procedure of System Flexibility Assessment

for $b = 1{:}B$
    for $n = 1{:}N$
        Initialization: Candidate Expansion Options, System Uncertainty Errors, Existing Units Information
        Randomly Generate Future Scenarios
        if in $\boldsymbol{n}$**th** scenario, the system operation constraints cannot be satisfied?
        Perform Re-expansion Planning (6.46)-(6.49)
        Adaptation Cost (n) = Adaptation Cost
        $n = n + 1$
        else

$n = n + 1$

end

$b = b + 1$

end

B. The System Flexibility Assessment Model

Stage II is to analyze the flexibility of the planned system, that is, whether the system needs to be re-expanded when faced with uncertain prediction errors. The model in this part is mixed-integer nonlinear programming. The variables in the model are mixed. There are 2 types of decision variables, which are binary variables to determine the installation of feeder and substation. The objective function of this stage is shown below:

$$Min\ J_2 = \left\{ \frac{1}{(1+\sigma)^b} \left[\begin{aligned} & \left(\pi_b^{ST} \cdot \overline{P^{ST}} \cdot \delta^{ST} \right) \\ & + \sum_{ij \in \Omega^{bus}} \left(\pi_{ij,b}^{Line} \cdot l_{ij}^{Line} \cdot \delta_{ij}^{Line} \right) \end{aligned} \right] \right\} \tag{6.46}$$

where π_b^{ST}, $\pi_{ij,b}^{Line}$ are the investment cost of substations and feeders; l_{ij}^{Line} is the length of the feeder; δ^{ST} and δ_{ij}^{Line} represent the quantities of expanded substations and feeders.

The constraints of power flow and substation are as follows:

$$S_{ij,t,y,b} - B_{ij}\left(\delta_{ij}^{Line,initial} + \delta_{ij}^{Line}\right)\left(\theta_{i,t,y,b} - \theta_{j,t,y,b}\right) = 0 \tag{6.47}$$

$$\left|S_{ij,t,y,b}\right| \le \left(\delta_{ij}^{Line,initial} + \delta_{ij}^{Line}\right)\overline{S_{ij,t,y,b}} \tag{6.48}$$

$$\begin{cases} 0 \le P_{t,y,b}^{ST,buy} \le \left(1 + \delta^{ST}\right)\overline{P_{t,y,b}^{ST,buy}} \\ 0 \le P_{t,y,b}^{ST,sell} \le \left(1 + \delta^{ST}\right)\overline{P_{t,y,b}^{ST,sell}} \end{cases} \tag{6.49}$$

where $\delta_{ij}^{Line,initial}$ denotes the initial quantities of the feeder at branch $i - j$. The constraints of nodal power balance, renewable energy, and BESS are mentioned above, which is:

(6.24), (6.27), (6.29)-(6.33), (6.38)

In this chapter, all the equations are satisfied: $\forall i,j \in \Omega^{bus}, \forall r \in \Omega^{R}, \forall k \in \Omega^{f\&s}, \forall s \in S, \forall t \in T, \forall y \in Y, \forall b \in B$.

6.5 Chapter Case Study

A. Experiment Settings and Uncertainty Prediction

In the proposed optimization problem, the transportation network planning in stage I is nonlinear programming, and the electricity system planning in stage I and stage II are mixed-integer quadratic programming and mixed-integer nonlinear programming, respectively. In the first stage of the two-stage optimization problem, each period of the power system planning has 9,396 variables, 6,240 equality constraints, and 10,800 inequality constraints. All of the problems can be solved by SCIP of OPTI toolbox in MATLAB. The advantage of this solver is that it can quickly find feasible solutions through pre-solving when facing complex mixed-integer nonlinear problems, but the disadvantage is that it may be easily trapped in the local optimum. The program of uncertainty prediction is implemented in the Python platform. The simulations were performed on a PC with a 3.2 GHz Intel (R) Core (TM) i7-8700 CPU and 16GB RAM. The solving time of multi-period network planning problems is about 17 minutes, and the remaining problems are usually solved within 1 minute, which is acceptable for long-timescale planning problems. The proposed two-stage integrated network co-planning method is conducted on the modified IEEE 33-bus microgrid and the 20-node transportation network. The basic parameters of the systems are quoted from [105] and [77]. To verify the effectiveness of the proposed method and model, three cases are established:

Case 1: Consider the BESS composed of fresh batteries or SLBs, simultaneously.

Case 2: Only consider the BESS composed of fresh batteries.

Case 3: Only consider the BESS composed of SLBs.

Case 1 is selected as the base case to verify whether the proposed model can reasonably select different types of BESS. Case 2 and case 3 are established to confirm which system has a lower cost when all BESS in the system are only consisted of fresh batteries or SLBs compared with case 1. Comparing case 2 and case 3, the BESS of case 2 only considers fresh batteries. Therefore, the rated capacity and power of its BESS will be higher than the BESS of case 3, which could lead to a lower system operation cost in case 2. The main reasons for designing these three cases are that case 1 is to test the effectiveness of the proposed model, that is, whether the system can make a reasonable choice between the two types of BESS. Case 2 and case 3 are the control groups that compare with case 1 in terms of renewable energy investment cost, system operating cost, battery investment cost, total system cost, and system flexibility. Furthermore, only fresh batteries or SLBs can be chosen to install under the setup of case 2 and 3. However, there is no limitation in case 1, hence, the impact of the rated capacity and power on system operation can be obtained through the comparison between case 1 and other cases. In the above cases, the total planning period of the system in stage I is 20 years, of which a period of 5 years is divided into 4-period blocks. After the completion of the first stage of simulation, all three cases will be evaluated for flexibility in stage II. The system parameters about BESS, microgrid, and transportation network are shown in Table 6-1, and Table 6-2. Regarding the O&M cost of batteries, according to the BESS Economic Analysis Report of World Bank Group in 2020 [126], BESS's O&M cost is about 3%-4.5% of its investment cost. Considering that the investment cost of SLBs is much lower than that of fresh batteries, and we assume that SLBs require more maintenance costs. Therefore, in this experiment, we set the investment cost of BESS composed of fresh batteries as the standard, and the O&M cost of BESS composed of fresh batteries and SLBs are 3% and 4.5% of that standard, respectively.

TABLE 6-1 MAIN PARAMETERS OF BESS

Fresh		SLB	
Parameter	***Value***	***Parameter***	***Value***
$\pi_{k,y,b}^{BESS}$	356.0$/kWh	$\pi_{k,y,b}^{BESS}$	73.0$/kWh
$\overline{E_{k,i,t,y,b}^{BESS}}$	700 kWh	$\overline{E_{k,i,t,y,b}^{BESS}}$	560 kWh
$u_k^{eff,ch}$	0.9	$u_k^{eff,ch}$	0.72
$u_k^{eff,dis}$	0.9	$u_k^{eff,dis}$	0.72
Parameter	***Value***	***Parameter***	***Value***
kp	1	$SOH_{k,i}^{safety}$(%)	60
$\underline{SOH_{k,i,b}}$(%)	40	$\overline{SOH_{k,i,b}}$(%)	100, 80

Before the start of the two-stage simulation, GANs are used for uncertainty prediction to generate future scenarios. The uncertain factors that need to be predicted in this chapter include wind speed, traffic flow, load, and solar exposure. The architecture and specific parameter settings of GANs in this article are quoted [49], and various historical data come from AEMO, BOM, and Highways England [128-129]. The comparison between the generated result sample and the real historical data is shown in Figure 6-4. It can be seen that the results of most data predictions, such as the time and amount of peak values, are not much different from the original data. There is a slight delay in the time of wind speed, load, and solar data, respectively, but this will not have much impact on the subsequent optimization results.

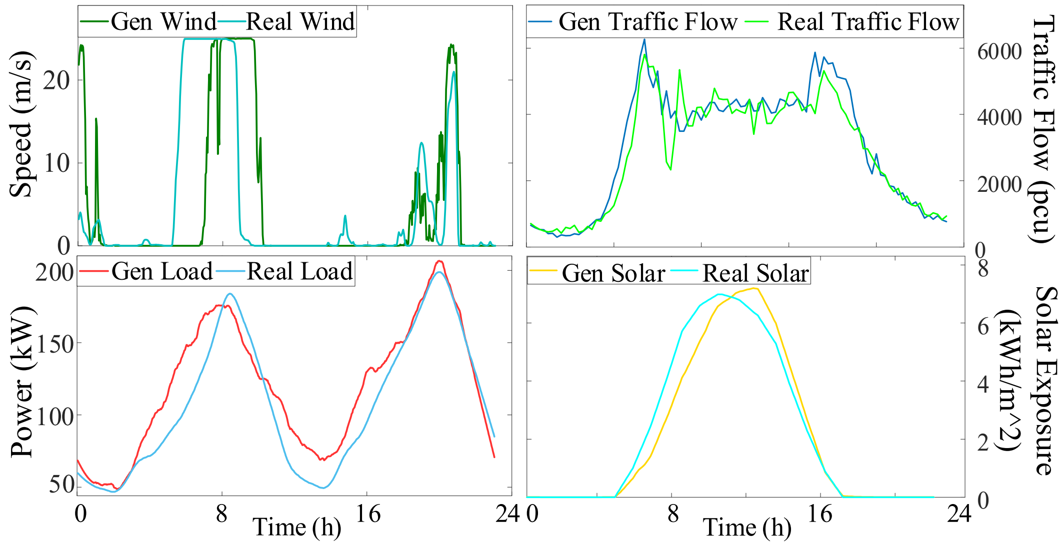

Figure 6-4 Comparison of generated data and historical data

TABLE 6-2 MAIN PARAMETERS SETTING OF STAGE I AND STAGE II

Parameter	***Value***	***Parameter***	***Value***
$\pi_{r,b}^{Re}$ (Solar)	3000 $	$\pi_{r,b}^{Re}$ (Wind)	60000 $
P_i^{CP}	3.6 kW	$P_{i,t}^{FCS}$	35 kW
β	80%	$\pi_{y,b}^{Carbon}$	25.53 $/ton
$\pi_{ij,b}^{Line}$	50000 $/KM	π_b^{ST}	365000 $/MW

B. Numerical Analysis of Stage I

After the iteration of the first period, the network topology of case 1 is shown in Figure 6-5. According to the final result of case 1, 90 PV panels are installed at bus 6, 9, 22, 26, 28; 72 PV panels are added at bus 15; and 10 wind generators are built at bus 6, 21, 25, 26; 8 wind generators are established at bus 18.

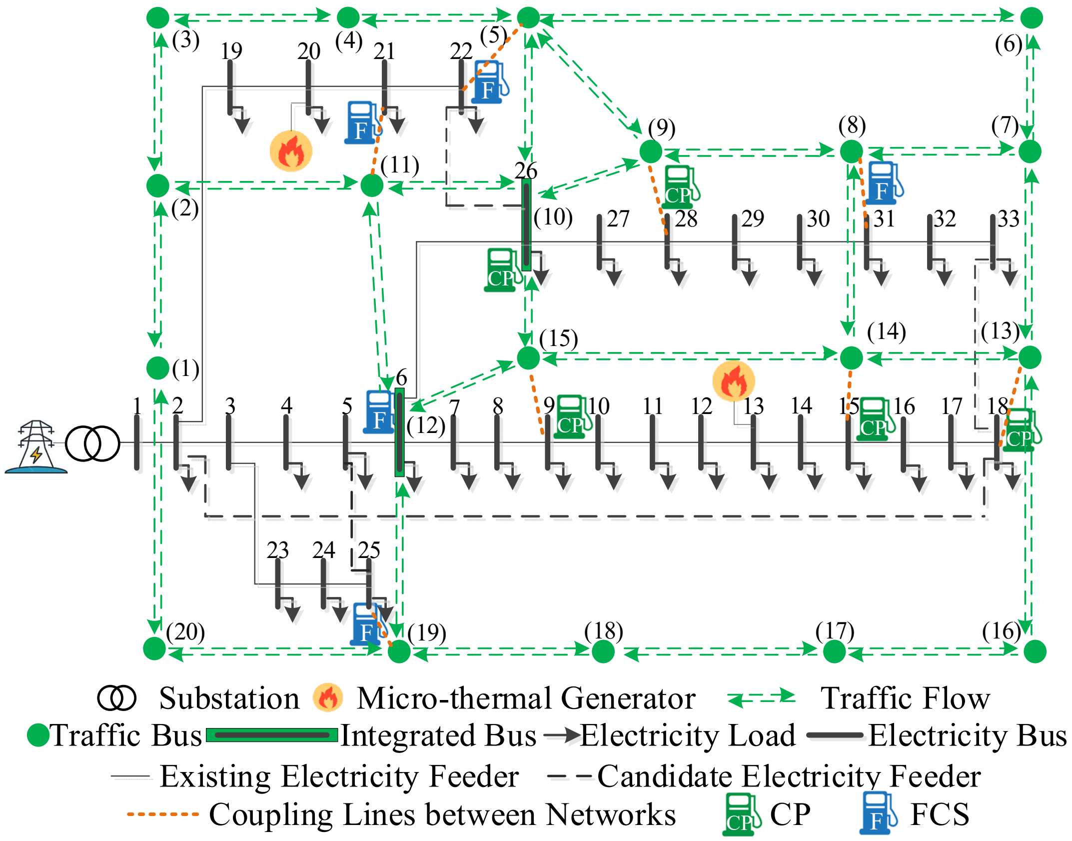

Figure 6-5 Network topology diagram of microgrid and transportation network

In case 1, the validity of SOH safety margin constraints was verified by comparison. The result is shown in Figure 6-6. When the BESS life is sufficient, the constraint does not affect the charging and discharging behavior of the BESS basically, but once the remaining SOH is insufficient, the constraint will restrict its operation. By allowing battery charging and discharging only when necessary, it is ensured that the battery life will not fall below the set value within a planned period.

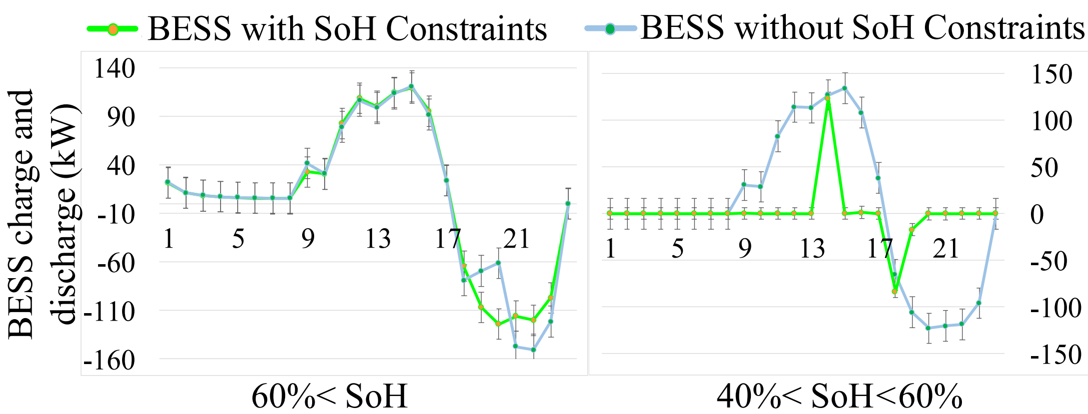

Figure 6-6 Comparison of the system with or without SOH constraints

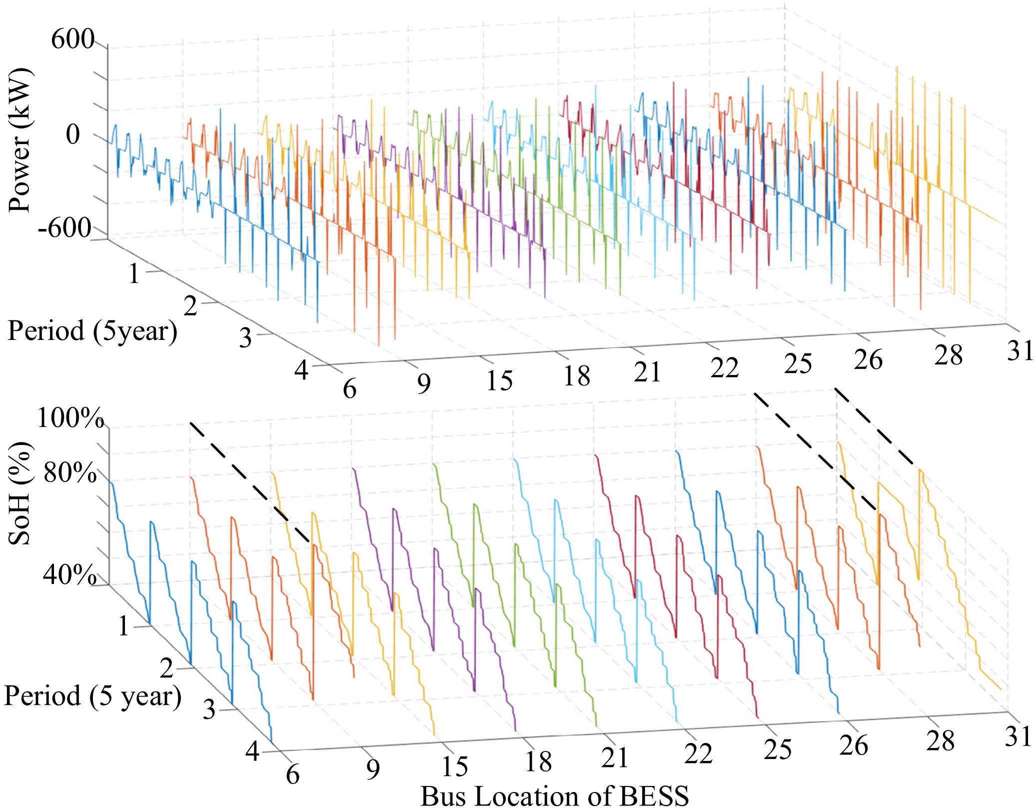

Figure 6-7 BESS operation and its multiple life cycles

Figure 6-7 further shows the BESS situations during the entire planning horizon in case 1, including charging and discharging behavior, selection, installation, and retirement for replacement. Among them, according to the SOH values, it can be known that the system has installed BESS composed of fresh batteries at the bus 31 in the third, 9, 28 in the fourth-period blocks, respectively. The BESS installed in the system on the remaining buses are all composed of SLBs. The results in the figure prove the effectiveness of the proposed model simultaneously, that is, replace the BESS whose SOH is lower than its set safety value to ensure the secure and reliable operation of the system.

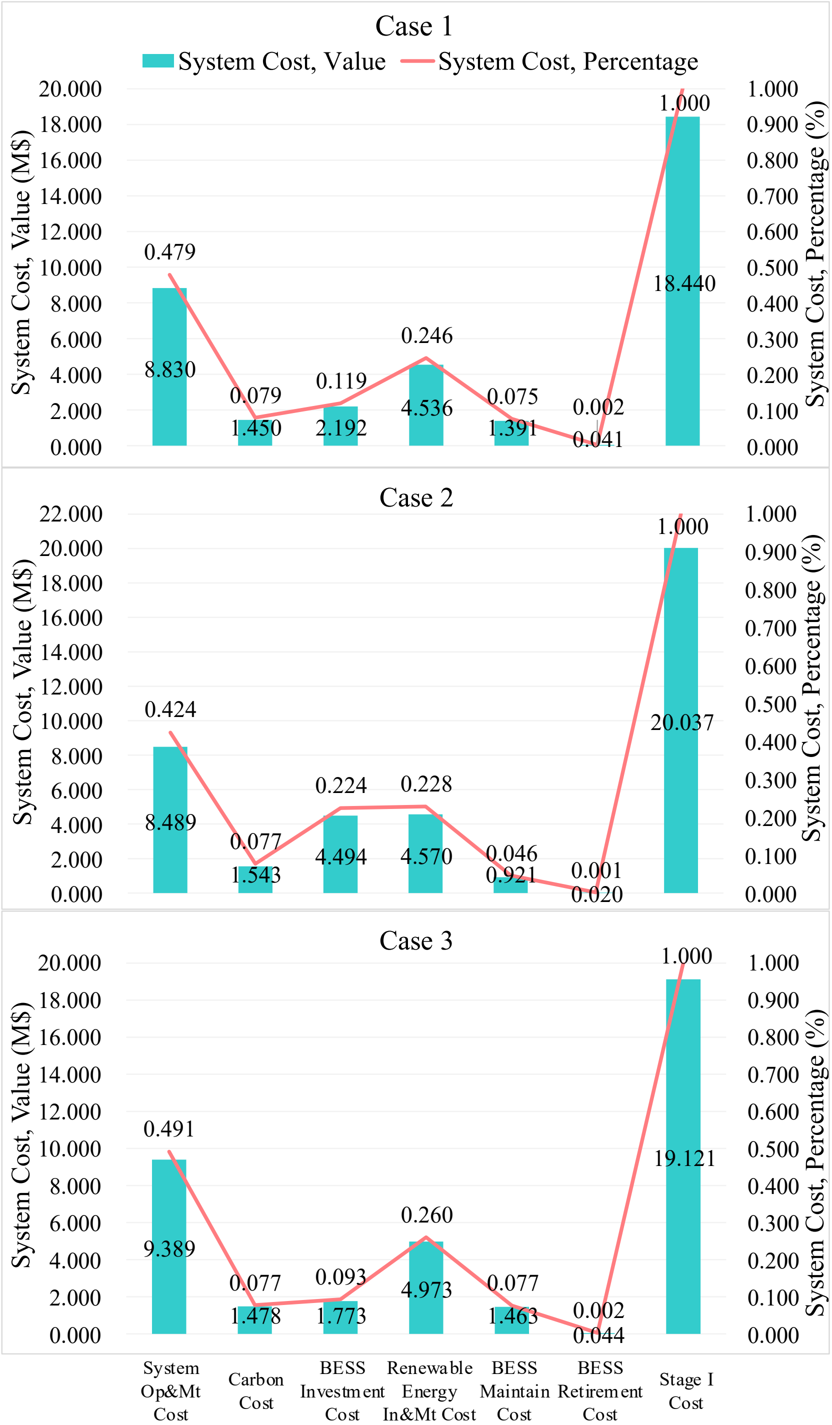

Figure 6-8 System cost comparison between various cases

Subsequently, comparing stage I optimization results among the three cases, it can be concluded that comprehensive consideration of the echelon utilization of BESS composed of fresh batteries and SLBs can usefully reduce system costs. The results are shown in Figure 6-8. The system total cost of case 1 is the lowest of the three cases, which is about \$18.440 million. The total costs of case 2 and case 3 are about \$20.037 million and \$19.121 million, respectively. Among them, it can be seen that because the

BESS in case 2 is all made up of fresh batteries, the investment cost of BESS is the highest among all cases. However, due to the longer period of lifespan, its BESS retirement costs are also the lowest. On the contrary, the BESS investment cost in case 3 is the lowest, but its system operating and maintenance cost is the highest among the three cases. Although the planning scheme of BESS composed of SLB in Case 3 will increase the remaining cost of the system, due to its extremely low BESS investment cost, Case 3 can still achieve a lower total system cost than Case 2. In summary, case 1 combines the advantages of the other two cases. While significantly declining the investment cost of BESS, the remaining system costs can also be controlled within an acceptable range, thereby greatly reducing the total cost of the system.

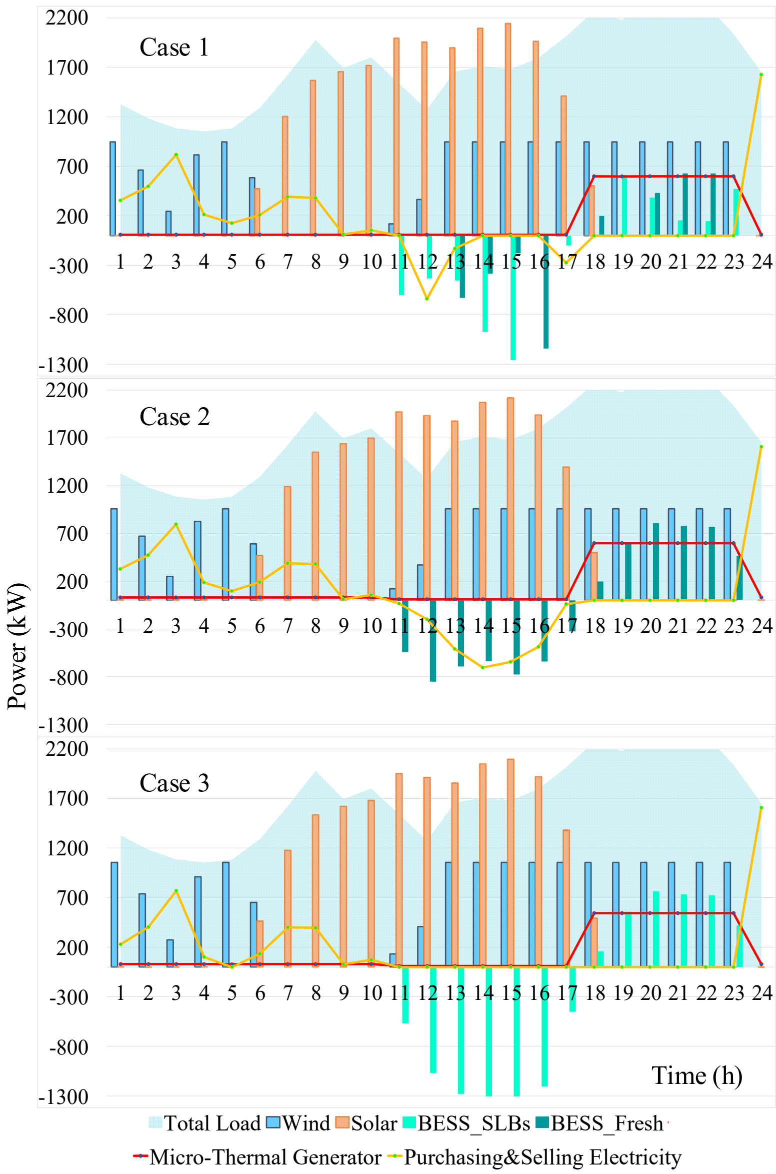

Figure 6-9 The system operation situations of each case

Compare the operation of the system in the fourth period of the three cases, as shown in Figure 6-9. In this figure, BESS_SLBs and BESS_Fresh respectively represent the charge and discharge curves of BESS composed of SLBs and fresh batteries. It can be seen that case 1 and case 2 need to sell electricity to deal with the electricity generated by renewable energy, and the electricity sold by case1 is less than case2. During the operation of the microgrid, due to the price difference between the purchasing and selling of electricity, the system usually does not choose to sell electricity actively when the capacity of the BESS is sufficient. In case 2, the SOH of all BESS did not fall below their set safe value in the third period, but in this period, it would cause insufficient available SOH. Due to the safety margin constraint of BESS, the system restricts its charging and discharging behavior.

C. Feasibility analysis of the proposed method

In the second stage, the flexibility analysis for the planning results of stage I is carried out, and the results are shown in Figure 6-10. The system flexibility analysis method in this chapter applies the empirical cumulative distribution function (CDF). It can intuitively display the probability of a particular value of adaptation cost.

TABLE 6-3 PROBABILITY AND VALUE OF ADAPTATION COSTS IN THREE CASES

	1 M$	2 M$	3 M$	4 M$	5 M$
Case 1	55.00%	38.75%	27.50%	16.25%	6.25%
Case 2	66.25%	43.75%	28.75%	15.00%	3.75%
Case 3	65.00%	48.75%	37.50%	20.00%	11.25%
	Maximum Adaptation Cost				
Case 1	5.85 M$				
Case 2	5.60 M$				
Case 3	5.95 M$				

As shown in Table 6-3, when the adaptation cost is 4 million dollars, the probability of occurrence of case 2 is about 15%, which is the lowest of the three cases. This proves that the system flexibility of case 2 is the highest at this moment. The probability of occurrence of case 1 and case 3 is approximately 16.25% and 20%, respectively. However, it should be noted that the system flexibility of case 1 is higher than that of case 2 when the adaptation cost is less than \$3 million. As the prediction errors of parameters such as future load and wind speed gradually increase, that is, after the adaptation cost is greater than \$3.5 million, the system flexibility of case 2 progressively exceeds that of case 1. To sum up, the systems of case 1 and case 2 have good flexibility. In case 3, because BESS is entirely composed of SLBs, the system is slightly lacking feasibility when it faces uncertain errors.

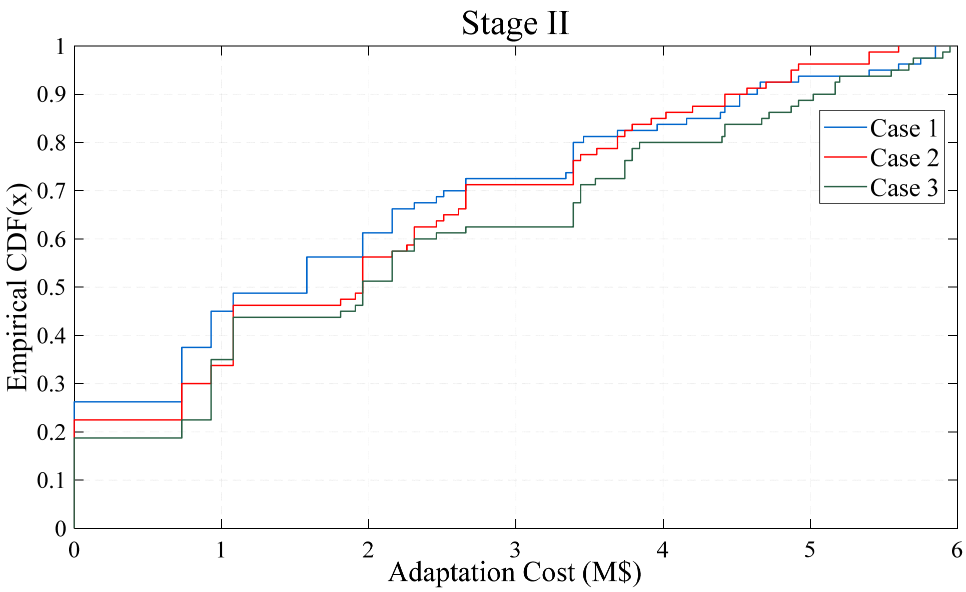

Figure 6-10 Empirical CDF of three cases

6.6 Chapter Summary

This chapter proposes an advanced two-stage collaborative system planning model, which considers the echelon utilization of retired on-board batteries. According to the multiple life cycles of the BESS, the cyclic replacement of the battery during the entire planning period can be realized. Moreover, through the analysis of flexibility, the performance of the system in the face of uncertain errors can be measured more intuitively. The model is implemented in an integrated network, which includes an IEEE 33-bus test system and a 20-node transportation network. The simulation results prove that reasonable utilization of SLBs can reduce the cost of the system to a certain extent while ensuring the flexibility of the system.

The number of retired EV batteries will experience explosive growth shortly, how to rationally reuse or recycle these batteries is an urgent issue that currently needs to be considered. Regarding the pricing of SLBs, since the price of SLBs will greatly affect their applicability, it is necessary to discuss the relevant price components in detail, for example, the studies can further consider its operating arbitrage ability when pricing. In the planning direction, in addition to applying retired EV batteries to the microgrid, as a backup power source in the power network or participating in the frequency regulation auxiliary service market is an approach to effectively utilizing its residual value, which method can usefully improve investment profitability of BESS and shorten the payback period of investment. Besides, the low SOH value of BESS may lead to serious results such as the sharp increase of power loss during the charging and discharging process and inaccurate SOC estimation. The influence of these factors on the planning results needs to be carefully considered. Furthermore, the impact of battery retirement on the environment is rarely discussed by studies currently. For example, how much impact the reasonable secondary utilization of retired batteries will have on carbon emissions is a question worthy of analysis. By studying the above problems, we can understand the characteristics of SLBs more clearly and make full development of their residual value.

Chapter 7 Conclusion and Future Work

This thesis constructs a comprehensive carbon management framework to model the low-carbon transition of power systems, optimizing system planning and operation to reduce emissions thoroughly at both system and societal levels.

Within this framework, the emission reduction targets encompass various emissions from Scope 1 to Scope 3. Firstly, inspired by existing methods for the retiring and retrofitting of CFPPs, this paper considers the source of system emissions, namely, emissions from fuel combustion, and proposes a comprehensive model and framework for CFPPs transformation planning. Subsequently, coordinated emission reduction FIS-based strategies are proposed, considering the bilateral characteristics of supply and demand. Under the premise of unquantifiable emission reduction intentions on the demand side, an active carbon target model is proposed, and the contribution of spatiotemporal carbon response to emission reduction is analyzed. Finally, considering the residual value of electric vehicle SLBs, cascading utilization planning for SLBs is proposed. Simulation and result analysis are mainly based on IEEE benchmark test systems of different network levels. The test results verify the advantages of the proposed model and methods in terms of effectiveness, scalability, and flexibility.

Although this thesis covers a broad spectrum of areas in the direction of low-carbon transition in power systems, there are undoubtedly still many research directions that can be further explored. Additionally, this paper involves many assumptions and premises, such as construction cycles, equipment aging, and consumer willingness, which may prevent the full achievement of the simulation results during the actual system transition process. These issues also need further discussion in future research. The following summarizes some directions:

- The coupling of artificial intelligence: With the development of methods such as deep learning and reinforcement learning, traditional parameter prediction strategies like load forecasting and price prediction are undergoing transformation. With the rise of large-scale language models, traditional methods of data analysis, forecasting, risk assessment management, and decision support are also gradually being replaced by artificial intelligence. However, how to effectively utilize these new artificial intelligence methods to improve or replace existing processes is a question that requires careful consideration. In this process, it is necessary to comprehensively consider the impact of artificial intelligence technology on aspects such as the security, reliability, and privacy of power systems, to ensure stable operation of the system and secure protection of user data.

- The coupling of power systems with the climate system on a long-term scale: The coupling between power systems and the climate system is essential in current planning and operational processes. Although short-term climate forecast results are commonly used, long-term changes in the climate system, such as the long-term trends of temperature, wind speed, solar radiation, etc., can significantly impact the current system planning outcomes, thereby affecting economic viability and system reliability. Therefore, in future planning and operational processes of power systems, it is necessary to consider the impacts of long-term climate changes further to enhance the resilience and anti-interference capability of the system.
- Lifecycle Assessment: Conduct comprehensive lifecycle assessments to evaluate the environmental impacts of different low-carbon transition strategies, deeply considering factors such as equipment manufacturing, operation, and decommissioning.
- Policy and Regulatory Frameworks: In recent years, countries have been accelerating the advancement of their emission reduction policies, and the mechanisms and scopes related to carbon markets have also been continuously adjusted. It is necessary to further analyze the effectiveness of existing policies and regulatory frameworks in promoting low-carbon transition and identifying opportunities for improvement or development of new market mechanisms.

Bibliography

[1] "State and Trends of Carbon Pricing 2021", World Bank, 2021. [Online]. Available: https://openknowledge.worldbank.org/handle/10986/35620.

[2] "Australia's plan to reach our net zero target by 2050," Australian Government, 26-Oct-2021. [Online]. Available: https://www.minister.industry.gov.au/ministers/taylor/media-releases/australias-plan-reach-our-net-zero-target-2050.

[3] "Draft law shows Germany plans to revise key emissions target for Energy Sector," Reuters, 05-Jul-2022. [Online]. Available: https://www.reuters.com/business/energy/draft-law-shows-germany-plans-revise-key-emissions-target-energy-sector-2022-07-05/.

[4] K. Appunn, "Parliament amends energy transition laws, weakens 2035 renewables target," Clean Energy Wire, 13-Jul-2022. [Online]. Available: https://www.cleanenergywire.org/news/parliament-amends-energy-transition-laws-weakens-2035-renewables-target.

[5] "National Greenhouse Gas Inventory Quarterly Update: March 2022," DCCEEW, 01-Aug-2022. [Online]. Available: https://www.dcceew.gov.au/climate-change/publications/national-greenhouse-gas-inventory-quarterly-update-march-2022.

[6] Congressional Budget Office, "Emissions of carbon dioxide in the Electric Power Sector," Congressional Budget Office, D.C., USA, Dec. 2022.

[7] "Sources of Greenhouse Gas Emissions," EPA, 05-Aug-2022. [Online]. Available: https://www.epa.gov/ghgemissions/sources-greenhouse-gas-emissions.

[8] "Electricity-sector-emissions-and-generation-data-2020-21," National Greenhouse and Energy Reporting, 28-Feb-2022. [Online]. Available: https://www.cleanenergyregulator.gov.au/NGER/National%20greenhouse%20and%20energy%20reporting%20data/electricity-sector-emissions-and-generation-data/electricity-sector-emissions-and-generation-data-2020-21.

[9] Y. Yang, J. Qiu, J. Ma, and C. Zhang, "Integrated grid, coal-fired power generation retirement and GESS planning towards a low-carbon economy," Int. J. Electr Power Energy Syst., vol. 124, p. 106409, Jan. 2021.

[10] G. He, D. S. Mallapragada, A. Bose, C. F. Heuberger, and E. Gencer, "Hydrogen Supply Chain Planning With Flexible Transmission and Storage Scheduling," IEEE Trans. Sustain. Energy, vol. 12, no. 3, pp. 1730–1740, Jul. 2021.

[11] Y. Tao, J. Qiu, S. Lai, J. Zhao, and Y. Xue, "Carbon-Oriented Electricity Network Planning and Transformation," IEEE Trans. Power Syst., vol. 36, no. 2, pp. 1034–1048, Mar. 2021.

[12] N. Zhang et al., "An Efficient Power System Planning Model Considering Year-round Hourly Operation Simulation," IEEE Trans. Power Syst., pp. 1–1, 2022, doi: 10.1109/TPWRS.2022.3146299.

[13] P. Denholm, D. J. Arent, S. F. Baldwin, D. E. Bilello, G. L. Brinkman, J. M. Cochran, W. J. Cole, B. Frew, V. Gevorgian, J. Heeter, B.-M. S. Hodge, B. Kroposki, T. Mai, M. J. O'Malley,

B. Palmintier, D. Steinberg, and Y. Zhang, “The challenges of achieving a 100% renewable electricity system in the United States,” Joule, vol. 5, no. 6, pp. 1331–1352, 2021.

[14] S. Impram, S. Varbak Nese, and B. Oral, “Challenges of renewable energy penetration on power system flexibility: A survey,” Energy Strategy Reviews, vol. 31, p. 100539, 2020.

[15] M. S. Alam, F. S. Al-Ismail, A. Salem, and M. A. Abido, “High-level penetration of renewable energy sources into grid utility: Challenges and solutions,” IEEE Access, vol. 8, pp. 190277–190299, 2020.

[16] Y. Lu, F. Cohen, S. M. Smith, and A. Pfeiffer, “Plant conversions and abatement technologies cannot prevent stranding of power plant assets in 2 °C scenarios,” Nature Commun, vol. 13, no. 1, p. 806, Feb. 2022.

[17] C. Kang et al., “Carbon Emission Flow From Generation to Demand: A Network-Based Model,” IEEE Trans. Smart Grid, vol. 6, no. 5, pp. 2386–2394, Sep. 2015.

[18] M. J. Ghadi, A. Rajabi, S. Ghavidel, A. Azizivahed, L. Li, and J. Zhang, “From active distribution systems to decentralized microgrids: A review on regulations and planning approaches based on operational factors,” Appl. Energy, vol. 253, p. 113543, Nov. 2019.

[19] Z. Lu, L. Bai, J. Wang, J. Wei, Y. Xiao, and Y. Chen, “Peer-to-Peer Joint Electricity and Carbon Trading based on Carbon-aware Distribution Locational Marginal Pricing,” IEEE Trans. Power Syst., pp. 1–1, 2022, doi: 10.1109/TPWRS.2022.3167780.

[20] C. Shao, K. Li, Z. Hu, and M. Shahidehpour, “Coordinated Planning of Electric Power and Natural Gas Distribution Systems With Refueling Stations for Alternative Fuel Vehicles in Transportation System,” IEEE Trans. Smart Grid, vol. 13, no. 5, pp. 3558–3569, Sep. 2022.

[21] B. Zeng, J. Zhang, X. Yang, J. Wang, J. Dong, and Y. Zhang, “Integrated Planning for Transition to Low-Carbon Distribution System With Renewable Energy Generation and Demand Response,” IEEE Trans. Power Syst., vol. 29, no. 3, pp. 1153–1165, May 2014.

[22] Y. Cheng, N. Zhang, B. Zhang, C. Kang, W. Xi, and M. Feng, “Low-Carbon Operation of Multiple Energy Systems Based on Energy-Carbon Integrated Prices,” IEEE Trans. Smart Grid, vol. 11, no. 2, pp. 1307–1318, Mar. 2020.

[23] C. Sabillon Antunez, J. F. Franco, M. J. Rider, and R. Romero, “A New Methodology for the Optimal Charging Coordination of Electric Vehicles Considering Vehicle-to-Grid Technology,” IEEE Transactions on Sustainable Energy, vol. 7, no. 2, pp. 596–607, Apr. 2016.

[24] M. Jacoby, "It’s time to get serious about recycling lithium-ion batteries", Chemical & Engineering News, 2020. [Online]. Available: https://cen.acs.org/materials/energy-storage/time-serious-recycling-lithium/97/i28.

[25] L. C. Casals, B. Amante García, and C. Canal, “Second life batteries lifespan: Rest of useful life and environmental analysis,” Journal of Environmental Management, vol. 232, no. 354–363, pp. 354–363, Feb. 2019.

[26] E. Hossain, D. Murtaugh, J. Mody, H. M. R. Faruque, Md. S. Haque Sunny, and N. Mohammad, “A Comprehensive Review on Second-Life Batteries: Current State, Manufacturing Considerations, Applications, Impacts, Barriers & Potential Solutions, Business Strategies, and Policies,” IEEE Access, vol. 7, pp. 73215–73252, 2019.

[27] D. Strickland, L. Chittock, D. A. Stone, M. P. Foster, and B. Price, “Estimation of Transportation Battery Second Life for Use in Electricity Grid Systems,” IEEE Transactions on Sustainable Energy, vol. 5, no. 3, pp. 795–803, Jul. 2014.

[28] Aemo.com.au, 2021. [Online]. Available: https://aemo.com.au/-

/media/files/electricity/nem/planning_and_forecasting/inputs-assumptions-methodologies/2021/aurecon-cost-and-technical-parameters-review-2020.pdf?la=en.
[29] "Battery Pack Prices Cited Below $100/kWh for the First Time in 2020, While Market Average Sits at $137/kWh | BloombergNEF", BloombergNEF, 2021. [Online]. Available: https://about.bnef.com/blog/battery-pack-prices-cited-below-100-kwh-for-the-first-time-in-2020-while-market-average-sits-at-137-kwh/.
[30] Y. Deng, Y. Zhang, and F. Luo, "Operational Planning of Centralized Charging Stations Using Second-Life Battery Energy Storage Systems," IEEE Transactions on Sustainable Energy, pp. 1–1, Jun. 2020.
[31] Afdc.energy.gov, 2021. [Online]. Available: https://afdc.energy.gov/files/u/publication/battery_second_life_faq.pdf.
[32] W. Shen, J. Qiu, K. Meng, X. Chen, and Z. Y. Dong, "Low-Carbon Electricity Network Transition Considering Retirement of Aging Coal Generators," IEEE Trans. Power Syst., vol. 35, no. 6, pp. 4193–4205, Nov. 2020.
[33] J. Guo, Y. Li, Y. Shen, J. Yu, and Y. Chen, "A Novel Incentive Mechanism for CCHP-Based Microgrids in Spinning Reserve," IEEE Trans. Power Syst., vol. 36, no. 3, pp. 1697–1712, May 2021.
[34] W. Liu, S. Chen, Y. Hou, and Z. Yang, "Trilevel Mixed Integer Optimization for Day-Ahead Spinning Reserve Management of Electric Vehicle Aggregator With Uncertainty," IEEE Trans. Smart Grid, vol. 13, no. 1, pp. 613–625, Jan. 2022.
[35] "CCS IN 2022," Global CCS Institute, https://status22.globalccsinstitute.com.
[36] "Capturing global attention: Carbon capture, utilisation and storage," CSIRO,https://www.csiro.au/en/news/All/Articles/2023/September/CCUS-explainer.
[37] H. Saboori and R. Hemmati, "Considering Carbon Capture and Storage in Electricity Generation Expansion Planning," IEEE Trans. Sustain. Energy, vol. 7, no. 4, pp. 1371–1378, Oct. 2016.
[38] A. Xuan, X. Shen, Q. Guo, and H. Sun, "Two-stage Planning for Electricity-Gas Coupled Integrated Energy System with Carbon Capture, Utilization, and Storage Considering Carbon Tax and Price Uncertainties," IEEE Trans. Power Syst., pp. 1–13, 2022.
[39] MIT Energy Initiative Symposium, "Retrotting of coal-fired power plants for CO2 emissions reductions," Massachusetts Institute of Technology, MA, USA, MITEI-Symposium-09-001-RP, Mar. 2009.
[40] S. Ladage, M. Blumenberg, D. Franke, A. Bahr, R. Lutz, and S. Schmidt, "On the climate benefit of a coal-to-gas shift in Germany's electric power sector," Sci. Rep., vol. 11, no. 1, p. 11453, Jun. 2021.
[41] "Transalta achieves full phase-out of coal in Canada," TransAlta, 28-Jun-2022. [Online]. Available: https://transalta.com/newsroom/transalta-achieves-full-phase-out-of-coal-in-canada/.
[42] S. M. Jordaan, A. W. Ruttinger, K. Surana, D. Nock, S. M. Miller, and A. P. Ravikumar, "Global mitigation opportunities for the life cycle of natural gas-fired power," Nature Clim. Chang., vol. 12, no. 11, pp. 1059–1067, Nov. 2022.
[43] M. Farhoumandi, F. Aminifar and M. Shahidehpour, "Generation Expansion Planning Considering the Rehabilitation of Aging Generating Units", IEEE Transactions on Smart Grid, vol. 11, no. 4, pp. 3384-3393, 2020.

[44] Q. Wang, X. Zhang, C. Yi, Z. Li, and D. Xu, “A Novel Shared Energy Storage Planning Method Considering the Correlation of Renewable Uncertainties on the Supply Side,” IEEE Trans. Sustain. Energy, vol. 13, no. 4, pp. 2051–2063, Oct. 2022.

[45] Y. Luo, B. Zeng, W. Zhang, Y. Liu, Q. Shi, and W. Liu, “Coordinative Planning of Public Transport Electrification, RESs and Energy Networks for Decarbonization of Urban Multi-Energy Systems: A Government-Market Dual-Driven Framework,” IEEE Trans. Sustain. Energy, vol. 15, no. 1, pp. 538–555, Jan. 2024.

[46] M. Z. Oskouei, B. Mohammadi-Ivatloo, O. Erdinc, and F. G. Erdinc, “Optimal Allocation of Renewable Sources and Energy Storage Systems in Partitioned Power Networks to Create Supply-Sufficient Areas,” IEEE Trans. Sustain. Energy, vol. 12, no. 2, pp. 999–1008, Apr. 2021.

[47] G. Pulazza, N. Zhang, C. Kang, and C. A. Nucci, “Transmission Planning With Battery-Based Energy Storage Transportation For Power Systems With High Penetration of Renewable Energy,” IEEE Trans. Power Syst., vol. 36, no. 6, pp. 4928–4940, Nov. 2021.

[48] C. Zhang, Y. Ding, Q. Wang, Y. Xue, and J. Østergaard, “Uncertainty-averse TRANSCO planning for accommodating renewable energy in CO2 reduction environment,” J. Mod. Power Syst. Clean Energy, vol. 3, no. 1, pp. 24–32, Mar. 2015.

[49] Y. Chen, Y. Wang, D. Kirschen and B. Zhang, "Model-Free Renewable Scenario Generation Using Generative Adversarial Networks", IEEE Transactions on Power Systems, vol. 33, no. 3, pp. 3265-3275, 2018.

[50] C. Zhang, J. Qiu, Y. Yang and J. Zhao, "Trading-oriented battery energy storage planning for distribution market", International Journal of Electrical Power & Energy Systems, vol. 129, p. 106848, 2021. Available: 10.1016/j.ijepes.2021.106848.

[51] P. Mancarella, "MES (multi-energy systems): An overview of concepts and evaluation models", Energy, vol. 65, pp. 1-17, 2014.

[52] J. Qiu, H. Yang, Z. Dong, J. Zhao, K. Meng, F. Luo and K. Wong, “A linear programming approach to expansion co-planning in gas and electricity markets”, IEEE Transactions on Power Systems, vol. 31, no. 5, pp. 3594-3606, 2016.

[53] Y. Tao, J. Qiu, S. Lai, and X. Sun, “Coordinated Planning of Electricity and Hydrogen Networks with Hydrogen Supply Chain for Fuel Cell Electric Vehicles,” IEEE Trans. Sustain. Energy, vol. 14, no. 2, pp. 1010–1023, Apr. 2023, doi: 10.1109/TSTE.2022.3232596.

[54] S. Lai, J. Qiu, and Y. Tao, “Credit-Based Pricing and Planning Strategies for Hydrogen and Electricity Energy Storage Sharing,” IEEE Trans. Sustain. Energy, vol. 13, no. 1, pp. 67–80, Jan. 2022, doi: 10.1109/TSTE.2021.3103886.

[55] Y. Tao, J. Qiu, S. Lai, and J. Zhao, “Integrated Electricity and Hydrogen Energy Sharing in Coupled Energy Systems,” IEEE Trans. Smart Grid, vol. 12, no. 2, pp. 1149–1162, Mar. 2021, doi: 10.1109/TSG.2020.3023716.

[56] J. Qiu, Z. Y. Dong, J. H. Zhao, K. Meng, Y. Zheng and D. J. Hill, ”Low Carbon Oriented Expansion Planning of Integrated Gas and Power Systems,” IEEE Transactions on Power Systems, vol. 30, no. 2, pp. 1035-1046, 2015.

[57] G. Liu, J. Liu, J. Zhao, J. Qiu, Y. Mao, Z. Wu, and F. Wen, “Real-time corporate carbon footprint estimation methodology based on appliance identification,” IEEE Trans. Ind. Inform., vol. 19, no. 2, pp. 1401–1412, 2023.

[58] Y. Tao, J. Qiu, S. Lai, X. Zhang, and G. Wang, “Collaborative Planning for Electricity

Distribution Network and Transportation System Considering Hydrogen Fuel Cell Vehicles," IEEE Trans. Transp. Electrific., vol. 6, no. 3, pp. 1211–1225, Sep. 2020.

[59] Z. Yan, C. Li, Y. Yao, W. Lai, J. Tang, C. Shao, and Q. Zhang, "Bi-level carbon trading model on demand side for integrated electricity-gas system," IEEE Trans. Smart Grid, pp. 1–1, 2022.

[60] Y. Yang, J. Qiu, and C. Zhang, "Distribution Network Planning Towards a Low-Carbon Transition: A Spatial-Temporal Carbon Response Method," IEEE Transactions on Sustainable Energy, vol. 15, no. 1, pp. 429 - 442, Jan. 2024.

[61] Y. Yang, J. Qiu, C. Zhang, J. Zhao, and G. Wang, "Flexible Integrated Network Planning Considering Echelon Utilization of Second Life of Used Electric Vehicle Batteries," IEEE Trans. Transp. Electrific., vol. 8, no. 1, pp. 263–276, Mar. 2022.

[62] M. Yan et al., "Blockchain for Transacting Energy and Carbon Allowance in Networked Microgrids," IEEE Trans. Smart Grid, vol. 12, no. 6, pp. 4702–4714, Nov. 2021.

[63] Y. Cheng, N. Zhang, Z. Lu, and C. Kang, "Planning Multiple Energy Systems Toward Low-Carbon Society: A Decentralized Approach," IEEE Trans. Smart Grid, vol. 10, no. 5, pp. 4859–4869, Sep. 2019.

[64] B. S. Palmintier and M. D. Webster, "Impact of Operational Flexibility on Electricity Generation Planning With Renewable and Carbon Targets," IEEE Trans. Sustain. Energy, vol. 7, no. 2, pp. 672–684, Apr. 2016.

[65] X. Sun, J. Qiu, Y. Yi, and Y. Tao, "Cost-Effective Coordinated Voltage Control in Active Distribution Networks With Photovoltaics and Mobile Energy Storage Systems," IEEE Trans. Sustain. Energy, vol. 13, no. 1, pp. 501–513, Jan. 2022.

[66] A. Bouallaga, A. Merdassi, A. Davigny, B. Robyns, and V. Courtecuisse, "Minimization of energy transmission cost and CO2 emissions using coordination of electric vehicle and wind power (W2V)," pp. 1-6, 2013.

[67] K. Zhang, C. Mao, J. Lu, D. Wang, X. Chen, and J. Zhang, "Optimal control of state-of-charge of superconducting magnetic energy storage for wind power system," IET Renew. Power Gener., vol. 8, no. 1, pp. 58-66, Jan. 2014.

[68] J. Lin, J. Qiu, Y. Yang, and W. Lin, "Planning of Electric Vehicle Charging stations considering fuzzy selection of Second Life Batteries," IEEE Trans. Power Syst., vol. 39, no. 3, pp. 5062–5076, May 2024. doi:10.1109/tpwrs.2023.3324001

[69] "Transport emissions", Climate Action, 2022. [Online]. Available: https://ec.europa.eu/clima/eu-action/transport-emissions_en. [Accessed: 29- Jan- 2022].

[70] Y. Tao, J. Qiu, S. Lai, X. Sun, and J. Zhao, "Adaptive Integrated Planning of Electricity Networks and Fast Charging Stations Under Electric Vehicle Diffusion," IEEE Trans. Power Syst., vol. 38, no. 1, pp. 499–513, Jan. 2023.

[71] T. Wu, X. Wei, X. Zhang, G. Wang, J. Qiu, and S. Xia, "Carbon-Oriented Expansion Planning of Integrated Electricity-Natural Gas Systems With EV Fast-Charging Stations," IEEE Trans. Transp. Electrific., vol. 8, no. 2, pp. 2797–2809, Jun. 2022.

[72] J. Zhu et al., "Coordination Planning of Integrated Energy System and Electric Vehicle Charging Station Considering Carbon Emission Reduction," IEEE Trans. on Ind. Applicat., vol. 59, no. 6, pp. 7555–7569, Nov. 2023.

[73] C. Li, Z. Dong, G. Chen, B. Zhou, J. Zhang, and X. Yu, "Data-Driven Planning of Electric Vehicle Charging Infrastructure: A Case Study of Sydney, Australia," IEEE Trans. Smart Grid, vol. 12, no. 4, pp. 3289–3304, Jul. 2021.

[74] W. Wei, L. Wu, J. Wang, and S. Mei, “Expansion Planning of Urban Electrified Transportation Networks: A Mixed-Integer Convex Programming Approach,” IEEE Trans. Transp. Electrific., vol. 3, no. 1, pp. 210–224, Mar. 2017.

[75] H. Zhang, S. J. Moura, Z. Hu, W. Qi, and Y. Song, “Joint PEV Charging Network and Distributed PV Generation Planning Based on Accelerated Generalized Benders Decomposition,” IEEE Trans. Transp. Electrific., vol. 4, no. 3, pp. 789–803, Sep. 2018.

[76] C.-M. Chan, C.-N. Lu, and Y. L. Lo, “Optimal Use of Existing Distribution Feeders to Accommodate Transportation Electrification,” IEEE Trans. Intell. Transport. Syst., vol. 16, no. 4, pp. 1941–1950, Aug. 2015.

[77] W. Yao, J. Zhao, F. Wen, Z. Dong, Y. Xue, Y, Xu, K, Meng, "A Multi-Objective Collaborative Planning Strategy for Integrated Power Distribution and Electric Vehicle Charging Systems", IEEE Transactions on Power Systems, vol. 29, no. 4, pp. 1811-1821, 2014.

[78] B. Lin and X. Li, “The effect of carbon tax on per capita CO2 emissions,” Energy Policy, vol. 39, no. 9, pp. 5137–5146, 2011.

[79] Y.-J. Zhang, T. Liang, Y.-L. Jin, and B. Shen, “The impact of carbon trading on economic output and carbon emissions reduction in China’s industrial sectors,” Applied Energy, vol. 260, p. 114290, 2020.

[80] C. Pankhurst, C. A. Cañizares, and K. Bhattacharya, “A Decentralised Transactive Energy Market Considering Physical System Constraints,” IEEE Trans. Smart Grid, vol. 15, no. 3, pp. 3165–3177, May 2024.

[81] G. Li, J. Yang, F. Wu, X. Zhu, S. Ke, and Y. Li, “A Market Framework for a 100% Renewable Energy Penetration Spot Market,” IEEE Trans. Sustain. Energy, vol. 14, no. 3, pp. 1569–1584, Jul. 2023.

[82] Z. Zhu, K. W. Chan, S. Bu, B. Zhou, and S. Xia, “Nash Equilibrium Estimation and Analysis in Joint Peer-to-Peer Electricity and Carbon Emission Auction Market With Microgrid Prosumers,” IEEE Trans. Power Syst., vol. 38, no. 6, pp. 5768–5780, Nov. 2023.

[83] H. Huang et al., “Blockchain-Enabled Carbon and Energy Trading for Network-Constrained Coal Mines With Uncertainties,” IEEE Trans. Sustain. Energy, vol. 14, no. 3, pp. 1634–1647, Jul. 2023.

[84] S. Cheng, S. C. Scholes, W. Kong, C. Gu, and F. Li, “Carbon-Oriented Electricity Balancing Market for Dispatchable Generators and Flexible Loads,” IEEE Trans. Power Syst., vol. 38, no. 6, pp. 5648–5659, Nov. 2023.

[85] Z. Liang, M. Bao, Y. Ding, Y. Hou, and Y. Song, “A Two-Stage Framework for Exploiting the Multi-Elasticity of Multi-Energy Demands in Integrated Electricity and Gas Markets,” IEEE Trans. Power Syst., vol. 39, no. 2, pp. 3196–3210, Mar. 2024.

[86] A. Awad, T. EL-Fouly and M. Salama, "Optimal ESS Allocation for Load Management Application", IEEE Transactions on Power Systems, vol. 30, no. 1, pp. 327-336, 2015.

[87] Y. Zhang, Z. Dong, F. Luo, Y. Zheng, K. Meng and K. Wong, "Optimal allocation of battery energy storage systems in distribution networks with high wind power penetration", IET Renewable Power Generation, vol. 10, no. 8, pp. 1105-1113, 2016.

[88] A. Gabash and P. Li, "Flexible Optimal Operation of Battery Storage Systems for Energy Supply Networks", IEEE Transactions on Power Systems, vol. 28, no. 3, pp. 2788-2797, 2013.

[89] B. Xu, Y. Shi, D. Kirschen and B. Zhang, "Optimal Battery Participation in Frequency Regulation Markets", IEEE Transactions on Power Systems, vol. 33, no. 6, pp. 6715-6725,

2018.
[90] J. Qiu, J. Zhao, H. Yang, D. Wang, and Z. Y. Dong, “Planning of solar photovoltaics, battery energy storage system and gas micro turbine for coupled micro energy grids,” Applied Energy, vol. 219, pp. 361–369, Jun. 2018.
[91] Y. Zheng, Y. Song, A. Huang, and D. J. Hill, “Hierarchical Optimal Allocation of Battery Energy Storage Systems for Multiple Services in Distribution Systems,” IEEE Transactions on Sustainable Energy, vol. 11, no. 3, pp. 1911–1921, Jul. 2020.
[92] A. Hussain, V. Bui and H. Kim, "Optimal Sizing of Battery Energy Storage System in a Fast EV Charging Station Considering Power Outages", IEEE Transactions on Transportation Electrification, vol. 6, no. 2, pp. 453-463, 2020.
[93] J. Vetter et al., "Ageing mechanisms in lithium-ion batteries", Journal of Power Sources, vol. 147, no. 1-2, pp. 269-281, 2005.
[94] C. Ju, P. Wang, L. Goel and Y. Xu, "A Two-Layer Energy Management System for Microgrids With Hybrid Energy Storage Considering Degradation Costs", IEEE Transactions on Smart Grid, vol. 9, no. 6, pp. 6047-6057, 2018.
[95] W. Chen, J. Qiu, J. Zhao, Q. Chai and Z. Dong, "Bargaining Game-Based Profit Allocation of Virtual Power Plant in Frequency Regulation Market Considering Battery Cycle Life", IEEE Transactions on Smart Grid, pp. 1-1, 2021.
[96] V. V. Viswanathan and M. Kintner-Meyer, “Second Use of Transportation Batteries: Maximizing the Value of Batteries for Transportation and Grid Services,” IEEE Transactions on Vehicular Technology, vol. 60, no. 7, pp. 2963–2970, Sep. 2011.
[97] J. Neubauer and A. Pesaran, “The ability of battery second use strategies to impact plug-in electric vehicle prices and serve utility energy storage applications,” Journal of Power Sources, vol. 196, no. 23, pp. 10351–10358, Dec. 2011.
[98] G. He, Q. Chen, C. Kang, P. Pinson, and Q. Xia, “Optimal Bidding Strategy of Battery Storage in Power Markets Considering Performance-Based Regulation and Battery Cycle Life,” IEEE Transactions on Smart Grid, vol. 7, no. 5, pp. 2359–2367, Sep. 2016.
[99] T. Dragicevic, H. Pandzic, D. Skrlec, I. Kuzle, J. M. Guerrero, and D. S. Kirschen, “Capacity Optimization of Renewable Energy Sources and Battery Storage in an Autonomous Telecommunication Facility,” IEEE Transactions on Sustainable Energy, vol. 5, no. 4, pp. 1367–1378, Oct. 2014.
[100] D. Tran and A. M. Khambadkone, “Energy Management for Lifetime Extension of Energy Storage System in Micro-Grid Applications,” IEEE Transactions on Smart Grid, vol. 4, no. 3, pp. 1289–1296, Sep. 2013.
[101] C. J. Rydh and B. A. Sandén, “Energy analysis of batteries in photovoltaic systems. Part I: Performance and energy requirements,” Energy Conversion and Management, vol. 46, no. 11–12, pp. 1957–1979, Jul. 2005.
[102] A. Zahedmanesh, K. Muttaqi and D. Sutanto, "A Cooperative Energy Management in a Virtual Energy Hub of an Electric Transportation System Powered by PV Generation and Energy Storage", IEEE Transactions on Transportation Electrification, pp. 1-1, 2021.
[103] K. Bradbury, L. Pratson and D. Patiño-Echeverri, "Economic viability of energy storage systems based on price arbitrage potential in real-time U.S. electricity markets", Applied Energy, vol. 114, pp. 512-519, 2014.
[104] R. Walawalkar, J. Apt and R. Mancini, "Economics of electric energy storage for energy

arbitrage and regulation in New York", Energy Policy, vol. 35, no. 4, pp. 2558-2568, 2007.
[105] Y. Zhang, Y. Xu, H. Yang, Z. Y. Dong, and R. Zhang, "Optimal Whole-Life-Cycle Planning of Battery Energy Storage for Multi-Functional Services in Power Systems," IEEE Transactions on Sustainable Energy, pp. 1–1, 2020.
[106] R. Bartnik and Z. Buryn, Conversion of coal fired power plants to cogeneration and combined cycle: Thermal and Economic Effectiveness. London, UK: Springer, 2011.
[107] R. Bartnik, The modernization potential of gas turbines in the coal-fired power industry: Thermal and economic effectiveness. London, UK: Springer, 2013.
[108] J. Qiu, Z. Y. Dong, J. Zhao, Y. Xu, F. Luo, and J. Yang, "A Risk-Based Approach to Multi-Stage Probabilistic Transmission Network Planning," IEEE Trans. Power Syst., vol. 31, no. 6, pp. 4867–4876, Nov. 2016.
[109] S. Fang, Y. Xu, Z. Li, Z. Ding, L. Liu, and H. Wang, "Optimal Sizing of Shipboard Carbon Capture System for Maritime Greenhouse Emission Control," IEEE Trans. Ind. Appl., vol. 55, no. 6, pp. 5543–5553, Nov. 2019.
[110] S. Hochreiter and J. Schmidhuber, "Long Short-Term Memory," Neural Comput., vol. 9, no. 8, pp. 1735–1780, 1997.
[111] M.-T. Luong, H. Pham, and C. D. Manning, "Effective Approaches to Attention-based Neural Machine Translation," Sep. 2015.
[112] Reality check: Why CCS has no role in Australia's energy system, Dec-2020. [Online]. Available: https://apo.org.au/sites/default/files/resource-files/2020-12/apo-nid309981.pdf.
[113] E. S. Rubin, J. E. Davison, and H. J. Herzog, "The cost of CO2 Capture and Storage," Int. J. Greenhouse Gas Control, vol. 40, pp. 378–400, 2015.
[114] California ISO, Demand trend. [Online]. Available: https://www.caiso.com.
[115] "Australian Government Bureau of Meteorology," Australia's official weather forecasts & weather radar - Bureau of Meteorology. [Online]. Available: http://www.bom.gov.au/.
[116] "Capital Costs and Performance Characteristics for Utility Scale Power Generating Technologies," U.S. eia, Feb-2020. [Online]. Available: https://www.eia.gov/analysis/studies/powerplants/capitalcost/pdf/capital_cost_AEO2020.pdf.
[117] "Economic Manuscripts: Appendix I: Production, Consumption, Distribution, Exchange", Karl Marx: Critique of Political Economy Appendix I, 1857.
[118] Y. Wang, J. Qiu, and Y. Tao, "Optimal power scheduling using data-driven carbon emission flow modelling for Carbon Intensity Control," IEEE Trans. Power Syst., vol. 37, no. 4, pp. 2894–2905, 2022.
[119] M. Chen et al., "Aggregated Model of Data Network for the Provision of Demand Response in Generation and Transmission Expansion Planning," IEEE Trans. Smart Grid, vol. 12, no. 1, pp. 512–523, 2021.
[120] M. Chen, C. Gao, M. Shahidehpour, and Z. Li, "Incentive-Compatible Demand Response for Spatially Coupled Internet Data Centers in Electricity Markets," IEEE Trans. Smart Grid, vol. 12, no. 4, pp. 3056–3069, Jul. 2021.
[121] G. He, J. Michalek, S. Kar, Q. Chen, D. Zhang, and J. F. Whitacre, "Utility-Scale Portable Energy Storage Systems," Joule, vol. 5, no. 2, pp. 379–392, Feb. 2021.
[122] X. Sun, J. Qiu, and J. Zhao, "Real-time volt/var control in active distribution networks with data-driven partition method," IEEE Trans. Power Syst., vol. 36, no. 3, pp. 2448–2461, May

2021.
[123] D. Watling, “User equilibrium traffic network assignment with stochastic travel times and late arrival penalty,” European Journal of Operational Research, vol. 175, no. 3, pp. 1539–1556, Dec. 2006.
[124] Yosef Sheffi, Urban transportation networks : equilibrium analysis with mathematical programming methods. Englewood Cliffs, N.J.: Prentice-Hall, 1985.
[125] J. H. Zhao, J. Foster, Z. Y. Dong, and K. P. Wong, “Flexible Transmission Network Planning Considering Distributed Generation Impacts,” IEEE Transactions on Power Systems, vol. 26, no. 3, pp. 1434–1443, Aug. 2011.
[126] J. H. Zhao, Z. Y. Dong, P. Lindsay, and K. P. Wong, “Flexible Transmission Expansion Planning With Uncertainties in an Electricity Market,” IEEE Transactions on Power Systems, vol. 24, no. 1, pp. 479–488, Feb. 2009.
[127] Openknowledge.worldbank.org, 2021. [Online]. Available: https://openknowledge.worldbank.org/bitstream/handle/10986/33971/Economic-Analysis-of-Battery-Energy-Storage-Systems.pdf?sequence=1&isAllowed=y.
[128] "Operational deamnad data.", Aemo.com.au, 2020. [Online]. Available: https://www.aemo.com.au/energy-systems/electricity/national-electricity-market-nem/data-nem/operational-demand-data.
[129] "Highways England - Open Data", Tris.highwaysengland.co.uk, 2020. [Online]. Available: http://tris.highwaysengland.co.uk/detail/trafficflowdata.